MULTIELECTRODE MICROSTIMULATION FOR TEMPORAL LOBE EPILEPSY

A Thesis
Presented to
The Academic Faculty

by

Sharanya Arcot Desai

In Partial Fulfillment
of the Requirements for the Degree
Doctor of Philosophy in the
School of Engineering

Georgia Institute of Technology
December 2013

MULTIELECTRODE MICROSTIMULATION FOR TEMPORAL LOBE EPILEPSY

Approved by:

Dr. Steve M. Potter, Advisor
School of Biomedical Engineering
Georgia Institute of Technology

Dr. Pamela Bhatti
School of Electrical Engineering
Georgia Institute of Technology

Dr. Robert E. Gross, Advisor
School of Biomedical Engineering
Georgia Institute of Technology
Department of Neurosurgery
Emory University

Dr. Maysam Ghovanloo
School of Electrical Engineering
Georgia Institute of Technology

Dr. Joseph Manns
School of Psychology
Emory University

Date Approved: November 1st 2013

To my family

ACKNOWLEDGEMENTS

Like every other kid growing up in India, I wanted to be a doctor when I grew up too. But, this gradually evolved and by the time I was in my mid-teens, I was fixated on pursuing a career in Biomedical Engineering. This led me to eventually get dual degrees in Biological Sciences and Electrical and Electronics Engineering from BITS-Pilani, one of the best universities in India. After completing my undergraduate degrees, I left my country and came to the US for a PhD in Bioengineering. I thank Georgia Tech for making my first experiences in the US so wonderful and filled with memories that I will cherish for a very long time.

After interacting with 3-4 PIs in the department of BME, I was convinced that I would make the best fit in Dr. Steve Potter's Neuroengineering lab. Luckily for me, Steve also decided to recruit me to his lab. Over the past several years, I've realized he's the best advisor I could have possibly asked for. Steve is very sincere, punctual, honest and serves as a great example of these traits to all his graduate students, me especially. I've always felt that Steve knows the answer to everything. Even when I've taken rodent surgery and behavior related questions to him, he has never failed to guide me in the right direction. His 'there is a solution to every problem' attitude has inspired and helped me time and again in both my PhD and otherwise.

Thanks to Steve Potter and John Rolston, the already well-established collaboration between the Potter and Gross labs proved very useful to me. Bob Gross has been incredible with the level of trust he's had on me. He gave me full freedom in coming up with experiments/studies I wanted to pursue, setting up my own long term

behavior lab, deciding on which grants to apply to and when. Despite his extremely busy schedule, Bob has always found the time to attend to every lab-related issue. His expertise in the domain of deep brain stimulation (DBS) is amazing. I've learnt so much about translational DBS just by listening to him talk at lab meetings that it inspired me to pursue an internship at Medtronic Neuromodulation as part of my dissertation.

The rest of my thesis committee consisting of Joseph Manns, Pamela Bhatti and Maysam Ghovanloo have been incredibly accommodating with scheduling committee meetings and making themselves available even at short notices. Unlike most of my friends in the PhD program both at Georgia Tech and elsewhere, I've never had have the chance to complain about how scheduling committee meetings can be such a herculean task and I thank my committee for keeping it that way. Their suggestions and advice have played an important role in shaping this dissertation.

I thank John Rolston, my mentor during my 1st year of PhD for the myriad lessons in Neuroscience and Neuroengineering. He's truly had a lot of patience with me. I thank Otis Smart for the many conversations**,** both work related and otherwise. He has never failed to put a smile on my face even on my bad days. I thank Li Su for teaching me some key surgery techniques. I eventually became an excellent rodent neurosurgeon because of the countless lessons I've had from him and John. Claire-Anne has been someone I could run to with the millions of questions I've had on immunohistochemistry and she's always found the time to provide me with detailed answers. I thank Neal Laxpati of the Gross lab and Jon Newman and Riley Zeller-Townson of the Potter lab for being excellent collaborators.

I thank the 10 undergraduate students who have worked with me in both the Potter and Gross labs. Their motivation and drive has inspired me to work harder on several days. Jonathan Joe, Thomas Shiu and Alexandra Harrison have helped me with several different aspects of surgeries, epileptic rat monitoring, seizure counting and histology. Amit Parekh and Kevin Lindsay have been helped me setup my long-term behavior lab and with data analysis. Alexandria Harrison, a summer graduate student from Kazakhstan taught me a few digital signal processing tricks for data analysis. Caitlin Johansson and Aaron Morris worked with me on trying to replicate my sonicoplating results on *in vitro* multielectrodes arrays at Georgia Tech.

My fellow graduate students in the Potter and Gross labs namely Jack Tung, Ming-fai Fong, Michelle Kuylendall, Nathan Killian and Alex Calhoun have all helped me in one way or the other on the various projects I've worked on for this dissertation and I am very thankful for that.

At Medtronic, I've met and made friends with some of the finest people in the Neuromodulation business. I am grateful to Tim Dension for letting me get involved in some of the current high-profile research projects at Medtronic Neuromodulation. Ben Isaacson, Siddharth Dani and Pedram Afshar have collaborated with me on a paper we sent to the IEEE Neural Engineering conference this year and have become close friends in doing so. Dave Line, Dave Carlson and Scott Stanslaski deserve gold medals for the amount of patience they've had in going through the firmware architecture of Medtronic's neurostimulators with me, time and again. Eric Panken, the team manager of Algorithms and Data Sciences, has never failed to make me feel happy and important at Medtronic. Randy Jenson, Terry Ahrens and Duane Bourget have been very quick in

responding to the dozens of questions I've had on telemetry data streaming. I thank Ramona Sly for being so prompt with her replies to my numerous administration related questions. I have never before looked forward to getting back to work so eagerly the next day, as I did during my time at Medtronic.

I thank all my friends for their love and support. I specially thank He Zheng and Garth Thompson for making me feel at home during my initial days in the US.

Nothing would be possible without my parents. My father has been my biggest fan throughout my childhood. The fact that I made him happy and proud through my accomplishments has always pushed me to achieve more. My PhD would have meant the world to him and I wish he were present to watch me accomplish this feat. My mom knows me even better than I do myself. She has stood with me through all my crazy times and has had faith in me even during times when I have given up on myself. My brother is my biggest source of hope and optimism. His belief in me has been a very important factor in my success stories over the past several years.

I thank my husband, Sudesh Peram for being my strength, my mentor and my friend. I am grateful to him for pulling me through difficult times and for loving me for who I am.

I thank the Schlumberger Foundation for granting me the very generous Faculty for the Future fellowship for three years in a row. I and my work were also funded by the CURE Foundation, NSF EFRI 1238097, the Wallace H. Coulter Foundation, and NIH grant NS05480.

TABLE OF CONTENTS

Acknowledgements ..... **iv**

List of tables ..... **xii**

List of figures ..... **xiii**

List of abbreviations ..... **xvi**

Summary ..... **xvii**

CHAPTER I Introduction **1**

CHAPTER II Durably improving impedance of microelectrode arrays **12**

2.1 Introduction **13**

2.2 Methods and Materials **15**

2.2.1 Plating solution preparation 15

2.2.2 The electroplating setup 16

2.2.3 Surgery, recordings, stimulations and impedance measurements 18

2.3 Results **19**

2.3.1 Test for durability 19

2.3.2 Matching electrode impedance under different plating conditions 22

2.3.3 Chronic MMEA implantation in vivo 23

2.3.4 Single unit activity recorded on electroplated electrodes 24

2.3.5 Reduction in stimulation voltage 25

2.3.6 Reduction of stimulation artifacts 26

2.3.7 Thermal or Johnson-Nyquist noise 30

2.4 Discussion and Conclusion **32**

CHAPTER III C-fos immunohistochemistry study of spatial activation with deep brain stimulation 35

3.1 Introduction 36

3.2 Methods 39

3.2.1 Surgery 42

3.2.2 Immunohistochemistry 42

3.2.3 Cell counting 43

3.3 Results 46

3.3.1 Immunohistochemistry staining of electrically stimulated and control sections. 46

3.3.2 Neuronal activation distribution 48

3.3.3 Neuronal activation% and total number of neurons activated 50

3.3.4 Neuronal activation with microelectode arrays 51

3.4 Discussion 53

CHAPTER IV Open-loop electrical stimulation for epilepsy 57

4.1 Introduction 58

4.2 Methods and materials 61

4.2.1 Surgery 61

4.2.2 Recording and stimulation studies 64

4.2.3 Seizure classification and counting 67

4.2.4 Cognition test 67

4.2.5 Data analysis and test for significance 68

4.2.6 Immunohistochemistry 69

4.3 Results 69

4.3.1 Theta oscillations are significantly reduced in tetanus toxin epilepsy 69

4.3.2 Asynchronous theta microstimulation significantly reduces tetanus toxin epilepsy. 73

4.3.3 Neither theta synchronous stimulation nor asynchronous stimulation at higher frequencies reduced seizures 76

4.4 Discussion 79

CHAPTER V Behavioral deficits associated with tetanus toxin epilepsy. 82

5.1 Introduction 82

5.2 Methods 83

5.2.1 Surgery 83

5.2.2 Morris water maze task 84

5.2.3 Forced Swim test 85

5.2.4 Morris Water Maze test with electrical stimulation 86

5.3 Results 87

5.3.1 Dorsal and ventral tetanus toxin injected rats showed significant memory impairments when compared to saline injected controls. 88

5.3.2 Epileptic rats did not display significant depression compared to controls 90

5.3.3 Theta synchronous microstimulation was ineffective in improving memory in preliminary studies. 91

5.4 Discussion 92

CHAPTER VI Closed-loop stimulation for epilepsy. 94

6.1 Introduction 94

6.2 Methods 96

6.3 Results 98

6.3.1 Biomarker identification 98

6.3.2 Responsive closed-loop stimulation 102

6.3.3 Predictive closed-loop stimulation 104

6.4 Discussion 105

CHAPTER VII Development of a rapid algorithm prototyping tool for closed-loop deep brain stimulation systems. 107

7.1 Introduction 107

7.2 System overview 110

7.3 Characterizing system latencies 111

7.4 RESULTS 115

7.4.1 Latency characterization 115

7.4.2 Example applications 118

7.5 CONCLUSION 123

CHAPTER VIII Conclusion and Future Direction 125

8.1 CONCLUSION 125

8.2 FUTURE DIRECTIONS 128

Appendix 132

References 139

LIST OF TABLES

Table 2.1 Electroplating parameters for achieving same reduction in impedance via three different electroplating techniques. 23

Table 6.1 Interictal spike rate in 60 seconds prior to seizures normalized with respect to baseline interictal spike rate. 100

Table 7.1 Signal to detection latency with Medtronic's closed-loop research tool. .. 115

Table 7.2 Stimulation command to actuation latency with Medtronic's closed-loop research tool. 115

LIST OF FIGURES

Figure 1.1 Traditional deep brain stimulation and vagus nerve stimulation techniques. 3

Figure 2.1 The sonicoplating setup and microelectrode array. 17

Figure 2.2 Impedance spectra of microwire electrodes before and after durability test. 20

Figure 2.3 SEM images of electroplated microwire electrode tips. 21

Figure 2.4 Impedance spectra of in vivo implanted microwires over time. 24

Figure 2.5 Single unit recording on unplated and sonicoplated microwires. 25

Figure 2.6 Stimulation voltage requirements by the electroplated and unplated microwires. 26

Figure 2.7 Stimulation artifact waveform on unplated and electroplated microwires. 29

Figure 2.8 Amplitude and duration of stimulation artifact on the three types of electroplated and unplated microwires. 29

Figure 2.9 Quantifying thermal noise in vivo on electroplated and unplated microwires. 31

Figure 3.1 Spatial activation with macro, micro and sonicoplated microelectrode array. 39

Figure 3.2 Macroelectrode and microelectrode array used in this study. 40

Figure 3.3 Impedance spectroscopy of macroelectrode, microelectrode array and sonicoplated microelectrode array. 41

Figure 3.4 Experimental procedure for studying neuronal activation caused by electrical stimulation. 44

Figure 3.5 C-fos+/NeuN+ cell counting method. 45

Figure 3.6 Histology results with C-fos+/NeuN+ stained sections. 47

Figure 3.7 Neuronal activation distribution around electrode tracks. 49

Figure 3.8 Neuronal activation% and total number of neurons activated. 50

Figure 3.9 Neuronal activation with several microelectrodes. 51

Figure 3.10 Tissue damage caused by macro and microelectrode. 53

Figure 4.1 DAPI stained horizontal sections through dorsal hippocampus to confirm implantation site. 61

Figure 4.2 Seizures and interictal spikes in the tetanus toxin model of temporal lobe epilepsy. 63

Figure 4.3 Three different stimulation protocols tested through the microelectrode array. 64

Figure 4.4 Stimulator headstage with multiplexer. 67

Figure 4.5 Abnormal theta oscillations in the tetanus toxin model of epilepsy. 71

Figure 4.6 Seizure reduction is obtained with asynchronous distributed microstimulation in theta frequency range. 75

Figure 4.7 Some of the other stimulation protocols tested did not reduce seizures. .. 78

Figure 5.1 The Morris water maze setup. 84

Figure 5.2 Morris water task performance by epileptic and control rats. 88

Figure 5.3 Forced swim task performance by epileptic and control rats. 90

Figure 5.4 Morris water task with electrical stimulation in epileptic rat. 91

Figure 6.1 Temporal variation of interictal spikes with respect to seizures. 99

Figure 6.2 Two types of electrical closed-loop stimulation were performed in the tetanus toxin model of temporal lobe epilepsy. 102

Figure 6.3 Responsive closed-loop stimulation for epilepsy. 103

Figure 6.4 Predictive closed-loop stimulation for epilepsy. 104

Figure 7.1 The Medtronic closed-loop research tool. 110

Figure 7.2 Test setup for characterizing latencies of the closed-loop research too. 112

Figure 7.3 Oscilloscope screenshots showing signal and stimulation command transmission between the implanted pulse generator and algorithm on host computer. 114

Figure 7.4 Application of the closed-loop research tool for Parkinson's disease.... 119

Figure 7.5 Simulink model example for Parkinson's disease. 120

Figure 7.6 Application of the closed-loop research tool for essential tremor...... 121

Figure 7.7 Simulink model example with sensor fusion for essential tremor...... 122

Figure A.1 Optogenetic light stimulation in dorsal hippocampus with ChR2 expression...... 136

Figure A.2 Optogenetic light stimulation in dorsal hippocampus with ChR2 expression...... 137

LIST OF ABBREVIATIONS

1. API	Application Programming Interface
2. BNI	Bidirectional Neural Interface
3. DBS	Deep Brain Stimulation
4. DC electroplating	Direct Current electroplating
5. DMM	Distributed Multielectrode Microstimulation
6. INS	Implanted NeuroStimulator
7. MEA	Multi-Electrode Array
8. MMEA	Microwire Multi-Electrode Array
9. STS	Streaming Telemetry System

SUMMARY

Multielectrode arrays may have several advantages compared to the traditional single macroelectrode brain electrical stimulation technique including less tissue damage due to implantation and the ability to deliver several spatio-temporal patterns of stimulation. Prior work on cell cultures has shown that multielectrode arrays are capable of completely stopping seizure-like spontaneous bursting events through a distributed asynchronous multi-site approach. In my studies, I used a similar approach for controlling seizures in a rat model of temporal lobe epilepsy. First, I developed a new method of electroplating *in vivo* microelectrode arrays for durably improving their impedance. I showed that microelectrode arrays electroplated through the new technique called sonicoplating, required the least amount of voltage in current controlled stimulation studies and also produced the least amplitude and duration of stimulation artifact compared to unplated, DC electroplated or pulse-plated microelectrodes. Second, using c-fos immunohistochemistry, I showed that 16-electrode sonicoplated microelectrode arrays can activate 5.9 times more neurons in the dorsal hippocampus compared to a single macroelectrodes while causing < 77% the tissue damage. Next, through open-loop multisite asynchronous microstimulation, I reduced seizure frequency by ~50% in the rodent model of temporal lobe epilepsy. Preliminary studies aimed at using the same stimulation protocol in closed-loop responsive and predictive seizure control did not stop seizures. Finally, through an internship at Medtronic Neuromodulation, I worked on developing and implementing a rapid algorithm prototyping research tool for closed-loop human deep brain stimulation applications.

CHAPTER I

INTRODUCTION

The brain is an amazing organ. Made of basic ingredients such as sugars, proteins and lipids, it is incredible how so many different types of cells work together in such beautiful coordination. But even when a small fraction of these cells begin to work out of synchrony, severe disorders may result. One may draw an analogy between the brain and a large orchestra containing sections of woodwinds, strings, brass and percussion instruments. Coordination and synchronization between these instruments is crucial to producing good symphony. Even when a few of these instruments are played out of sync, chaotic sounds will result.

Epilepsy, affecting about 1% of the world's population, is a great example of a disorder where such coordination and synchronization is lost in the brain (Mormann et al. 2003). A population of neurons within the seizure focus firing out of coordination can generalize into tonic-clonic episodes, which can be severely disabling to the patient (Warren et al. 2010). Recently, through recordings on microelectrode arrays, very small seizures termed 'microseizures' were identified in the epileptic brain (Stead et al. 2010). These microseizures were found to be sparsely distributed and happened more frequently at the epileptic foci, sporadically evolving into generalized seizures by presumably recruiting more neurons to fire out of normal synchrony (Stead et al. 2010).

As of today, Vagus nerve stimulation (VNS; Figure 1.1) remains the only FDA approved electrical stimulation treatment for medically refractory epilepsy (Rolston et al.

2012). In VNS, spiral electrodes wound around the vagus nerve having projections to the nucleus of solitary tract, deliver intermittent stimulation (Schachter and Saper 1998). The nucleus of solitary tract in turn has projections to many different parts of the brain. Through mechanisms not fully understood, the VNS open-loop approach has been shown to reduce seizures by 50% in 40% of the patients (Rolston et al. 2012). Two recent clinical trials have investigated direct brain electrical stimulation for epilepsy. Neuropace's RNS (Sun et al. 2008) and Medtronic's SANTE (Fisher et al. 2010) performed deep brain stimulation where a single macro electrode was implanted within the epileptic focus in the former, or bilaterally in the anterior nucleus of the thalamus in the latter (Rolston et al. 2012). Both showed significant decrease in seizure frequency compared to unstimulated control. However, neither technique was effective in completely stopping seizures (Rolston et al. 2012).

The traditional method of performing brain stimulation is through macroelectrodes measuring 1.27 mm in diameter implanted within brain targets to be stimulated (Figure 1.1) (Butson and McIntyre 2006). In epilepsy, irrespective of the size of seizure focus (the region of interest for stimulation), electrodes of the same dimensions are implanted. Even with such a direct brain stimulation approach, side effects may result from the unnecessary stimulation of structures that lie outside the region of interest. Further, with macroelectrodes, there is a physical limitation on the number of spatial patterns of stimulation that can be delivered.

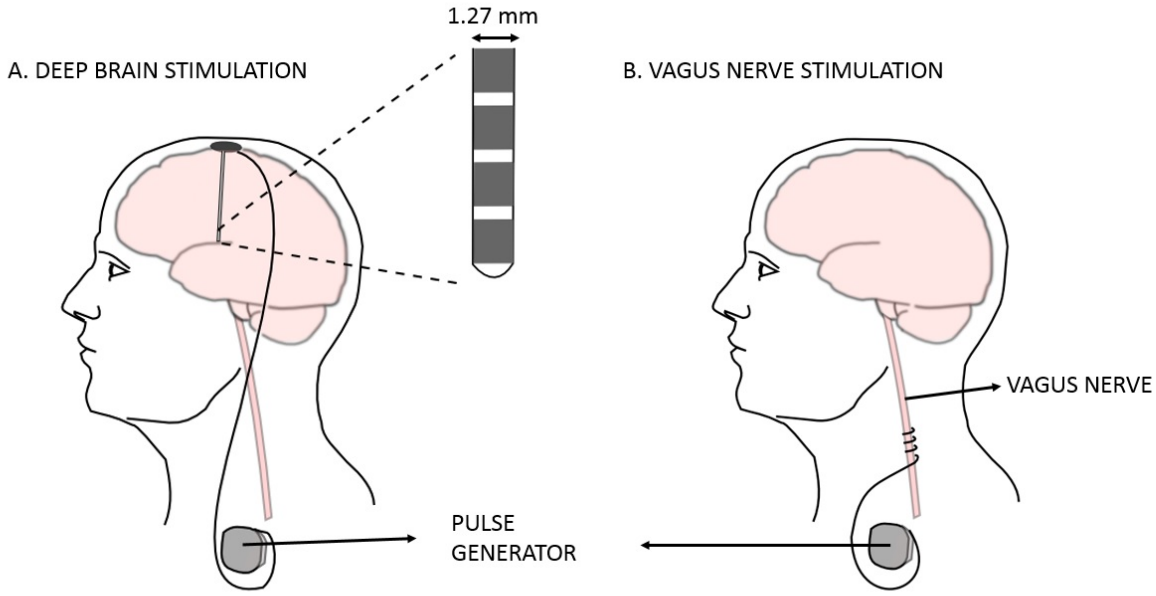

Figure 1.1 Traditional deep brain stimulation and vagus nerve stimulation techniques. (A) Deep brain stimulation involves implanting electrodes measuring 1.27 mm in diameter within deep brain structures such as the subthalamic nucleus for Parkinson's disease. A pulse generator connected to the electrodes is implanted below the clavicle of the patient. (B) Vagus nerve stimulation for epilepsy involves wrapping circular electrodes around the vagus nerve having projections to the nucleus of solitary tract.

An alternate approach to brain stimulation is to use multi microelectrode arrays through which several different spatio-temporal patterns of stimulation can be delivered while causing reduced tissue damage due to implantation. Further, the microelectrodes can be specifically targeted to specific cell layers or axon tracts that need to be stimulated. The width of these targets is often much smaller than the diameter of the macroelectrodes. Although multimicroelectrode arrays have been used commonly in brain machine interfaces (Donoghue 2002; Pais-Vieira et al. 2013), they have seldom been used in deep brain stimulation for treating brain disorders such as epilepsy, Parkinson's disease, essential tremor, etc.

In epilepsy and movement disorders such as Parkinson's disease and essential tremor, abnormal synchronization of certain neural populations has been considered to be the fundamental manifestation of the pathologic state (Perez Velazquez and Carlen 2000; Percha et al. 2005; Warren et al. 2010; Little et al. 2013). In trying to rescue the brain from such abnormal synchronizations, Tass et al. (Tass and Majtanik 2006) have shown that desynchronizing multi-site stimulation has anti-pathological effects in movement disorders and epilepsy. When brief bursts of high frequency pulses were delivered on multiple sites, they briefly perturb the phases of the different subpopulations affected within the target population. Due to the pathologically strong interactions, the neurons spontaneously relax from hyper-synchronized into a pronounced transient desynchronized state, and, finally, revert back to pathological synchrony if left unperturbed (Tass and Majtanik 2006). A similar concept was shown to be effective in controlling spontaneous *in vitro* array-wide, seizure-like bursting events in cultures of cortical neurons (Wagenaar et al. 2005). In 60 microelectrode array *in vitro* dishes with monolayer cultures grown over the electrode array, multi-site stimulation delivered on 25 randomly chosen microelectrodes was capable of completely stopping the culture-wide bursts (Wagenaar et al. 2005). This study further shows the potential benefits the multi microelectrode stimulation approach may have over single-site macroelectrode stimulation. When stimulation was delivered in a closed-loop fashion to maintain the background firing rate of the culture at a predefined value, the cultures were maintained burst-free at lower stimulation frequencies (Wagenaar et al. 2005).

Two other recent studies have displayed the power of closed-loop stimulation in controlling neural disorders. Both showed that closed-loop stimulation was more

effective than open-loop stimulation in Parkinson' Disease. The first study was done in human patients and used power in the beta frequency band as the biomarker for turning on electrical stimulation (Little et al. 2013), while the second study used single unit firing rate as the biomarker for performing stimulation in Parkinsonian non-human primates (Rosin et al. 2011). Additionally, in the realm of epilepsy, the Responsive neurostimulator system from Neuropace where the stimulator is turned on when seizures are detected has produced similar seizure reduction when compared to the open-loop SANTE and VNS systems (Rolston et al. 2012). With closed-loop, there is a saving on battery life with the subsequent consequence of requiring patients to undergo fewer battery replacement surgeries which can be both a financial burden and strenuous to the patient and his/her family. Moreover, since stimulation will be turned on only when necessary, brain habituation and unnecessary side effects will be reduced. Hence, even though the RNS system has only shown comparable results to SANTE and VNS, the other benefits of the closed-loop stimulator may arguably make this treatment more preferable, in comparison.

Once implanted, the ideal closed-loop deep brain stimulation system should be invisible to the patients in that the device and control algorithms should function with no intervention from patients or his/her medical support team. In other words, it should appear as if the patient did not receive the implant in the first place. Furthermore, the system should be completely effective in rescuing the brain from the disease condition, while having no side effects. Some of the current challenges impeding the implementation of such systems are 1) Technology limitations 2) Lack of understanding

of stimulation interaction with brain tissue and 3) Lack of knowledge on effective stimulation parameters for disease control.

1) Technology limitations.

The major challenges of closed-loop systems derive from both the physical limitations of such systems and, paradoxically, their capabilities. The main physical limitation is the problem of stimulus artifacts, described further below (Rolston et al. 2011) (Wagenaar and Potter 2002). Trying to record an electrical signal, while simultaneously providing an extrinsic electrical signal, requires disentangling the extrinsic signal (stimulation) from the intrinsic signal (the neural activity). Recorded extracellular electrical signals are on the order of microvolts, whether single unit APs or LFPs. Electrical stimuli, on the other hand, are typically in the range of volts, a million-fold difference in amplitude. Therefore, recording equipment designed to operate at one range seldom works well at the other. Thus, when stimulation is amplified by the recording electronics, say at 1000×, a 5 V pulse becomes a 5000 V input. Since this exceeds the range of the electronics, they saturate at their maximal input value, often for a duration far exceeding the stimulus pulse itself. Depending on hardware filters and the amplifier's construction, this resetting can take from milliseconds to whole seconds (Rolston et al. 2011). During this time, the amplifier's output is not indicative of any neural signal, and therefore no useful information about the brain can be extracted.

Beyond saturation of the electronics, an additional problem is the electrical waveform produced by stimuli that are non-saturating. This waveform is often treated as a

deterministic response to stimulation (though it usually is not), and is superimposed upon the intrinsic neural signals.

2) Lack of understanding of stimulation interaction with brain tissue.

Deep brain stimulation (DBS) has been successful in stopping symptoms of brain disorders such as Parkinson's disease. But despite its success, very little is known about its mechanisms of actions including the spatial extent over which stimulation has an effect (Montgomery and Gale 2008). It is perhaps because of this reason that there has been very limited incremental success in improving therapy through deep brain stimulation, since the first success stories with DBS. Understanding the spatial extent of stimulation with varying stimulation parameters will definitely go a long way in optimizing treatment outcome (Chaturvedi et al. 2010). Further, new types of electrodes including microelectrode arrays discussed previously in this introduction, may have advantages compared to macroelectrode stimulation, especially when stimulating complex structures like the hippocampus. Knowing the spatial extent of neuronal tissue activated by different stimulation parameters will help in spacing out the individual electrodes in the microelectrode array for optimal stimulation of brain structures.

3) Lack of knowledge on effective stimulation parameters for disease control.

Another main challenge is the sheer number of possibilities unleashed by closed-loop stimulation. One approach to solving this complex problem is to break it up into two independent sub-problems A) Find effective stimulation parameters that control disease symptoms in open-loop stimulation. B) Find reliable biomarkers that can be used to turn on stimulation when a disease-prone brain state is detected. Some examples of

biomarkers include seizures in epilepsy (Sun et al. 2008) and power in beat band for Parkinson's disease (Little et al. 2013).

In this dissertation, a multielectrode microstimulation approach for epilepsy is explored. The focus in this dissertation is on temporal lobe epilepsy (TLE) which is the form of epilepsy most resistant to treatment by drugs (Helmstaedter 2002). Patients with TLE are also often not candidates for resection surgeries due to risk to memory, which is already impaired in a good fraction (Helmstaedter 2002). The broad aim of my work can be divided into 3 categories, which are each aimed at tackling the 3 limitations listed above. (A) Reducing stimulation artifact pickup for better brain activity sensing during stimulation with chronic implants. (B) Understanding the spatial extent of neuronal activation with deep brain stimulation using different electrode types. (C) Finding effective stimulation parameters that control disease symptoms in epilepsy.

A brief summary of the following chapters is given below

Chapter 2: Durably improving impedance of microelectrode arrays.

The impedance of implantable microelectrode arrays was durably reduced by a new technique called 'sonicoplating' in which DC electroplating of platinum black on the base metal was done under ultrasonic vibrations. This technique knocked off loosely bonded platinum black particles, retaining only the strong bonds leading to higher durability of the electroplated material compared to DC and pulsed plating techniques ($P<0.05$). The sonicoplated microelectrodes also had significantly reduced stimulation artifact pickup ($P<0.01$) and required less stimulation voltage ($P<0.005$) for delivering a set amount of current compared to unplated electrodes.

Chapter 3: C-fos immunohistochemistry study of spatial activation with deep brain stimulation.

C-fos immunohistochemistry was used to study the spatial extent of neuronal activation in voltage-controlled electrical stimulation studies using unplated microelectrodes, sonicoplated microelectrodes and unplated macroelectrodes in the dorsal hippocampus. With 4 hours of continuous 25 Hz, ± 1 V, 400 μs/phase, biphasic square pulse stimulation in anesthetized rats, it was found that by targeting an array of 16 sonicoplated microelectrodes into the pyramidal cell layer of the hippocampus, 5.9 times the neurons as a single macroelectrode can be activated with 23% less damage, overall.

Chapter 4: Open-loop electrical stimulation for epilepsy.

The tetanus toxin model of temporal lobe epilepsy was used in these studies. It was found that theta oscillations (center frequency ~7.5 Hz) are significantly reduced ($P<10^{-4}$) in the epileptic rats when compared to saline injected controls. Asynchronous distributed multi-site microstimulation delivered within the theta frequency range was effective in significantly reducing seizure frequency by ~50% whether delivered continuously or intermittently ($P<0.05$). Synchronous theta stimulation through the microelectrodes or theta pulse stimulation through macroelectrodes was ineffective in reducing seizures.

Chapter 5: Behavioral deficits associated with tetanus toxin epilepsy.

Through tests in the Morris water maze task, it was found that the tetanus toxin injected epileptic rats have significant ($P<0.05$) memory deficits compared to saline injected controls. Whether the injections were given in the dorsal or the ventral

hippocampus, similar deficits were observed. The epileptic rats however did not show any significant differences compared to saline injected controls in the forced swim test for depression. Preliminary studies with theta synchronous microstimulation delivered through microelectrode array failed to improve memory performance.

Chapter 6: Closed-loop electrical stimulation for epilepsy.

For performing closed-loop electrical stimulation, it is first important to find biomarkers that can be used to control stimulation. It was found that interictal spike frequency significantly ($P<0.005$) reduces in the 60-second time period prior to the onset of seizures compared to a baseline rate, which was calculated 60-360 prior to seizure onset. Delivering stimulation in both 1) Responsive fashion in response to seizures and 2) Predictive fashion in response to a decrease in interictal spike rate failed to stop seizures in preliminary tests.

Chapter 7: Development of a rapid algorithm prototyping tool for closed-loop deep brain stimulation systems.

As part of an internship at Medtronic Neuromodulation, I worked on designing and testing an Application programming interface (API) based closed-loop algorithm prototyping platform for DBS that will allow researchers/clinicians to rapidly design any closed-loop algorithm of interest to them in MATLAB/Simulink or LabVIEW on a host processor (laptop). Neural data is streamed into the laptop through telemetry and stimulation commands are sent through telemetry to implanted bi-directional neural interfaces. Two example closed-loop algorithms designed using this system are described.

Chapter 8: Conclusion and future directions.

In this chapter, I conclude my dissertation by discussing implications of my work and researching on some future directions for improvement.

Appendix.

Preliminary studies were performed for understanding spatial activation with optogenetic light stimulation in the dorsal hippocampus with c-fos immunohistochemistry. Some results and scope for improving experimental procedures are described.

CHAPTER II

DURABLY IMPROVING IMPEDANCE OF MICROELECTRODE ARRAYS[1]

Implantable microelectrode arrays (MEAs) have been a boon for neural stimulation and recording experiments. Commercially available MEAs have high impedances, due to their low surface area and small tip diameters, which are suitable for recording single unit activity. Lowering the electrode impedance, but preserving the small diameter, would provide a number of advantages, including reduced stimulation voltages, reduced stimulation artifacts and improved signal-to-noise ratio. Impedance reductions can be achieved by electroplating the MEAs with platinum (Pt) black, which increases the surface area but has little effect on the physical extent of the electrodes. However, because of the low durability of Pt black plating, this method has not been popular for chronic use. Sonicoplating (i.e. electroplating under ultrasonic agitation) has been shown to improve the durability of Pt black on the base metals of macro-electrodes used for cyclic voltammetry. This method has not previously been characterized for MEAs used in chronic neural implants. We show here that sonicoplating can lower the impedances of microwire multi-electrode arrays (MMEA) by an order of magnitude or more (depending

[1] Desai, S.A., Rolston, J.D., Guo., L., Potter, S.M., (2010). Improving impedance of implantable microwire

on the time and voltage of electroplating), with better durability compared to pulsed plating or traditional DC methods. We also show the improved stimulation and recording performance that can be achieved in an *in vivo* implantation study with the sonicoplated low-impedance MMEAs, compared to high-impedance unplated electrodes.

2.1 Introduction

Implantable microelectrode arrays have been used to record and stimulate in a number of studies in different regions of the brain (Branner et al. 2001; Vetter et al. 2004; McCreery et al. 2006; Cogan 2008). Microwire multi-electrode arrays (MMEAs) have been used widely in studies requiring both chronic and acute (<1 day) recordings and stimulations (Nicolelis et al. 1997; Buzsaki 2004; Deadwyler and Hampson 2004; Shi et al. 2007; Ganguly et al. 2009; O'Doherty et al. 2009; Rolston et al. 2009; Venkatraman et al. 2009). They have especially gained prominence because of the wide range of array shapes and sizes available (including number of electrodes, length, spacing, insulation, diameter, impedance, tip shape, etc.), to suit different needs.

The stimulation parameters (voltage, pulse length, etc.) that are required to evoke neural responses using the MMEAs are dependent on the impedance of the electrodes. It would be ideal for the electrodes to have low impedance because this would directly reduce the amount of voltage required to produce a given current, and in turn evoke the desired response. Lowering the required stimulation voltage is expected to help avoid several problems:

First, when electrodes immersed in saline solutions are driven to high enough voltages, electrolysis occurs, wherein water is irreversibly split into O_2 and H_2 gases

(Merrill et al. 2005). For platinum (Pt) electrodes, Rose and Robblee (1990) (Rose and Robblee 1990) have reported that the maximum charge density that can be applied without the electrode potential exceeding the water window (or causing electrolysis of water) is 50-100 $\mu C/cm^2$ using anodic-first pulses and 100-150 $\mu C/cm^2$ using cathodic-first pulses. For platinum (Pt) electrodes of a few micrometers in diameter the electrolysis limit is determined to be above 1 V (at which oxidation of the electrode begins) or below -0.8 V (at which hydrogen evolution begins) (Rozman et al. 2000). Lowering the impedance of stimulating electrodes would allow for higher currents to be passed before causing electrolysis.

Second, in simultaneous stimulation and recording experiments, stimulation artifacts are undesirable because they make detection of action potential difficult or impossible in the time period for which they last (Wagenaar and Potter 2002) (Rolston et al. 2009). Signal processing algorithms like SALPA (Wagenaar and Potter 2002) suppress stimulation artifacts on the non-stimulating electrodes but do not work well on the stimulating electrode itself if the stimulus saturates the preamplifier, filters or analog-to-digital converter. Lowering the impedance of electrodes by increasing their surface area will also increase their capacitance. Increasing capacitance will have the effect of reducing the capacitive voltage for a given stimulation current. Since capacitive voltage is the main culprit in prolonging stimulation artifacts, lowering it should reduce the duration of the artifacts. Lower impedances allow reduced stimulation voltages and this will also reduce the amplitude of stimulation artifacts (Ross et al. 2004).

Third, thermal noise (also known as the Johnson-Nyquist noise) is directly proportional to electrode impedance (Johnson, 1928; Nyquist, 1928) and will also be

reduced by lowering the impedance of electrodes. Reducing thermal noise should help in improving the signal-to-noise ratio of neural recordings.

All this calls for MMEAs with reduced impedance. Ideally, impedance should be reduced by increasing surface area without increasing the physical extent of the electrodes. Otherwise, we would compromise on single unit selectivity and increase damage to tissue. Electroplated Pt black is non-toxic (Dymond et al., 1970) and has a high surface area but traditionally is very delicate and not suitable for chronic use. In the field of cyclic voltammetry, Marrese has shown that plating electrodes with Pt black under ultrasonic agitation increases their surface area with higher durability (Marrese, 1987). However, to the best of my knowledge, this technique has not previously been characterized for neural recording and stimulation on microelectrodes used in chronic implants.

Here, we study the durability of Pt black plated on MMEAs under ultrasonic vibration ("sonicoplating") in chronic implants. We also show explicitly the improvements that durably plated MMEAs can have over unplated MEAs for *in vivo* recording and stimulation performance. Pulsed plating is another technique that has been proposed for improving the durability of Pt black plating (Gladstein, 2001, 2005). We compared the durabilities of Pt black plated through sonicoplating, pulsed plating and DC plating by scanning electron microscopy (SEM), impedance spectroscopy and measurements of *in vivo* stimulation and recording.

2.2 Methods and Materials

2.2.1 Plating solution preparation

We followed the protocol for the plating solution from Marrese (1987). For 200 ml of chloroplatinic acid plating solution, we added 200 ml of ultrapure (>10Mohm/cm) water, 20 mg of lead acetate trihydrate (Sigma-Aldrich) (lead ions have been shown to increase the adherence of Pt black on the substrate), 5 µl of 1 N HCl and 2 g of chloroplatinic acid hydrate (Aldrich) at room temperature (25^{o}C).

2.2.2 The electroplating setup

The electroplating setup used consists of a cathode (the MMEA that is to be plated), an anode (a strip of Pt metal) and the electrolyte (Pt electroplating solution) immersed in a standard ultrasonic bath agitator (sonicator) (Sonicor model DSC-101TH) used to provide agitation in the ultrasonic frequency range. The sonicator that we used in our study had output vibrations of 40,000 Hz at 276 watts.

Voltage-controlled electroplating was performed on all trials at room temperature using the setup depicted in Figure 2.1. Input current for electroplating was provided by our open-source NeuroRighter multi-electrode electrophysiology setup (Rolston et al. 2009). The use of NeuroRighter made intermittent impedance measurements *in vivo* and *in vitro* fast and easy.

The MMEAs (Tucker-Davis Technologies) that we used in our experiments had sixteen electrodes of 33 µm diameter arranged in two rows of 8 electrodes, with 175 µm between electrodes within a row, and 1 mm between rows. The electrodes are made of a tungsten core insulated with polyimide. There is a thin layer of gold between the tungsten and polyimide which enables soldering of the electrode to the connector. The sixteen electrodes on the MMEA were divided into four groups of four interleaved electrodes

(each group had one electrode each from electrode numbers 1-4, 5-8, 9-12 and 13-16). We sonicoplated one of the four groups, pulsed plated the second, DC plated the third and left the fourth group unplated to serve as a control. The microwire electrodes were plated one at a time by the three different plating techniques until their impedances were brought down to the same level. This was made possible by interfacing a 16:1 multiplexer circuit with NeuroRighter. So that only the sonicoplated electrodes were exposed to sonication, the order of plating was 1) sonicoplating, followed by 2) pulsed plating followed by 3) DC plating.

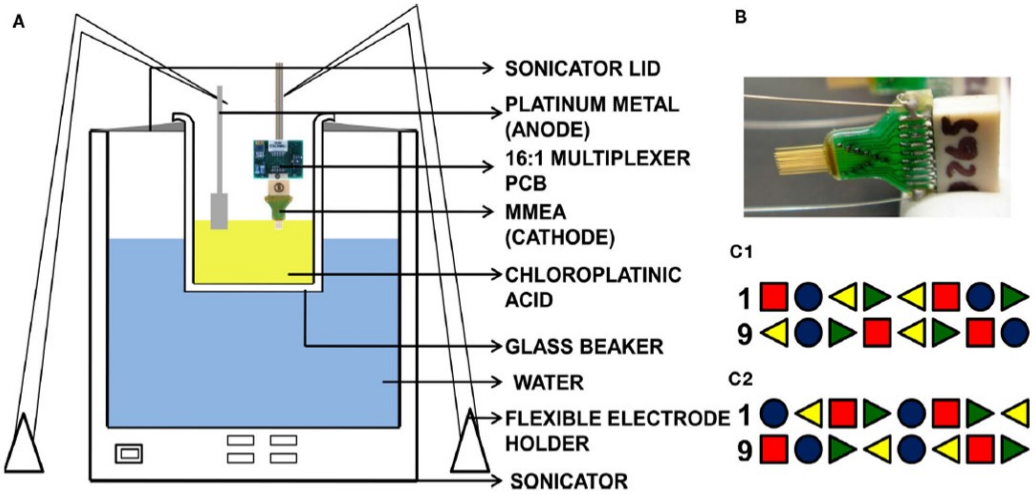

Figure 2.1 The sonicoplating setup and microelectrode array.
(A) Setup used in the sonicoplating experiment consists of a cathode (MMEA - the base metal to be electroplated), an anode (a strip of Pt metal) and the electrolyte (chloroplatinic acid plating solution) in a standard 500 ml Pyrex glass beaker placed in an ultrasonic agitator. Flexible arm probe holders are used to hold the MMEA and Pt counter-electrode. The same setup is used for pulsed plating and DC plating with the ultrasonic agitator switched off. Electroplating current comes from NeuroRighter, which is programmed to deliver voltage-controlled DC current or pulsed current of appropriate amplitude and duration. (B) MMEA (Tucker Davis Technologies) with tungsten electrodes insulated with polyimide. (C) Of the sixteen electrodes in the microwire array, four are sonicoplated (red square), four are pulsed plated (green right triangle), four are DC plated (yellow left triangle) and four are left unplated (blue circle). (C1) and (C2)

show the sixteen plated and unplated electrodes in MMEAs used in our durability and in vivo studies respectively. Time and voltage for plating were chosen so that the three types of plating produced similar final impedance values.

2.2.3 Surgery, recordings, stimulations and impedance measurements

Animal work was conducted in accordance with the National Institute of Health Guide for the Care and Use of Laboratory Animals and approved by the Emory University Institutional Animal Care and Use Committee. An adult male Sprague-Dawley rat weighing ≥ 350 g was used for our *in vivo* durability, stimulation and recording tests. For the duration of the surgery, the rat was kept anesthetized with 1-3% inhaled isofluorane. A craniectomy was made over the right dorsal hippocampus, centered at 3.5 mm posterior and 2.8 mm lateral to bregma. The dura was removed with a sterile needle. An electroplated 18-electrode MMEA, whose impedances were brought down to the same levels by the three different plating methods on 4 electrodes each (according to the method in the previous section was slowly implanted into the brain to a depth of ~3.7 mm (in addition to the 16 normal electrodes, the MMEA also had two longer (6 mm) ground and reference electrodes). Skull screws were implanted and dental acrylic was applied to seal the craniectomy. Buprenorphine (0.05 mg/kg) was injected and the rat was allowed to rest for 6 days before subsequent impedance studies began.

Impedances were measured by stimulating with sine waves of amplitude 1 μA across the frequency range of 10 to 10000 Hz. To compare stimulation voltages required (for a fixed simulation current) on the three different types of plated and unplated electrodes; ten ±10 μA biphasic current-controlled pulses of 800 μs duration (50% duty cycle) were delivered on one electrode at a time while simultaneously recording (at 25

kHz) from all sixteen electrodes. Stimulation artifacts (<1 ms) on the non-stimulating electrodes were removed in real-time with the SALPA algorithm (Wagenaar and Potter 2002).

2.3 Results

2.3.1 Test for durability

We tested the durability of the Pt black plating by subjecting an electroplated 16-electrode MMEA, whose impedances were brought down to the same levels by the three different plating methods on 4 electrodes each (according to the procedure in the methods section) to additional sonication in physiological saline solution. The hypothesis is that additional sonication will remove any loosely bonded Pt black particles, showing which plating technique produces the most durably plated layer. As seen from Figure 2.2, at the end of sixty minutes of ultrasonic agitation in saline, all three types of plated electrodes showed an increase in the impedance levels compared to their impedance values immediately after plating, indicating that there is a loss in Pt black plated by all three methods. However this increase was much more pronounced in the DC and pulsed plated electrodes. As seen from Figure 2.2 A-C, at 1 kHz there is a 63 ± 16% increase in the impedance of the sonicoplated electrodes after sixty minutes of additional sonication as opposed to 297 ± 18% increase and 353 ± 72 % increase in the pulsed plated and DC plated cases.

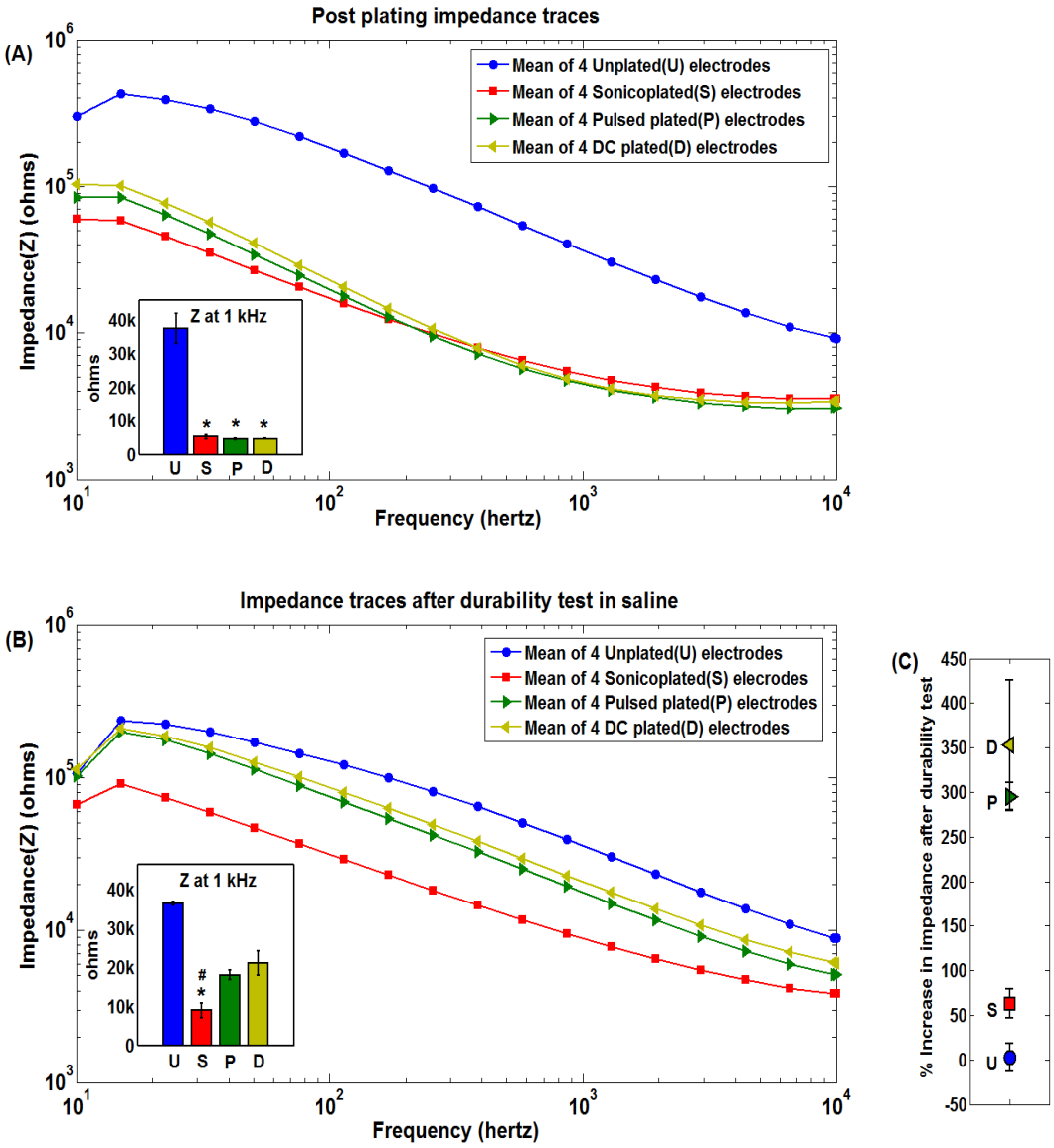

Figure 2.2 Impedance spectra of microwire electrodes before and after durability test. (A) Post plating mean impedance spectra of the three types of plated and unplated electrodes. Each log-log plot shows the mean impedance value of four electrodes that were subject to the same type of plating treatment. The inset at the bottom left shows the mean impedance values of the three types of plating at 1 kHz (blue – unplated , red – sonicoplated , green – pulsed plated , yellow – DC plated) with the error bars representing the standard error of the mean. Impedance values were recorded in physiological saline solution with the help of NeuroRighter (Rolston et al. 2009),*p<0.001 (t-test) compared to unplated electrodes (B) Mean impedance traces of the same electrodes after being subject to sixty minutes of sonication in saline.*p = 0.001 compared to control; #p<0.05 compared to pulsed plated and DC plated electrodes. (C) Percentage increase in the impedance values after sixty minutes of

additional sonication in saline. Values are calculated from the mean post plating and post additional sonication values at 1 kHz for the three types of plated and the unplated electrodes.

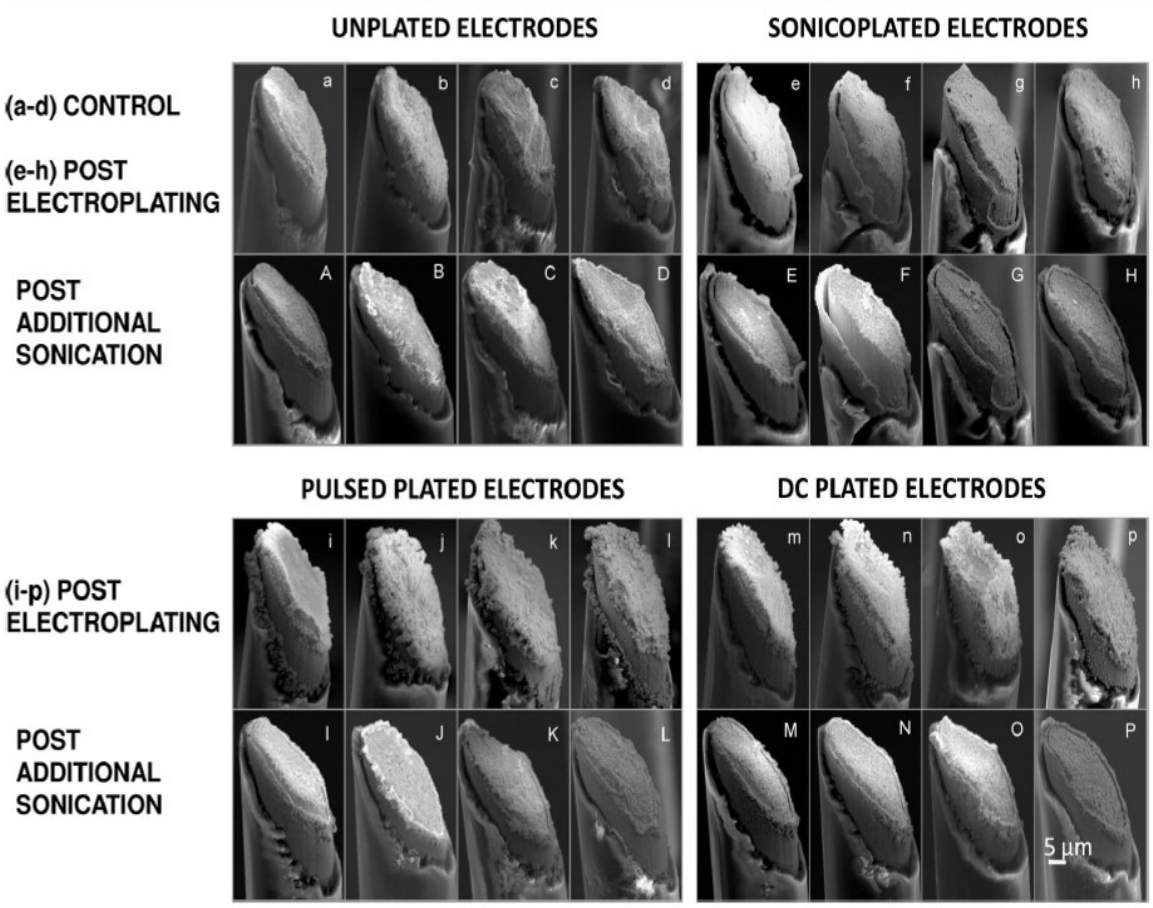

Figure 2.3 SEM images of electroplated microwire electrode tips.
SEM images of microwire electrode tips that are cut at a 45 degree angle. Small letters (starting with (e)) denote images of electrodes whose impedances are brought down to the same level by the three different plating methods. (a-d) unplated electrodes (e-f) sonicoplated electrodes (i-l) pulsed plated electrodes (m-p) DC plated electrodes. Capital letters denote SEM images of the same electrodes after 60 minutes of ultrasonic agitation in saline. (A-D) unplated electrodes (E-F) sonicoplated electrodes (I-L) pulsed plated electrodes (M-P) DC plated electrodes.

Scanning Electron Microscopy (SEM) was carried out before and after the durability test to see if there was a difference in surface morphology of the Pt black plating formed by the three plating techniques. As seen from Figure 2.3, there was a remarkable difference in the way Pt black plating forms by the three plating techniques. In the sonicoplated electrodes (e-h in Figure.2.3), there is a more uniform, thin layer of plating formed when compared to the pulsed plated (i-l) and the DC plated cases (m-p) where Pt black forms distinct lumps. This is presumably because in the case of sonicoplating, only those Pt black particles that formed strong bonds with either the base metal or with other Pt particles remain attached during the process of plating. Via this nano-scale type of Darwinian selection during sonicoplating (Marrese, 1987), the weaker bonds are broken and the weakly bonded Pt particles leave the plating, forming a more uniform and adherent Pt layer on the base metal. The DC and pulsed plating techniques, on the other hand, presumably allow weak and strong bonds to remain in the plating. This is suggested by the loss of many Pt lumps upon one-hour sonication of the pulsed and DC plated electrodes.

2.3.2 Matching electrode impedance under different plating conditions

We did a number of pilot experiments to come up with an estimate of the time and voltage required for the three plating techniques to undergo a similar reduction in impedance. Table 2.1 reports the values used for this study, showing that the sonicoplating technique requires more time and voltage than the other two plating techniques. Since plating under ultrasonic agitation allows only strong bonds to remain, knocking off weakly bonded Pt particles, it requires more net charge for this method to achieve a similar reduction in impedance.

Table 2.1 Electroplating parameters for achieving same reduction in impedance via three different electroplating techniques.

Treatment	Microwire MEA used in durability test (Tips cut at 45°) Mean Preplating Impedance at 1kHz ~ 37kΩ Mean Postplating Impedance at 1kHz ~ 5kΩ	Microwire MEA used *in vivo* (Tips cut at 90°) Mean Preplating impedance at 1kHz ~ 21kΩ Mean Postplating impedance at 1kHz ~ 1.7kΩ
Sonicoplating	**100 seconds of -2 V DC with the sonicator on**	**200 seconds of -2 V DC with the sonicator on**
Pulsed plating	**15 seconds of -1.5 V, 100 Hz square pulses (50% duty cycle) with the sonicator off**	**170 seconds of -1.5 V, 100 Hz square pulses (50% duty cycle) with the sonicator off**
DC plating	**10 seconds of -1 V DC with the sonicator off**	**100 seconds of -1 V DC with the sonicator off**

2.3.3 Chronic MMEA implantation in vivo

In order to look at the improvements that reducing impedance can have in an actual recording and stimulation experiment and also to look at the durability of Pt black plating in a chronic study, we implanted an electroplated MMEA (according to the method in section 2.2, with no sonication of pulsed or DC plated electrodes) into a rat's hippocampus and followed the impedances over a period of three weeks. As seen from Figure 2.4, the difference in the impedances between the three types of plating was not as noticeable as in our durability test in saline. However, it should be noted that the impedances in an *in vivo* environment are affected by variable factors such as gliosis (Rudge et al. 1989; Polikov et al. 2005) making it difficult to follow the impedance contributions of the electrodes themselves. The impedances on the plated electrodes remained significantly lower than the unplated electrodes at 3 weeks post implantation ($p < 0.001$, t-test). In fact, the sonicoplated electrodes had, on average, lower impedances

than electrodes with other types of plating, throughout the course of three weeks ($p < 0.35$).

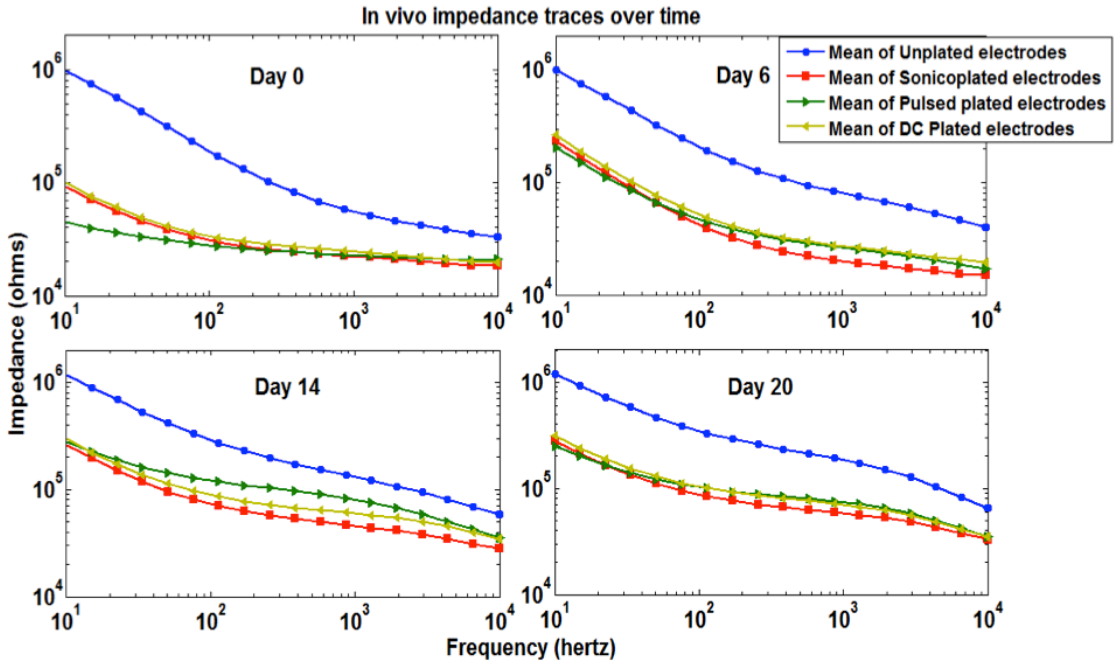

Figure 2.4 Impedance spectra of in vivo implanted microwires over time.
Mean impedance spectra of the three types of plated and unplated electrodes in an *in vivo* MMEA immediately after implantation (A) and after 6 (B), 14 (C) and 20 (D) days.

2.3.4 **Single unit activity recorded on electroplated electrodes**

To confirm that the electroplated Pt black increased the surface area of electrodes without compromising single-unit selectivity (e.g. from an increase in the electrode's physical extent), We looked at five minutes of spontaneous recording on the plated and unplated electrodes. Clustering of spontaneous action potentials recorded on each electrode was performed using Wave_clus (Quiroga et al. 2004). Each type of electroplated electrode recorded normal single unit action potential waveforms similar to

the unplated electrodes indicating that the increase in electrode surface is achieved without losing out on single-unit selectivity (Figure 2.5).

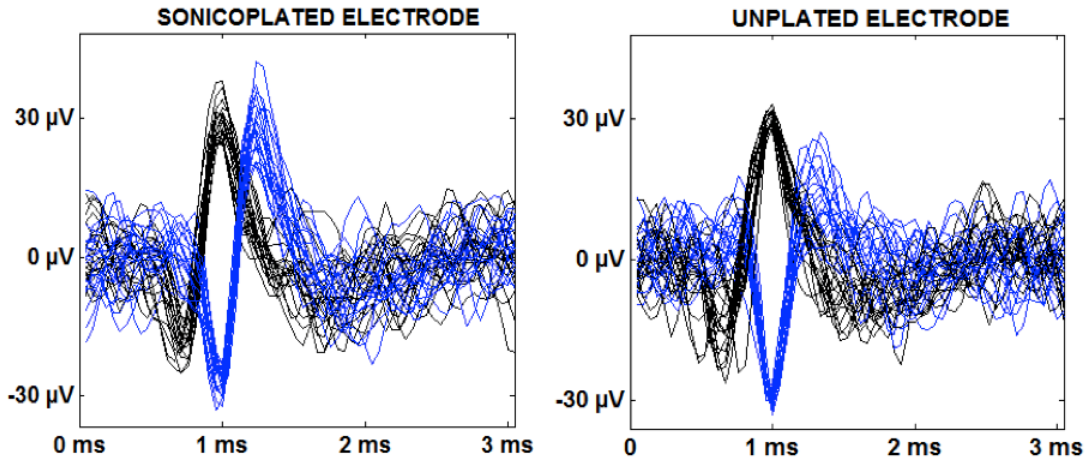

Figure 2.5 Single unit recording on unplated and sonicoplated microwires.
Multiple separable spike waveforms recorded on a single sonicoplated and an unplated electrode in a five-minute spontaneous recording. The blue and black traces show two distinct units with twenty of their action potential waveforms overlaid.

2.3.5 Reduction in stimulation voltage

By Ohm's law, the stimulation voltage required to pass a given current is directly proportional to the electrode impedance. Therefore, lowering impedance would directly translate to lowering the stimulation voltage required to evoke a response. This was verified experimentally in a chronically implanted MMEA as depicted in Figure 2.6. The sonicoplated electrodes had the lowest mean impedance of the three types of plating, and as expected had the maximum reduction in stimulation voltage. For a stimulation current of 10 µA, the unplated electrodes required a mean voltage of about 1.13 V, whereas the

sonicoplated electrodes required a mean voltage less than 0.64 V. This is a 43% reduction in stimulation voltage.

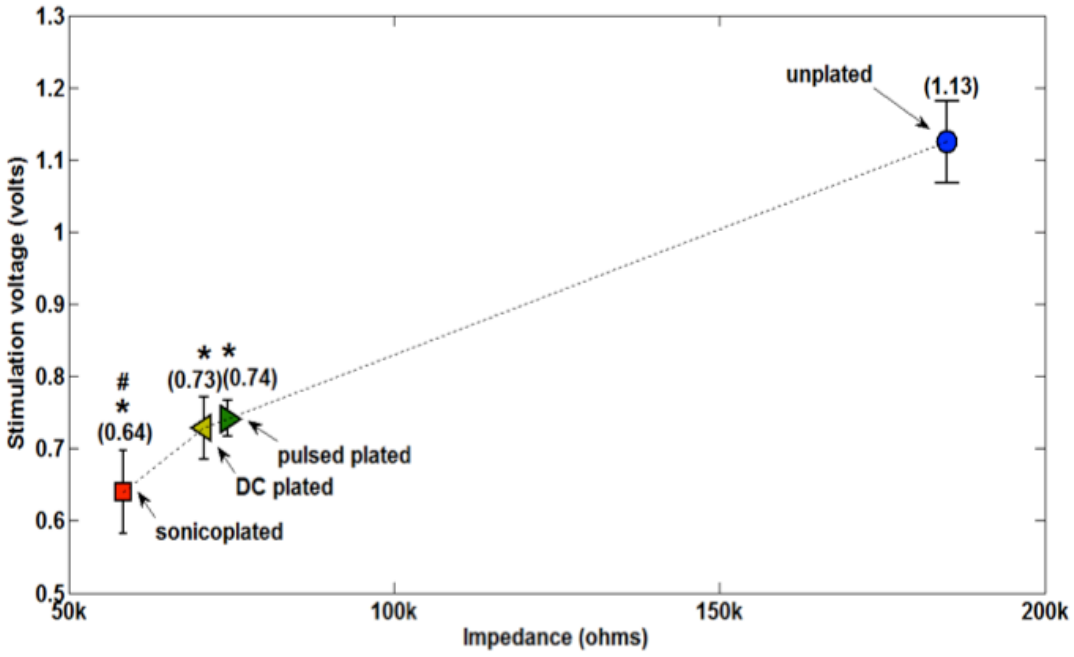

Figure 2.6 Stimulation voltage requirements by the electroplated and unplated microwires.
Stimulation voltages required on electrodes of different impedances to deliver an output current of 10 µA. For a fixed output current set in NeuroRighter, the stimulation voltage was measured on all electrodes on Day 20 post implantation. Data represents mean±SEM on the four electrodes that have the same type of plating. Values in parentheses show the mean. *$p<0.003$ compared with unplated electrodes; #$p<0.21$ compared with pulsed plated and DC plated electrodes.

2.3.6 Reduction of stimulation artifacts

Extracellular electrical stimuli (~1 V) are typically 5 orders of magnitude larger than extracellularly recorded neural signals (~10 µV). This makes recording spikes evoked by stimuli difficult due to large stimulation artifacts. Capacitive charge accumulation between the stimulating electrode and the surrounding tissue impedes or prevents the detection of spikes for the time period for which the stimulation artifacts

persist. In many cases, recording electronics become saturated for tens of milliseconds post stimulation (Rolston et al. 2009). As shown in Figure 2.7, a substantial reduction in the impedance on the stimulating electrode can reduce stimulation artifacts to a great extent. Since the sonicoplated electrodes require the lowest voltage for a 10 μA stimulus, compared to the other types of plating, they have the least stimulation artifact (in terms of amplitude and duration). The amplitudes and durations of the stimulation artifacts for the different types of plated electrodes compared to the unplated electrodes are quantified in Figure 2.8. The durations of the artifacts were reduced to about 8.6 ms on the sonicoplated electrodes compared to 482 ms in the unplated case. This is a 98% reduction in the duration of stimulation artifacts on the sonicoplated electrodes ($p < 0.01$). The amplitude of the artifacts was also reduced by 83% ($p < 0.005$). Similar reductions were observed on the unplated and DC plated electrodes too, but the results were best on the sonicoplated electrodes. These results were obtained *in vivo*, 20 days after implantation.

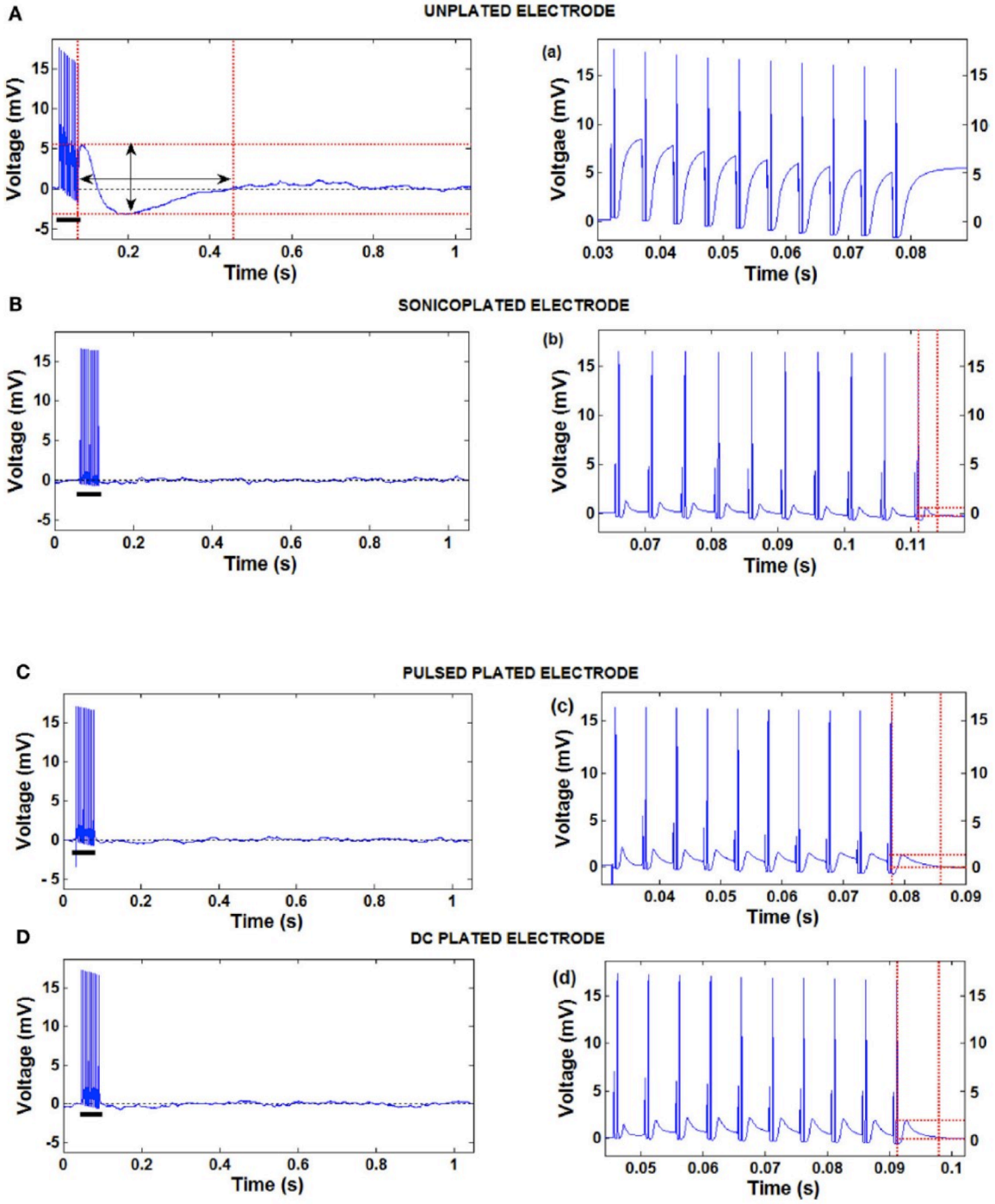
A
UNPLATED ELECTRODE
Voltage (mV)
Time (s)
(a)
Voltgae (mV)
Time (s)
B
SONICOPLATED ELECTRODE
Voltage (mV)
Time (s)
(b)
Voltage (mV)
Time (s)
C
PULSED PLATED ELECTRODE
Voltage (mV)
Time (s)
(c)
Voltage (mV)
Time (s)
D
DC PLATED ELECTRODE
Voltage (mV)
Time (s)
(d)
Voltage (mV)
Time (s)

Figure 2.7 Stimulation artifact waveform on unplated and electroplated microwires.
(Previous page) Stimulation artifacts on electrodes produced by a pulse train of ten 10 µA, 800 µs pulses on the same electrode. (A-D) Stimulation artifacts on one each of the three types of plated and the unplated electrodes. (a-d) Zoomed-in recordings of the high frequency part of the stimulation artifacts of the respective images on the left (shown with black bars). The dotted red lines show the amplitude and duration of the stimulation artifacts. Amplitude of the stimulation artifact was measured as the difference between the local maxima and local minima following the last pulse delivered. Duration was measured as the time between the last pulse delivered and the time for the voltage to return to 1% of the baseline voltage.

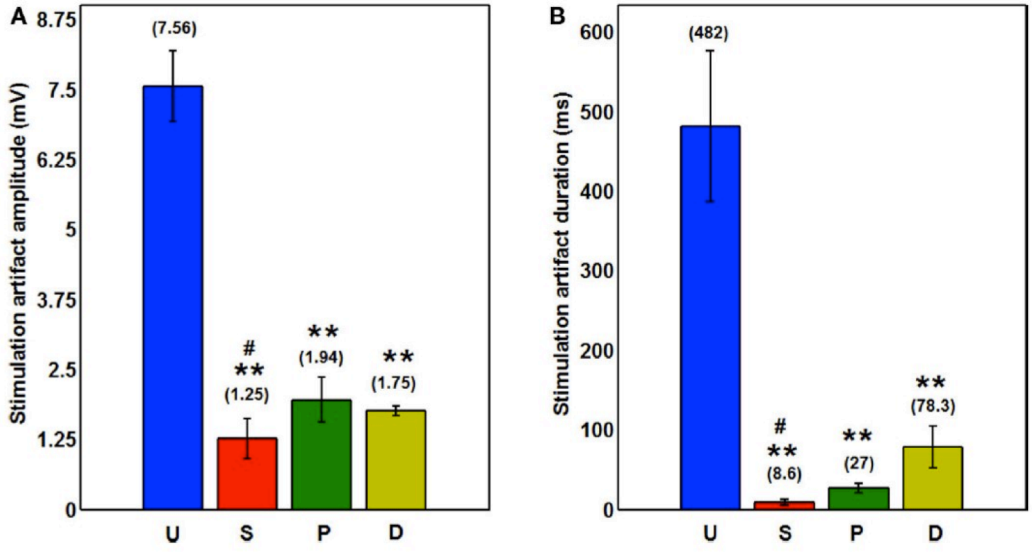

Figure 2.8 Amplitude and duration of stimulation artifact on the three types of electroplated and unplated microwires.
(A) Amplitude of the stimulation artifact on the three types of plated and unplated electrodes after ten 10 µs pulses are delivered. Mean±SEM values on the four electrodes of each type of plating are shown graphically. Values in parentheses show the mean.*$p<0.005$ compared to unplated electrodes; #$p<0.27$ compared to pulsed plated and DC plated electrodes. (B) Duration of the stimulation artifacts with mean in parentheses and error bars showing standard error.*$p<0.01$ compared to unplated electrodes; #$p<0.07$ compared to pulsed plated and sonicoplated electrodes.

2.3.7 Thermal or Johnson-Nyquist noise

Thermal noise is the electronic noise generated by the thermal agitation of the charge carriers (usually electrons) inside an electrical conductor at equilibrium, which happens regardless of any applied voltage and depends on the electrode impedance. Thermal noise is commonly believed to be one of the main contributors to noise in MEA recordings (Heuschkel et al. 2002).

Thermal noise is quantified by the formula $v^2 = 4k_BTZ$ (1)

Where v is the noise amplitude (in units of volts per √Hz), k_B is Boltzmann's constant, T is the temperature, and Z is the impedance. Hence, noise varies with the square root of the impedance of the electrode. So, decreasing the impedance of the electrodes should decrease the thermal noise. We made a spontaneous recording on an unplated electrode in an awake and behaving rat and compared this with recordings on the same electrode made after the animal was euthanized by an injection of euthasol. Our intention was to eliminate all biological sources of noise while keeping the physical environment surrounding the electrode constant. We observed an action-potential free recording on an unplated electrode to have an RMS amplitude of about 120 μV in an awake and behaving animal (The RMS includes frequencies in the 1 Hz to 9 kHz range). We also noticed that movement artifacts don't contribute much to recorded activity.

A continuous recording was made before and after a lethal dose of euthasol. Figure 2.9(A) shows brain activity ceasing ~13 min post-injection. At this time, the total noise recorded on the same unplated electrode had an RMS amplitude of about 9 μV. Because brain activity ceases within thirteen minutes after circulation ceases, it can be

safely assumed that most of the 9 µV noise observed is thermal noise and noise due to electromagnetic interference (EMI).

Hence, thermal noise and EMI together contribute less than 10% to the total noise. We compared noise levels on the three types of plated electrodes and the unplated electrodes in a euthanized animal (Figure 2.9 (B)). As can be seen from the figure, there is no significant difference ($0.3 < p < 0.6$) between the noise levels on the different types of plated and unplated electrodes in a euthanized animal, showing that a decrease in thermal noise levels is not measurable and may be obscured by noise from EMI.

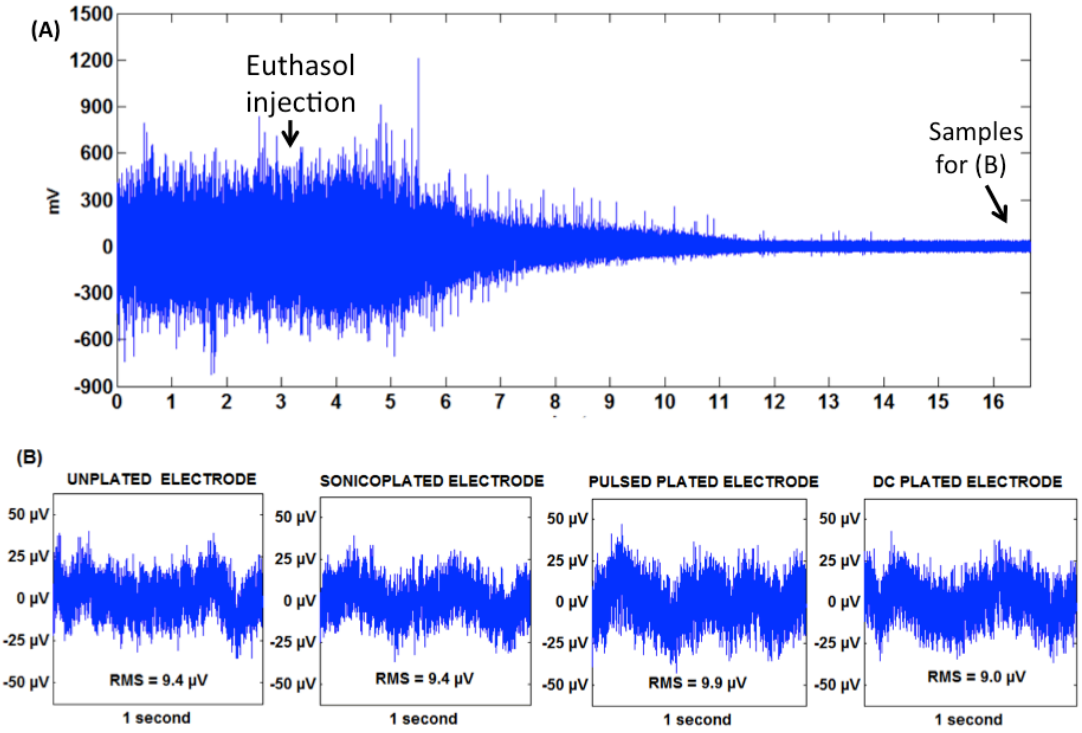

Figure 2.9 Quantifying thermal noise in vivo on electroplated and unplated microwires.
(A) A seventeen minute recording from a rat on an unplated electrode showing the cessation of neural activity after an injection of euthasol. (B) (L-R) recording on an unplated, sonicoplated, pulsed plated and DC plated electrode in a euthanized rat. Mean RMS noise levels on the three types of plated and unplated electrodes are shown in the respective plots.

2.4 Discussion and Conclusion

We have introduced and characterized the technique of sonicoplating (plating under ultrasonic agitation) of Pt black on MMEAs for increased durability compared to traditional plating techniques.

A test for durability was performed by subjecting MMEAs (whose electrode impedances were reduced to the same extent by the sonicoplating method and the traditional DC and pulsed plating methods) to an hour of ultrasonic agitation in a standard saline solution. Sonicoplated electrodes were able to withstand this durability test much better than those plated by the other two methods. Improved durability is important, especially in chronic studies, where it is required to record or stimulate in the same regions of the brain sometimes even over the period of a few months. Even in acute studies, the plating has to be durable enough to withstand the process of being implanted into the brain, penetrating through pia mater and brain tissue. Poor durability has been one of the main reasons why Pt black plated MEAs are seldom used.

Lowering impedance on MMEAs has a direct effect on lowering the required stimulation voltage in current controlled stimulations. This can have two important consequences. Firstly, reduced voltage while stimulating would mean less power is dissipated in the brain in the form of heat; leading to less tissue damage (Power is directly proportional to electrode impedance). This can be of great practical importance for experiments or therapeutic treatments requiring persistent or high-frequency stimulation. Secondly, since stimulation voltage is reduced by this method, stimuli are less likely to exceed the water window that occurs at voltages of above 1 V (at which oxidation of the

electrode begins) or below -0.8 V (at which hydrogen evolution begins) (Rozman et al. 2000) causing the irreversible breakdown of water into O_2 and H_2 gases (Merrill et al. 2005). Hence, lowering impedance will increase the range of currents that one can use without hitting the water window and causing irreversible electrolytic damage in the brain.

Stimulation artifacts result because of charge accumulation in the interface between the electrodes and the surrounding tissue immediately after stimulation. These artifacts can often last 500 ms or even longer (Figure 2.8) and have amplitudes that are about ten times the amplitude of physiological action potentials, making spike detection difficult or even impossible immediately after stimulation. Evoked responses can occur in as little as 1 ms after a stimulation (Wagenaar and Potter 2002; Rolston et al. 2009), hence it is important to reduce the duration of stimulation artifacts to as short as possible. A substantial reduction in the electrode impedance can greatly reduce the problem of stimulation artifacts. Since sonicoplating of Pt black maintains low impedance values for long periods of time, this technique helps get rid of stimulation artifacts, potentially making spike detection possible even a few milliseconds after stimulation on the stimulating electrode (Figure 2.8), and even sooner on non-stimulation electrodes.

Thermal noise or Johnson-Nyquist noise, electromagnetic interference (EMI) from nearby electronics and biological signals of no interest to the investigator are believed to be the main contributors to noise in neural recordings. We have shown that contributions from thermal noise and electromagnetic interference make up less than 10% of the total noise when using electrodes with typical microwire impedances and that no significant

reduction in thermal and EMI noise is observed with lowered impedances. Hence, a reduction in the thermal noise (if any) is obscured by effects from biosignals and EMI.

This is only the first basic analysis of the benefits of sonicoplating for chronic MMEAs. Similar sonicoplating techniques that Potter and Pine developed in the mid 1990s have proven useful for recording or stimulating cultured networks using planar MEAs in vitro (Pancrazio et al. 1998; Maher et al. 1999; Ross et al. 2004). We continued to record action potentials from our longest-living cortical culture (Potter and DeMarse 2001) for well over a year, from MEA electrodes that were sonicoplated. One study demonstrated the efficacy of a sonicoplated polyimide sieve electrode at recording and stimulating re-grown peripheral nerves, weeks after implantation (Ramachandran et al. 2006). However, they did not conduct an analysis of the long-term effects of sonication on the Pt coatings used. It is likely that sonicoplating can be extended to other high-surface-area conductive coatings than Pt black, for example, conductive polymers like PEDOT, which are also electrodeposited (Xiao et al., 2004).

As more closed-loop applications are used, in the laboratory and in the clinic (Arsiero et al. 2007), the ability to both stimulate and record from the same or nearby electrodes becomes more urgent. Sonicoplating can help overcome one hurdle for such stimulate-record applications, the stimulation artifact.

Since it has now proven useful on cyclic voltammetry electrodes, multiwire MEAs, polyimide sieve electrodes, and planar MEAs, it is likely that sonicoplating will be generally applicable to all electrode types in which a durable reduction in impedance is desirable. This may also include macroelectrodes used for deep brain stimulation (Gross et al. 2004).

CHAPTER III

C-FOS IMMUNOHISTOCHEMISTRY STUDY OF SPATIAL ACTIVATION WITH DEEP BRAIN STIMULATION[2]

Microelectrode arrays (wire diameter < 50 μm) were compared to traditional macroelectrodes for Deep Brain Stimulation (DBS). Understanding the neuronal activation volume may help solve some of the mysteries associated with DBS i.e., its mechanisms of action. We used C-fos immunohistochemistry to investigate neuronal activation in the rat hippocampus caused by multi-micro- and macroelectrode stimulation. At ±1 V stimulation at 25 Hz, microelectrodes (33 μm diameter) had a radius of activation of 100 μm, which is 50% of that seen with 150 μm diameter macroelectrode stimulation. Macroelectrodes activated about 5.8 times more neurons than a single microelectrode, but displaced ~20 times more neural tissue. The sphere of influence of stimulating electrodes can be significantly increased by reducing their impedance. By ultrasonic electroplating (sonicoplating) the microelectrodes with platinum to increase their surface area and reduce their impedance by an order of magnitude, the radius of activation increased by 50 μm and more than twice the number of neurons were activated within this increased radius compared to unplated microelectrodes. We suggest that a

[2] Desai, S.A., Gutekunst, C-A., Potter, S.M., Gross, R.E., Deep brain stimulation macroelectrodes compared to multiple microelectrodes in rat hippocampus (in prep.)
Desai, S.A., Gutekunst, C-A., Potter, S.M., Gross, R.E., (2012) Analyzing neuronal activation with macroelectrode vs. microelectrode array stimulation. Conf Proc IEEE Eng Med Biol Soc, 2012.2012:p.4144-7.

new approach to DBS, one that uses multiple high-surface area microelectrodes, may be more therapeutically effective due to increased neuronal activation.

3.1 Introduction

Despite its great success, very little is known about the mechanisms of action of Deep Brain Stimulation (DBS) (McIntyre et al. 2004; Mayberg et al. 2005; Perlmutter and Mink 2006). DBS involves electrically stimulating electrode(s) implanted within deep brain structures like the Subthalamic Nucleus for Parkinson's disease (Kumar et al. 1998; Benabid et al. 2009). In practice, a battery connected to leads is implanted in the chest region of patients below the clavicle and the leads end in electrodes, which are typically 1.27 mm in diameter. Electrodes are implanted within the brain structure that would receive either chronic or intermittent electrical stimulation (Greenberg et al. 2006). Stimulation parameters are fine-tuned depending on initial clinical outcomes (Volkmann et al. 2006). DBS has been the popular alternative in cases where drugs have proven ineffective (Greenberg et al. 2006; Cusin et al. 2010; Anderson et al. 2012). Understanding the spatial extent of influence of electrical stimulation will help solve some of the mysteries associated with DBS.

Multielectrode array (MEA) microstimulation (Desai et al. 2010) may have advantages when compared to single macroelectrode stimulation for several reasons, especially when stimulating complex structures like the hippocampus, which is an important locus in the etiology of temporal lobe epilepsy (Velasco et al. 2001; Velasco et al. 2007). These reasons include: 1) Microelectrodes with diameters of tens of micrometers may be specifically targeted towards particular cell layers, which may not be

possible with a macroelectrode (1.27 mm in diameter) whose diameter is bigger than these targets. 2) With an MEA, one or a few microelectrodes may be simulated at a time, which would enable spatio-temporal patterns of stimulation that are not possible to perform with a single macroelectrode. 3) Tissue damage caused by implanting microelectrodes will be less, compared to macroelectrode implantation. To validate 1) and 2), a systematic analysis of the radius of activation with macroelectrode and microelectrode stimulation would be necessary. Moreover, such an understanding will help in spacing out the individual electrodes in the microelectrode array to achieve desired activation patterns.

Reducing impedance of microelectrodes provides several advantages, like reduced stimulation artifact, reduced voltage requirements for current controlled stimulation, and reduced thermal noise leading to improved signal to noise ratio of neural recording (Ferguson et al. 2009; Desai et al. 2010). Additionally, reducing the impedance would mean injecting more current in voltage controlled stimulation experiments (Desai et al. 2010), which may in turn lead to more effective brain stimulation.

Several simulation studies by Cameron McIntyre (McIntyre et al. 2004; Chaturvedi et al. 2010; Butson et al. 2011), Warren Grill (Grill 1999; Wei and Grill 2009) and others have estimated the electrical fields and activating functions surrounding electrode tracks, but this needs validation in living neuronal tissue. A recent study by Histed, et al., (Histed et al. 2009) used 2-photon calcium imaging to study patterns of cell activation using microelectrodes in the superficial layers of cortex. Although this technique has great temporal and spatial resolution, it cannot be used in deep brain structures like thalamus or hippocampus because brain tissue strongly scatters light and imaging becomes impossible

beyond a depth of 1 mm (Helmchen and Denk 2005). The results from the Histed, et al., study will certainly serve as a guiding point for understanding electrical stimulation interaction with neuronal populations, but cannot be directly translated to other brain regions which have different cytoarchitecture and projection patterns (Histed et al. 2009).

C-fos is an immediate early gene which has been used extensively as a metabolic marker to study seizure pathways and neuroanatomical connections, and to analyze neuronal populations activated by a wide range of stimuli including neuroactive drugs and brain stimulation techniques (Dragunow and Faull 1989; Saryyeva et al. 2011). The Fos protein in conjunction with Jun has been shown to regulate transcription of genes that contain AP-1 binding sites and are involved in cell growth and proliferation (Kerr et al. 1988; Morgan and Curran 1991). Transient induction of C-fos mRNA and protein has been reported in several studies following neuronal excitation (Morgan and Curran 1991). There is also evidence that C-fos is induced in glial cells following neural insult. The mRNA reaches peak values at 30-45 minutes post-stimulation and decays with a half-life of 12 minutes. C-fos protein synthesis follows mRNA expression and it is turned over with a half-life of about 2 hours (Muller et al. 1984). Given these long activation and decay time scales, this technique lacks temporal resolution. However, it provides single-cell spatial resolution and can be used to visualize and count individual neurons activated by electrical stimulation as shown in Saryyevaa et. al., (Saryyeva et al. 2011). In this chapter, we used c-fos immunohistochemistry to study neuronal activation caused by DBS in the dorsal hippocampus using macroelectrode, microelectrode and electroplated microelectrode stimulation.

3.2 Methods

All animal procedures were conducted in accordance with the National Institute of Health Guide for the Care and Use of Laboratory Animals and approved by the Emory University Institutional Animal Care and Use Committee.

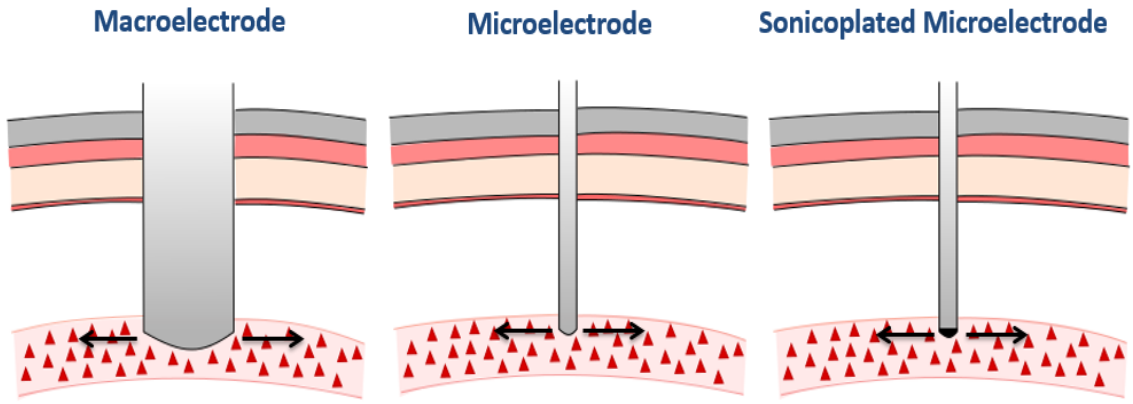

Figure 3.1 Spatial activation with macro, micro and sonicoplated microelectrode array. The above figure depicts the aim of this chapter which is to find the spatial extent of activation in the dorsal hippocampal pyramidal cell layers with macroelectrode, microlectrode and sonicoplated microelectrode stimulation. The figure is a cartoon showing the three types of electrodes implanted through the skull, dura and pia mater into the hippocampal cell layer (not drawn to scale).

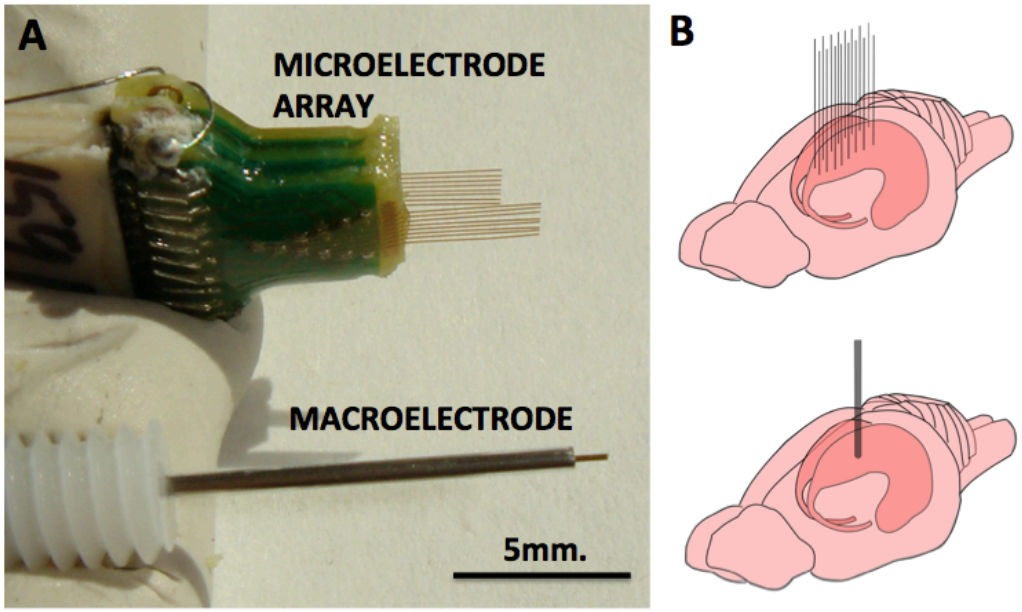

Figure 3.2 Macroelectrode and microelectrode array used in this study.
(A) Pictures of Microelectrode array (MEA) and macroelectrode of the type that were used in this study. Each of the 16 electrodes of the MEA measure 33 µm in diameter and the macroelectrode measures 150 µm (excluding insulation). (B) The approximate implantation positions of the MEA and the macroelectrode in the rodent dorsal hippocampus.

Twenty-four rats were used in this study. Rats were divided into three groups of 8. Rats in group 1 had a single macroelectrode (150 µm diameter, vendor: Plastics One, VA) aimed towards the CA3 cell layer of the dorsal hippocampus. Rats in groups 2 and 3 had a microelectrode array with 16 electrodes measuring 33 µm in diameter, arranged in two rows of 8 electrodes each (vendor: TDT, FL). Row 1 was targeted towards the CA1 cell layer of the dorsal hippocampus and row 2 was targeted towards the CA3 cell layer of the dorsal hippocampus. The difference between groups 2 and 3 is that group 2 had unplated microelectrodes while the microelectrodes in group 3 had their impedances reduced by an order of magnitude by our process of sonicoplating, as described in chapter 2 (Desai et al. 2010). Shown in figure 3.3 are impedance plots of a macroelectrode and microelectrode array before and after electroplating. Since microelectrodes in the MEA

were connected in parallel while being stimulated, it was necessary to make sure that the combined impedance of 15 microelectrodes (with and without electroplating) did not fall below 200 Ω since the maximum current delivering capacity of our setup is ±5 mA and we used ±1 V voltage-controlled stimulation in our study.

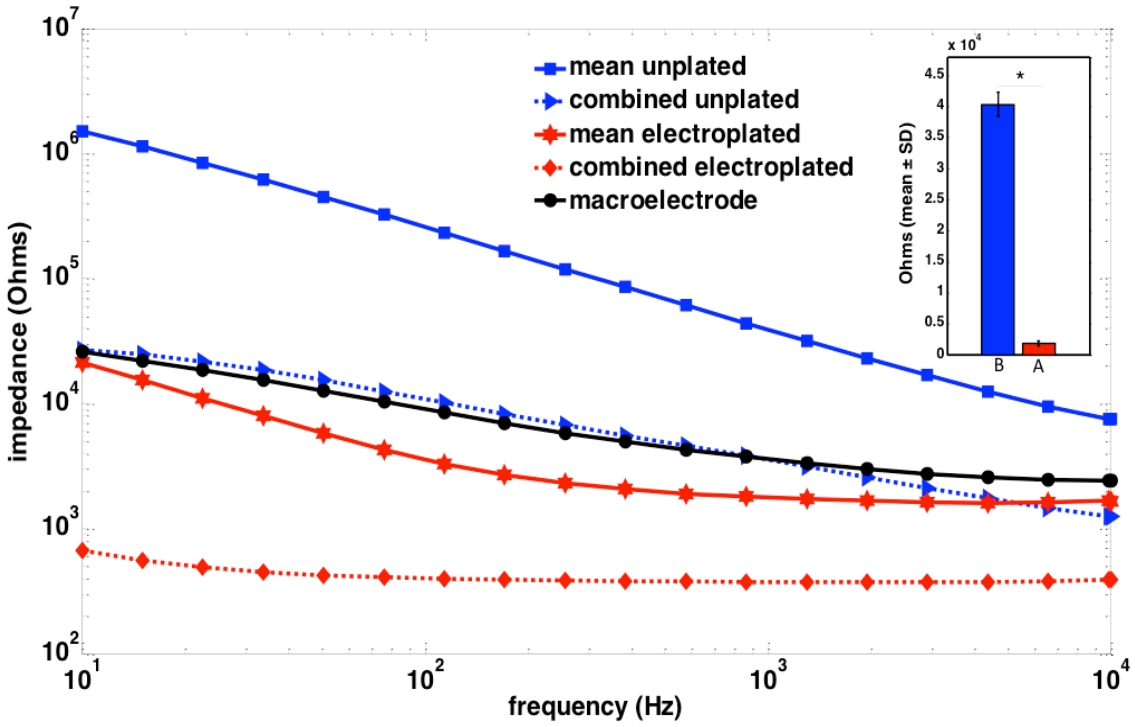

Figure 3.3 Impedance spectroscopy of macroelectrode, microelectrode array and sonicoplated microelectrode array.
Impedance spectra of a single macroelectrode (black), the mean impedance of a plated (red) and an unplated (blue) microelectrode array, and the combined impedance of 15 plated (red, dotted) and unplated (blue, dotted) microelectrodes that were connected in parallel for stimulation. The inset shows a bar graph representation of the mean ± standard deviation of the impedance plots of the 15 microelecrodes before (B; blue) and after (A; red) electroplating at 1 k Hz. * $P<0.05$.

3.2.1 Surgery

Each rat was anesthetized with 1.5-3% inhaled isoflurane before receiving a craniectomy over the right dorsal hippocampus. Each rat was then implanted with either a single macroelectrode (group 1), an unplated microelectrode array (group 2) or a sonicoplated microelectrode array (group 3). Half the rats in each group received four hours of ±1 V, 400 μs per phase, biphasic square pulses at 25 Hz. The remaining rats in each group served as controls and did not receive any stimulation. Electrical stimulation was delivered using our custom-built open-source electrophysiology suite, NeuroRighter (Rolston et al. 2009). In cases where the microelectrode array was stimulated, 25 Hz pulses were delivered synchronously through the electrodes. Both the macroelectrode and the MEA electrodes were insulated except at the tip. After 4 hours of implantation, electrodes were slowly removed from the brain.

3.2.2 Immunohistochemistry

Following electrode (macro, micro or sonicoplated micro) removal from the brain, each rat was deeply anesthetized with a lethal dose of Euthasol (130 mg/kg), injected intraperitoneally, and then perfused intracardially with 0.9% NaCl, followed with 4% paraformaldehyde in 0.1 M phosphate buffered saline at pH 7.2 (PBS) for 15 min at a rate of 20 ml per min. Brains were removed and cryoprotected in 30% sucrose at 4°C, and the region spanning the entire electrode site sectioned in the horizontal plane at 50 μm thickness using a freezing microtome, collected in series of 4 in 4% paraformaldehyde PBS, and rinsed in PBS. To identify the number and type of cells activated by the electrical stimulation, double immunofluorescence labeling for the immediate early gene,

c-Fos (Dragunow and Faull 1989), and the neuronal marker, NeuN (Mullen et al. 1992) was performed. Free-floating sections were rinsed in PBS, blocked in 5% normal donkey serum (NDS) and 0.1% Triton-X100 for 30 min and rinsed in PBS. After rinses in PBS, sections were incubated overnight at 4°C in rabbit anti-C-fos (1:5000; Calbiochem) and mouse anti-NeuN (1:1000; Millipore) in PBS containing 1% NDS. Sections were rinsed in PBS and incubated in Alexa 594-conjugated donkey anti-rabbit (1:1000; Jackson Immunoresearch) and Alexa 488-conjugated donkey anti-mouse (1:1000; Jackson Immunoresearch) in 1% NDS for 1 hr. All sections were additionally counterstained by incubation with the nuclear dye DAPI that labels all cell nuclei. Sections were rinsed in PBS, and then mounted on glass slides with Fluoromont-G mounting medium (SouthernBiotech) for fluorescence microscopy. For each double-label experiment, controls included omission of one or both primary antibodies. Sections were visualized using a Nikon eclipse E400 microscope equipped with 3 fluorescent cubes, a monochrome and color digital camera and Nikon BR software (Nikon Instruments Inc., Melville, NY). For each brain at least 2 series were stained and images corresponding to the tip of the electrodes were used for counting. Figure 3.4 shows an illustration of the experimental procedure.

3.2.3 Cell counting

In the horizontal sections (50 μm in thickness) at the tip of the electrode track, C-Fos+/NeuN+ cells surrounding the track were counted using ImageJ and compared between the various stimulation treatments. NeuN and DAPI staining was used to confirm the location of electrodes. Only those electrodes that landed within the hippocampal cell layers were taken into account for this study, other electrodes were

ignored. Student's t-test was used for analyzing the statistical significance between neuronal activation via the different types of electrodes.

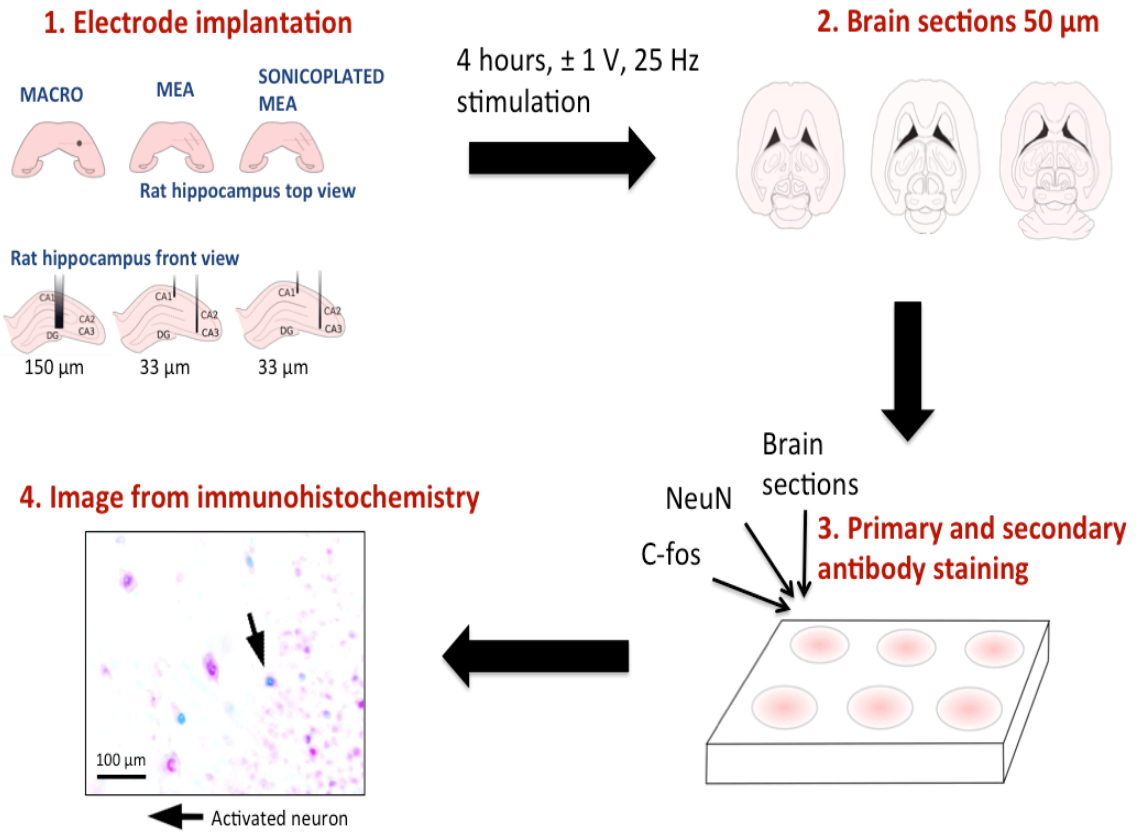

Figure 3.4 Experimental procedure for studying neuronal activation caused by electrical stimulation.

(1) Macroelectrode, microelectrode array or a sonicoplated microelectrode array was targeted towards the dorsal hippocampal pyramidal layer in rodent brain. 4 hours of ± 1 V, 25 Hz, 400 µs/phase biphasic square pulses were delivered with the rats under anesthesia. (2) Rats were euthanized and the brains sections were produced at 50 µm thickness. (3) Primary and secondary antibody staining was performed for c-fos (activity marker) and NeuN (neuronal marker). (4) Fluorescent imaging was performed to identify activated neurons (arrow shows an example).

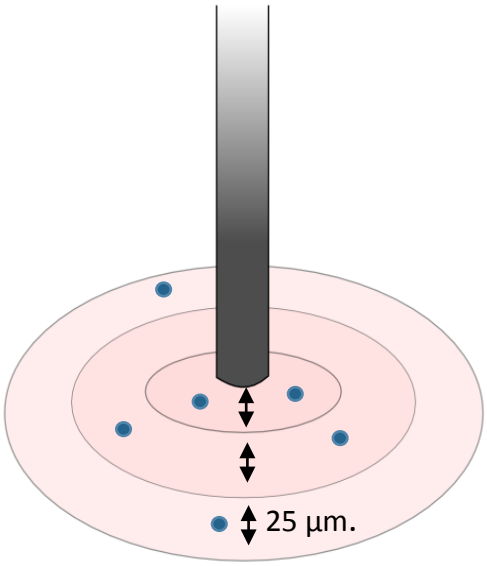

Figure 3.5 C-fos+/NeuN+ cell counting method.
Activated neurons were counted in ImageJ by drawing circles in increments of 25 µm. radius around the electrode tracks.

Microelectrodes used in this study were separated by 175 µm, but even with careful and slow implantation, they tended to deflect ending closer or farther than 175 µm. Circles in increments of 25 µm in radius were drawn around the electrode tracks in each case and the number of C-Fos+/NeuN+ cells were counted within each concentric circle pair in each type of electrode implanted condition (macro, micro, sonicoplated micro; stimulated, unstimulated; Figure 3.5). With microelectrode array implantation, C-Fos+/NeuN+ cells were assigned to the electrode that was closest to the cell. Cell counting was performed until two consecutive circles with no C-fos+/NeuN+ cells were encountered. For computing neuronal activation density, the number of neurons counted within each concentric circle pair was divided by the volume of tissue over which they were counted (h = 50 µm for these sections). Test for significance was performed using Student's t-test.

3.3 Results

3.3.1 Immunohistochemistry staining of electrically stimulated and control sections.

Whether the rats were implanted with macroelectrode, microelectrode array or sonicoplated microelectrode array, electrical stimulation resulted in C-fos expression limited to a region immediately surrounding the electrode track, suggesting that electrical stimulation has a limited radius of activation in the dorsal hippocampus (Figure 3.6). Most of the C-fos+ cells were also NeuN+. Local to the site of implantation, C-fos+ and NeuN- cells were also seen in some of the control and stimulated cases. However, since co-staining for glial cells was not performed, in this dissertation we refrain from discussing such C-fos+/NeuN- cells in more detail.

In rats implanted with a macroelectrode or a microelectrode array that did not undergo any electrical stimulation, no C-fos+/NeuN+ was detected surrounding the electrode tracks (Figure 3.6). These results confirm that it is the electrical stimulation and not the process of electrode implantation itself that is responsible for the increased neuronal C-fos expression seen in the stimulated animals. Dorsal hippocampal sections contralateral to the site of implantation and stimulation did not show C-fos+ in all three cases of stimulation (macro, micro and sonicoplated micro). This suggests that C-fos activation is contained within the hemisphere that received the electrical stimulation

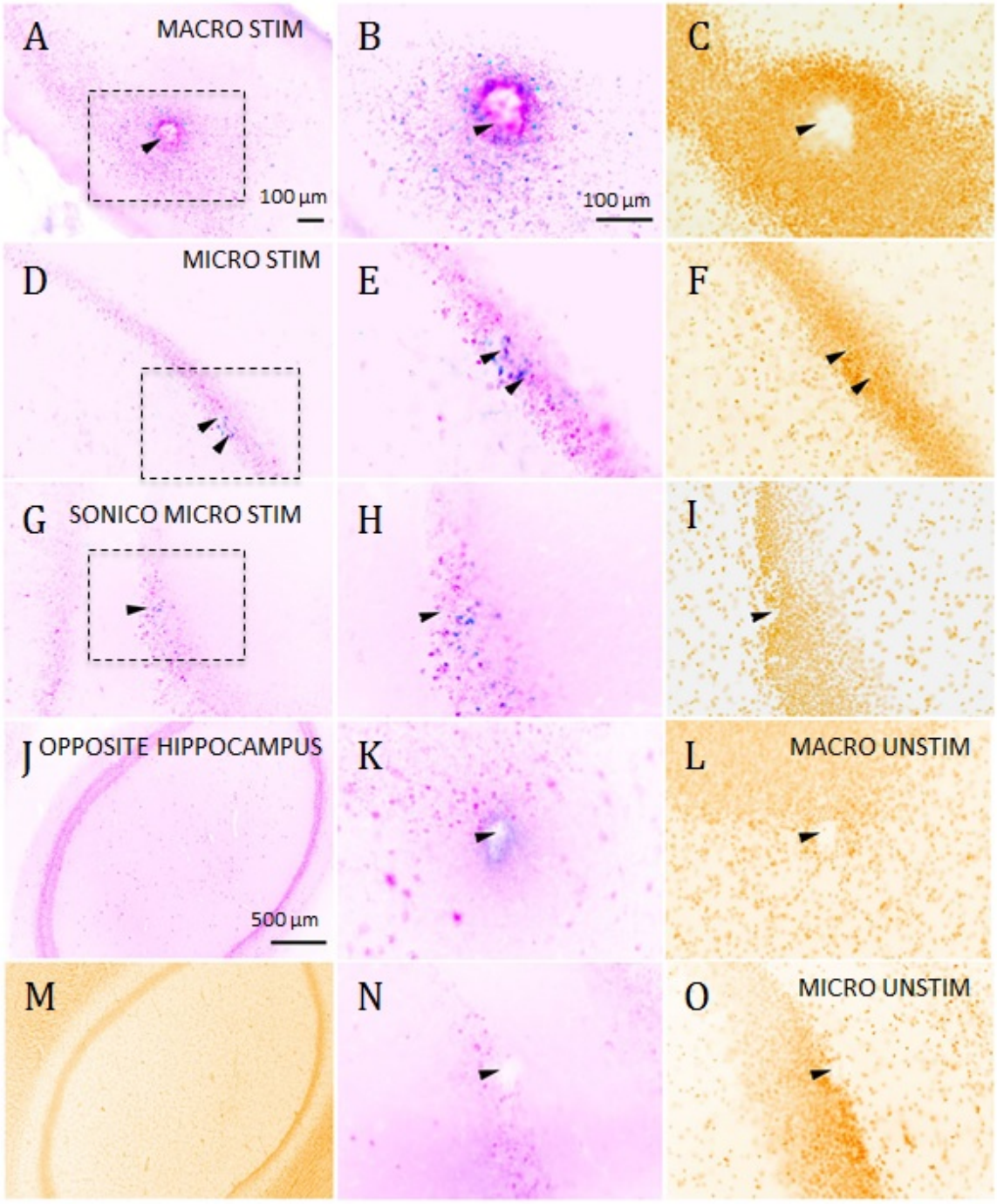

Figure 3.6 Histology results with C-fos+/NeuN+ stained sections.
Representative horizontal sections through the dorsal hippocampus of rats implanted with a macroelectrode (A-C), a microelectrode array (D-F), or a sonicoplated microelectrode array (G-I) stimulated and stained for C-fos (blue), NeuN (pink) and the nuclear marker DAPI (mustard). Macroelectrode and microelectrode implanted dorsal hippocampal sections from rats that did not receive any stimulation are shown in K-L

and N-O respectively. J, M are sections of the dorsal hippocampus contralateral to the site of macrostimulation. The region within the dotted box in A, D and G is shown at higher magnification in B, E and H, and C, F and I. Location of implanted electrodes is indicated with arrows. Scale bar (for all except J, M): 100 µm. J, M Scale bar: 500 µm.

3.3.2 Neuronal activation distribution

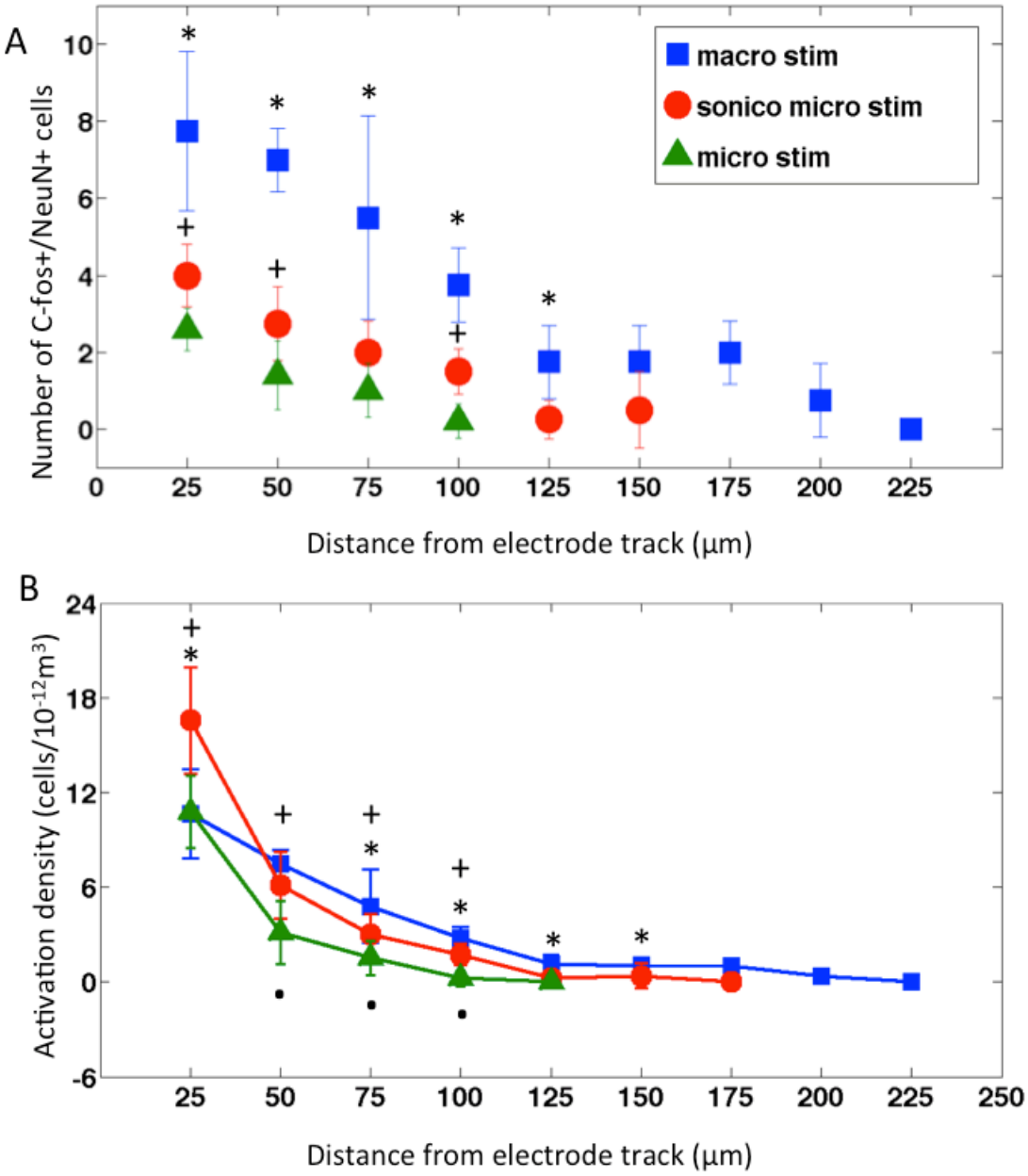

Figure 3.7 Neuronal activation distribution around electrode tracks.
(Previous page) (A) Number of C-fos expressing neurons within concentric circles in 25 μm radius increments surrounding implanted and stimulated macroelectrode (macro; blue squares, n = 4), sonicoplated microelectrode (sonico micro; red circles, n = 4) and unplated microelectrodes (micro; green triangles, n = 4). Inset shows the mean ± SD (standard deviation). * $P<0.05$ between macroelectrode, sonicoplated microelectrode and unplated microelectrode (where data is present). + $P<0.05$ between sonicoplated and unplated microelectrode. (B) Mean ± SD neuronal activation density (number of C-fos+/NeuN+ cells/m^3) with macroelectrode (macro), sonicoplated microelectrode (sonico micro) and microelectrode (micro) stimulation around the electrode tracks; * $P<0.05$ between macroelectrode and sonicoplated microelectrode; + $P<0.05$ between sonicoplated and unplated microelectrode; ˙ $P< 0.05$ between unplated microelectrode and macroelectrode.

Macroelectrodes have the largest activation radius, followed by sonicoplated microelectrodes and then unplated microelectrodes. When stimulated at 25 Hz, ± 1V, for 4 hours, macroelectrodes had a maximum radius of activation of 200 μm. Single microelectrodes on the other hand had a radius of activation of 100 μm. By sonicoplating the microelectrodes and reducing their impedance by an order of magnitude but performing stimulation at the same fixed voltage of ± 1V, the radius of activation was increased to 150 μm (Figure 3.7 A). The control cases, where electrodes were implanted but no stimulation was performed, had no C-fos+/NeuN+ cells (Figure 3.6).

The sonicoplated microelectrodes show higher activation density in the first 25μm concentric cylindrical volume (height 50 μm) around the electrode track, when compared to micro and macro electrodes (Figure 3.7 B). Notice that the microelectrode and sonicoplated microelectrode have high activation densities in the first concentric cylindrical volume surrounding the electrode track and that this rapidly falls with

distance. The macroelectrodes on the other hand have a more linear activation density pattern with increasing distance from electrode track.

3.3.3 Neuronal activation% and total number of neurons activated

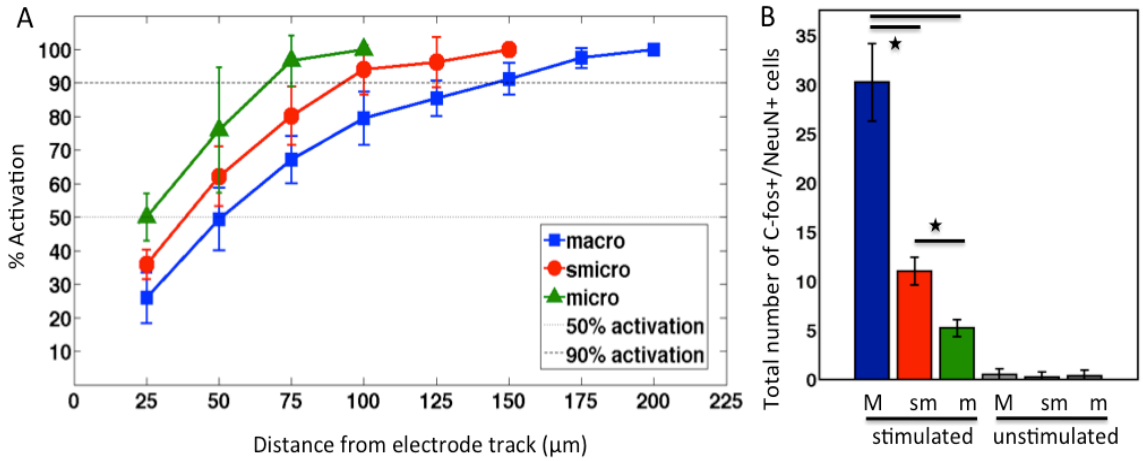

Figure 3.8 Neuronal activation% and total number of neurons activated.
(A) Mean ± SD percentage of neuronal activation in 25 µm radius increments surrounding implanted and stimulated electrodes. (B) Bar graphs showing the mean ± SD number of C-fos+/NeuN+ cells with macroelectrode (M), sonicoplated microelectrode (sm) or unplated microelectrode (m) , with and without stimulation. * P<0.05.

The cumulative activation figure (3.8 A) shows that with macroelectrode stimulation, 50% of activated neurons (AN_{50}) were within a radius of 50.7 µm from the electrode track whereas 90% of activated neurons (AN_{90}) were within a radius of 144.7 µm. For sonicoplated microelectrodes AN_{50} was 38.3 µm AN_{90} was 92.7 µm. For a single microelectrode that was unplated, AN_{50} was 25 µm and AN_{90} was 70 µm.

A single macroelectrode activates 30.25 ± 3.95 neurons surrounding the electrode track in the dorsal hippocampus in one 50 µm brain section, compared to 5.2 ± 0.84 neurons with a single microelectrode. Sonicoplating and reducing the impedance of the

microelectrodes by an order of magnitude resulted in a 52.7% increase in the number of neurons activated (11 ± 1.41). In all the unstimulated controls, the number of C-fos+/NeuN+ was not statistically different from background C-fos activation levels (Figure 3.8 B).

3.3.4 Neuronal activation with microelectode arrays

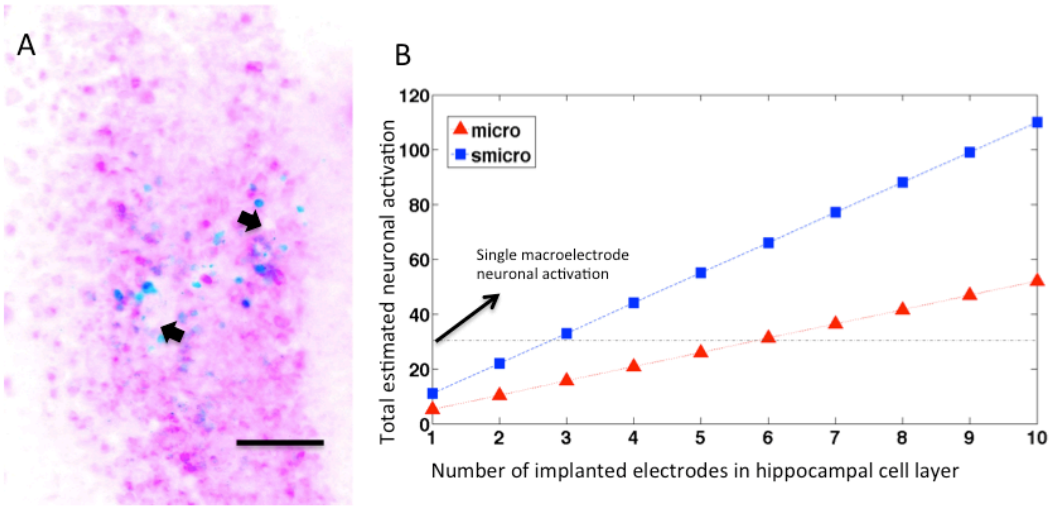

Figure 3.9 Neuronal activation with several microelectrodes.
(A) Representative horizontal section through the dorsal hippocampus of a rat implanted with a microelectrode array. The image shows two microelectrode tracks (depicted with arrows) ending within the hippocampal pyramidal cell layer. The section is stained for C-fos (blue) and NeuN (pink). Scale bar: 100 µm. (B) Estimated neuronal activation in 50 µm brain sections with multiple unplated and sonicoplated microelectrodes (micro, smicro respectively) implanted in the hippocampal cell layer. The horizontal black dotted line shows the mean number of neurons activated by a single macroelectrode for comparison.

In cases where more than one microelectrode from the implanted microelectrode array ended within the pyramidal cell layer of dorsal hippocampus, the number of C-fos+/NeuN+ cells increased linearly with the number of electrodes within the cell layer

(Figure 3.9 A). If we extrapolate these results, it would take fewer than 6, 33-µm diameter unplated microelectrodes (which would occupy 28% volume compared to a macroelectrode) or fewer than 3, 33-µm diameter sonicoplated microelectrodes (13.3% volume compared to macroelectrode) to activate an equal number of neurons as a single macroeletrode (150 µm diameter). Alternatively, with 20 unplated or sonicoplated microelectrodes (which would occupy less volume compared to a single macroelectrode), 3.5 or 7.5 times more neurons would be activated when compared to single macroelectrode.

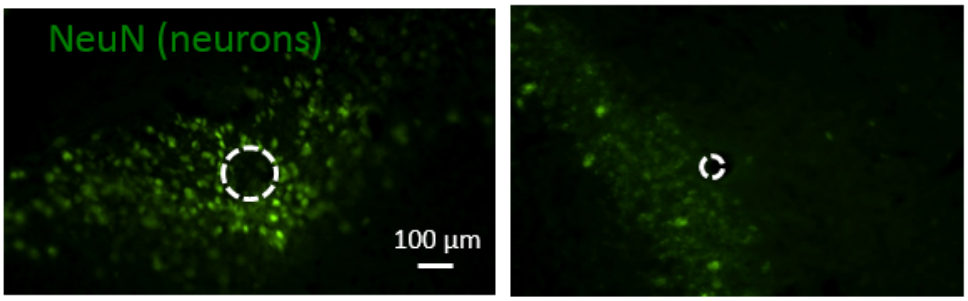

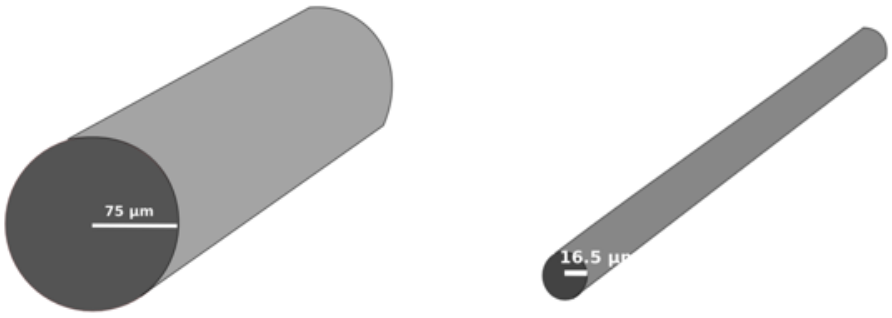

Volume of a macroelectrode (10^{-12} m^3)	Volume of a microelectrode (10^{-12} m^3)
63.617	3.079

Figure 3.10 Tissue damage caused by macro and microelectrode.
(Previous page) NeuN stained images show healthy neurons immediately surrounding the electrode tracks with both macroelectrode and microelectrode implanted in the dorsal hippocampus for 4 hours. Excluding insulation, a single macroelectrode displaces > 20 times the amount of brain tissue compared to a single microelectrode.

3.4 Discussion

Using C-fos immunohistochemistry, we have compared the radius of activation and the activation density following electrical stimulation through a macroelectrode, a microelectrode array and an electroplated microelectrode array in the dorsal hippocampus. Under the conditions tested, a macroelectrode has an activation radius of ~200 μm, a microelectrode has an activation radius of ~100 μm and an electroplated microelectrode has an activation radius of ~150 μm. Thus, a microelectrode array approach could be used when precise stimulation of narrow cell layers, such as the pyramidal cells layer of the CA1 and CA3 regions of the hippocampus is desired. By targeting unplated or electroplated microelectrodes to such target cell layers, stimulation of structures outside these targets can be minimized. The activation radius numbers presented in this dissertation would help in determining the spacing between microelectrodes in the microelectrode array. One method of achieving precise targeting of microelectrodes to specific cell layers would be through the use of movable microelectrodes (Rolston et al. 2011) whose depth can be individually adjusted using microdrives (Keating and Gerstein 2002). Using a macroelectrode whose diameter is larger than these targets would lead to stimulation of structures outside the target, giving rise to undesired side effects (Hariz 2002).

The macroelectrode and the microelectrode array used in this study are from different vendors and are made of different material. The macroelectrode measured 150 μm in diameter and was made of stainless steel with polyimide insulation, and the microelectrodes were made of tungsten with polyimide insulation and the electroplated material was platinum black. These materials have different charge storage capacities (Merrill et al. 2005) and hence may employ different degrees of capacitive vs. faradaic charge transfer mechanisms (Merrill et al. 2005; Cogan 2008). Therefore, the differences seen here between the three stimulation cases (macro, micro, sonicoplated micro) may arise not only due to the differences in their geometry, but also due to differences in the their material makeup. We note here that it is common for macroelectrodes to be built from material such as the stainless steel (Gimsa et al. 2005) that have lower charge storage capacity. Metals such as tungsten, platinum or platinum-iridium have higher charge storage capacities and are the popular choice for making microelectrodes (Stoney et al. 1968). The larger size of the macroelectrode gives it sufficient surface area to inject large currents safely (Mccreery et al. 1990). While we acknowledge that a direct comparison of the effects of increasing merely the size of electrodes on the activation radius required the electrodes to be made of the same material, we note here that a study of the nature performed here would still have high practical relevance, since materials such as platinum-iridium are rarely used to make macroelectrodes for animal studies.

Only one electrical stimulation parameter (± 1V, 400 μs/ phase, biphasic square pulses at 25 Hz) was tested in this work. Since different populations of neurons within the hippocampus have a preference, to fire when stimulated at distinct frequencies (Pike et al. 2000) (pyramidal cells have a lower frequency preference while fast spiking interneurons

prefer higher frequencies), we anticipate that stimulating at higher/lower frequencies and voltages will excite different populations and numbers of neurons (Wagenaar et al. 2004). A study performed in the pedunculopontine nucleus in rat 6-hydroxydopamine (6-OHDA) Parkinson's disease model using C-fos immunohistochemistry showed that 25 Hz stimulation activated more neurons when compared to 130 Hz stimulation (Saryyeva et al. 2011). The results reported here should be seen as a small but valuable step towards understanding the pros and cons associated with using microelectrode arrays vs. macroelectrodes for deep brain stimulation.

In chronic implantation studies, glial encapsulation of the implanted electrode increases the distance of the target neurons from the implanted electrode (Griffith and Humphrey 2006; Bewernick et al. 2010). Although we did not look into the effects of gliosis on the number of neurons activated, this process would cause a steady decrease in neuronal activation over time in voltage controlled stimulation studies due to increased impedance of the tissue-electrode interface (Butson et al. 2006). In chronic implantation experiments, changes in impedance over time should be closely monitored and stimulation parameters should be adjusted to account for this increased impedance to achieve better control of neural activation. Using a closed-loop electrophysiology setup such as NeuroRighter (Newman et al. 2012) will greatly help in automating this process.

As discussed in the results section, the macroelectrode used in this study measuring 150 μm in diameter would cause 20.67 times the tissue damage as a single microelectrode measuring 33 μm in diameter due to implantation (Figure 3.10). For human DBS electrodes, which are typically 1.27 mm in diameter, this ratio would be much larger. By positioning microelectrodes sufficiently close within a given target,

more neurons can be activated than using a single macroelectrode while causing less tissue damage.

CHAPTER IV

OPEN-LOOP ELECTRICAL STIMULATION FOR EPILEPSY[3]

Electrical brain stimulation has shown promise for reducing seizures in drug-resistant epilepsy, but the electrical stimulation parameter space remains largely unexplored. New stimulation parameters, electrode types, stimulation targets, etc. may be more effective in controlling seizures compared to currently available options. In this chapter we have explored a distributed multielectrode microstimulation (DMM) approach where electrical stimulation was delivered through 15 33-µm diameter electrodes implanted at the epileptic focus (dorsal hippocampus) in the rat tetanus toxin model of temporal lobe epilepsy. We have shown that theta (oscillations with center frequency ~7.5 Hz) is abnormal in this animal model during awake behaving conditions. Specifically, theta oscillations are significantly ($P< 10^{-4}$) reduced in amplitude when compared to saline-injected control rats. DMM with biphasic pulses delivered asynchronously on the 15 microelectrodes within the theta range (6-12 Hz/ electrode) was effective in reducing seizures by ~46% in open-loop stimulation studies ($P<0.05$). When theta stimulation (pulsed or sinusoidal) was delivered synchronously on the 15 microelectrodes or through a single macroelectrode, no effects on seizure frequency were

[3] Desai, S.A., Rolston, J.D., Potter, S.M., Gross, R.E., Anti-epileptic effects of asynchronous multielectrode theta microstimulation in a rodent model of temporal lobe epilepsy. (in prep.)

observed. High frequency stimulation (>16.66 Hz/per electrode) had a tendency to increase seizure frequency.

4.1 Introduction

Among the different types of epilepsies, temporal lobe epilepsy, where seizures begin from the temporal lobe of the brain, is the most drug resistant (Engel 1996). Electrical stimulation has shown limited but promising results for controlling seizures in cases where drugs have proven ineffective (Jobst 2010; Rolston et al. 2012). However, the electrical stimulation parameter space, including different spatio-temporal stimulation patterns, remains largely unexplored.

Microelectrode arrays have been used extensively for single/multi-unit recording and stimulation in the field of brain machine interfaces (Lebedev and Nicolelis 2006; O'Doherty et al. 2009; Pais-Vieira et al. 2013). With microelectrode arrays, several spatio-temporal patterns of stimulation can be delivered, which are not possible with the traditional deep brain stimulation macroelectrodes (Wagenaar et al. 2004; Wagenaar et al. 2005). While this technique has not been tested for controlling seizures in epilepsy, multielectrode arrays have provided several insights into the generation and propagation of seizures. For example, Stead et al., (Stead et al. 2010) have used high density microelectrodes to record microseizures that occur more frequency at the epileptic foci and are not picked up on macroelectrodes or even on adjacent microelectrodes spaced less than 1 mm. apart. These microseizures will occasionally evolve into large-scale clinical seizures. Stimulation through microelectrode arrays may have the advantage of

interacting with the epileptic network at such micro scales, preventing microseizures from maturing into disabling clinical seizures.

In support of this hypothesis, it was shown by Wagenaar et al. (Wagenaar et al. 2005) in cultures of cortical neurons that distributed low-frequency microstimulation through 25 microelectrodes on 64-electrode multielectrode arrays is capable of completely eliminating spontaneous culture-wide, seizure-like bursting events. Stimulation through a single microelectrode even at much higher frequencies, analogous to contemporary deep brain stimulation, on the other hand failed to stop the bursting events (Wagenaar et al. 2005). Single unit recording revealed that the distributed microstimulation approach, where stimulation pulses were delivered asynchronously on the 25 microelectrodes, increased tonic background firing rate of the culture, which prevented the bursts from occurring. Adjusting the stimulation rate in a closed-loop fashion based on ongoing culture-wide firing rate achieved better burst control at lower stimulation frequencies (Wagenaar et al. 2005). The effectiveness of the distributed microstimulation approach in reducing spontaneous seizures *in vivo* has not been tested before.

Another aspect of electrical stimulation that is crucial for determining therapy success is stimulation parameter selection, including stimulation frequency, waveform, amplitude and pulse-width. Often in deep brain stimulation, stimulation parameter selection is done empirically, based on trial and error (Moro et al. 2002). While this technique has produced reasonably good disease and symptom control for Parkinson's disease, etc., the mechanisms of action of the electrical stimulation remain largely unknown (Montgomery and Gale 2008). Additionally, undesirable side effects often result (Guehl et al. 2006). Stimulation parameter selection based on a thorough analysis

of the underlying disease state may be crucial for achieving complete disease control with minimal side effects. For applications in epilepsy, one such parameter space that deserves attention is the theta frequency range. Hippocampal theta oscillations (5-10 Hz) (Buzsaki 2002) have been known to have anti-epileptic effects in human patients with epilepsy. For example, fewer seizures occur during REM sleep and wakefulness, conditions during which hippocampal theta is prevalent (Montplaisir et al. 1987; Bland and Colom 1993). Additionally, theta has been reported to be abnormal in some rodent models of epilepsy. Colom et al., (Colom et al. 2006) have shown that theta is reduced in amplitude and shifted towards higher frequencies in the pilocarpine model of epilepsy. When theta was induced through injection of the muscarinic agonist, carbachol into the medial septum or through tail pinch, the number of epileptic spikes was drastically reduced. In another study by Miller et al., (Miller et al. 1994) it was shown that 4-8 Hz electrical stimulation or injection of carbachol at the medial septum stopped pentylenetetrazol induced facial-forelimb seizures within 5 seconds and stopped ictal activity during electrically induced status epilepticus within 10 seconds. Thus, hippocampal theta may represent a physiological state that is resistant to seizures.

For our studies, we chose the intrahippocampal tetanus toxin model of epilepsy, which is a non-lesional model of human temporal lobe epilepsy where treated rats exhibit spontaneous tonic-clonic seizures (Brace et al. 1985). Additionally, the model produces interictal spikes and high frequency oscillations similar to human epilepsy (Bragin et al. 1999; Rolston et al. 2010). Given the high number of spontaneous seizures (about 30 per day), low mortality rate and focal onset of seizures, this is an excellent model for studying the effects of electrical stimulation on focal spontaneous Racine scale 5 seizures

(Racine et al. 1972). Analyzing theta oscillations in a focal epilepsy model on non-anesthetized rats, will add another dimension to the relation between epilepsy and theta oscillations in the brain.

4.2 Methods and materials

All animal procedures were conducted in accordance with the National Institute of Health Guide for the Care and Use of Laboratory Animals and approved by the Emory University Institutional Animal Care and Use Committee. 46 male Sprage Dawley rats (~ 300 grams) were used in these studies.

4.2.1 Surgery

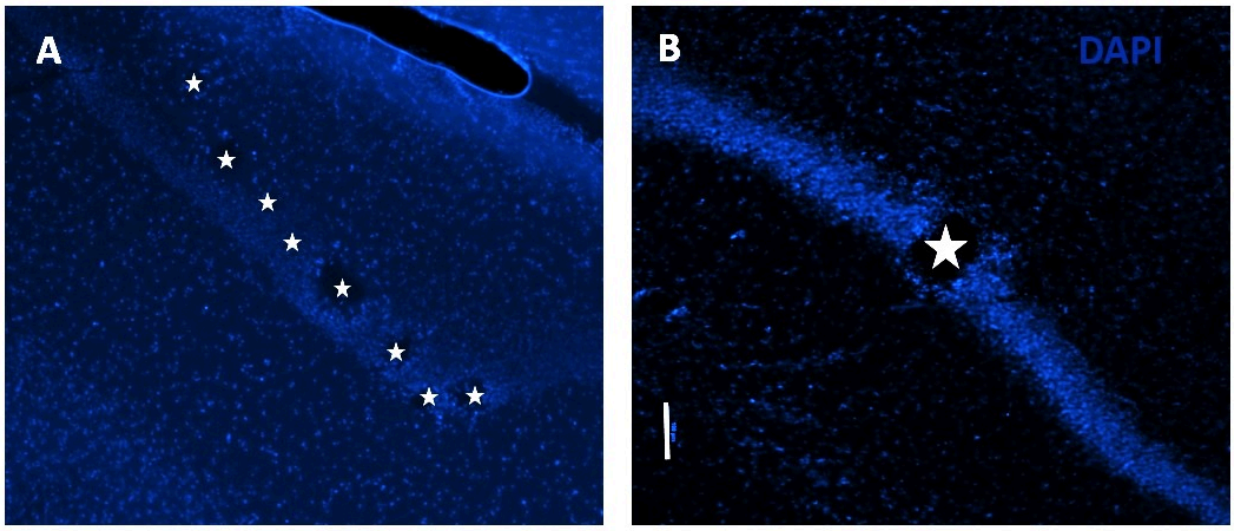

Figure 4.1 DAPI stained horizontal sections through dorsal hippocampus to confirm implantation site.
Tissue damage due to electrode implantation can be seen along the pyramidal cell layer in (A) MEA implanted and (B) macroelectrode implanted cases. Stars mark the electrode locations. Scale bar: 100 µm.

(A) Tetanus toxin/saline injection and microelectrode array implantation surgery:

24 rats underwent this procedure. Rats were anesthetized with 1.5-3% inhaled isoflurane before receiving a craniectomy over the right dorsal hippocampus. Five smaller craniectomies, including one over the cerebellum were made for skull screws. In 16 rats, 25 ng. of tetanus toxin in 500 nl. of sterile PBS was injected into the right dorsal hippocampus at coordinates 3.3 mm AP, 3.2 mm ML, 3.1 mm DV with respect to bregma. In the remaining rats (controls), 500 nl. of sterile PBS was injected at the same coordinates. A freshly pulled glass pipette was used to deliver the injections. Five minutes after the pipette was lowered into the brain, seven injections of tetanus toxin or saline spaced 30 seconds apart were made. All except one tetanus toxin injected rat were implanted with a sonicoplated microelectrode array (Desai et al. 2010) in the right dorsal hippocampus, ipsilateral to the injection site. One tetanus toxin injected rat was implanted with the microelectrode array in the left dorsal hippocampus contralateral to the injection site. Sonicoplating (DC electroplating with platinum black under ultrasonic vibration) was done to reduce impedance of microelectrode arrays by an order of magnitude as discussed in chapter 2 (Desai et al. 2010). Microelectrode arrays (Tucker-Davis Technologies, FL) consisted of 2 rows of 8 electrodes (33 μm diameter) each, with electrodes in the outer row measuring 4 mm. in length and electrodes in the inner row measuring 3 mm. in length. Distance between the two rows was 1 mm and electrodes within the same row were separated by 175 μm. Single unit and LFP recording was performed during implantation of the microelectrode array to ensure positioning of the microelectrodes within the CA1 and CA3 cell layers of the dorsal hippocampus. The skull screw over the cerebellum served as reference for recorded data and the remaining

skull screws tied together served as ground for stimulation. The craniectomy was closed with dental acrylic and rats were allowed to rest for a week. 7-10 days after surgery, tetanus toxin injected rats started exhibiting spontaneous Racine scale 5 seizures. Saline injected controls exhibited no seizures.

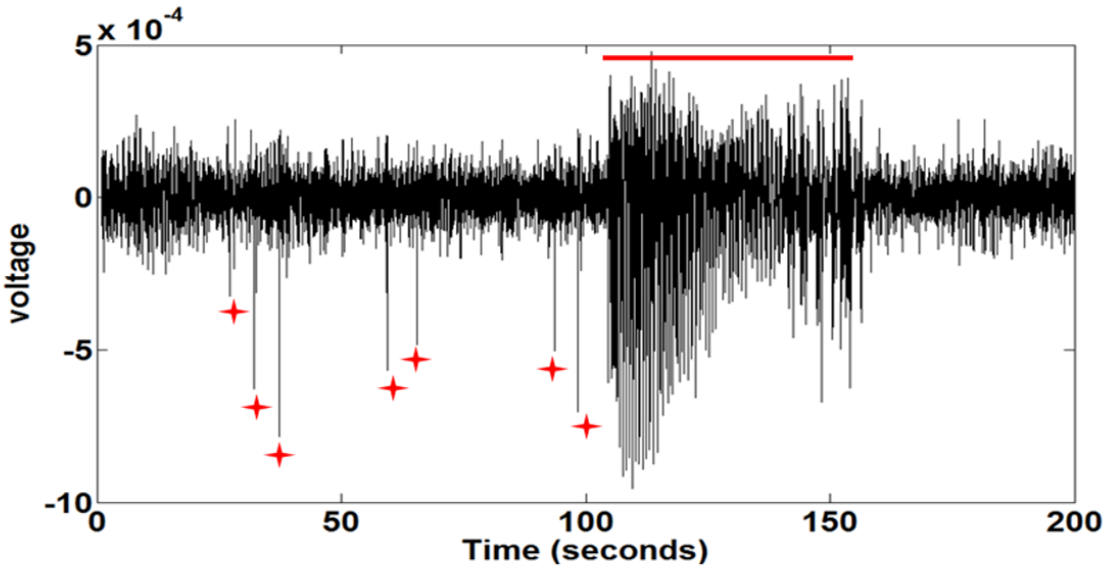

Figure 4.2 Seizures and interictal spikes in the tetanus toxin model of temporal lobe epilepsy.
A typical seizure (indicated by red bar), and interictal spikes (indicated by red plus symbols) recorded from the tetanus toxin model of temporal lobe epilepsy.

(B) Tetanus toxin injection and macroelectrode implantation surgery:

6 rats underwent this procedure. Rats were anesthetized, tetanus toxin was injected and skull screws were drilled exactly as described in the surgery section above (A). However, in this group a single macroelectrode (Plastics One, VA) measuring 150 µm. in diameter targeted towards the CA3 of the right dorsal hippocampus was

implanted instead of the microelectrode array. Procedure for closing the craniectomy, rest and recovery periods were similar to (A).

(C) Tetanus toxin/saline injection surgery:

16 rats underwent this procedure. Anesthesia and injection steps were the same as in Surgery section (A). One very small craniectomy was made over the right dorsal hippocampus pertaining to the injection coordinates, half the rats received tetanus toxin injection while the other half received saline injection. The scalp was stapled to close the craniectomy and rats were allowed to rest for one month. Between days 7-10 post surgery, observations were made while rats remained in their home cages to ensure expected development of seizures in the tetanus toxin injected rats. Rats in this group were used only for the Morris water maze spatial memory task, which began one month post-surgery.

4.2.2 Recording and stimulation studies

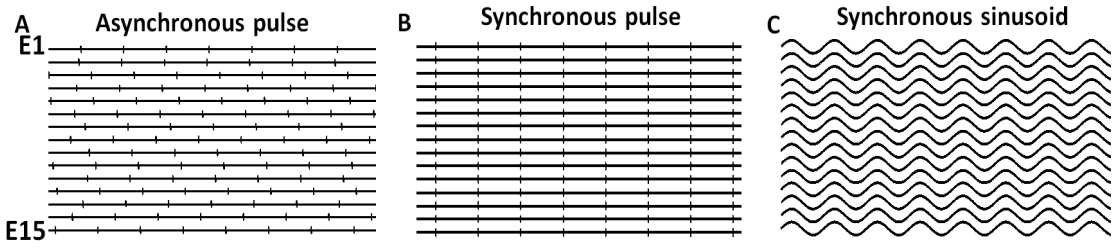

Figure 4.3 Three different stimulation protocols tested through the microelectrode array.

(A) Asynchronous pulse: Pulses are out of phase on the 15 electrodes. (B) Synchronous pulse: Pulses are delivered simultaneously on the 15 electrodes. (C) Synchronous sinusoid: Sinusoidal stimulation delivered in phase on the 15 electrodes. E1-E15: electrode 1 to electrode 15.

Our lab's custom-built open-source multichannel electrophysiology suite, NeuroRighter (Rolston et al. 2009; Rolston et al. 2009; Rolston et al. 2010; Newman et al. 2012) was used for all recording and stimulation studies. Neural data was recorded at 25 kHz. Neural signals in the 500 Hz-9 kHz band were used for analyzing single and multi-unit activity, and those in the 1 Hz - 2 kHz band were used for analyzing local field potentials. Triangle BioSystems International's (TBSI, NC) recording headstage was used for buffering and amplifying neural data by 100X before being sent to NeuroRighter's interface boards for filtering. Commutators (Tucker-Davis Technologies, FL) were used to reduce strain on rats and enabled them to move around freely in Plexiglass chambers during long recording and stimulation sessions.

Three different stimulation protocols were tested through the multielectrode arrays. (1) Asynchronous pulse (2) Synchronous pulse and (3) Synchronous sinusoid (Fig.4.3). Asynchronous stimulation involved distributing ±1 V, 400 μs per phase, square pulses asynchronously over 15 microelectrodes. Figure 4.3 (A) shows one example of asynchronous stimulation where square pulses at an aggregate frequency X, are distributed over 15 microelectrodes such that each microelectrode receives (X/15) Hz stimulation.

The electrode order for stimulation distribution was chosen randomly for each trial. A custom-built stimulation headstage with a 1:16 multiplexer that interfaces with TBSI's recording headstage was used for performing distributed asynchronous microstimulation. For synchronous pulse and sinusoidal stimulation, square pulses or sinusoidal waves were sent synchronously over 15 microelectrodes (Figure 4.3 (B, C)).

Recording and stimulation sessions began 7-10 days after surgery (except in one MEA implanted rat where recording was performed every day since surgery for one month) corresponding to the time when seizure frequency stabilized in epileptic rats. For each of the stimulation protocols tested, one hour of spontaneous data was recorded before and after 1 hour of stimulation. The one-hour pre-stimulation, stimulation and post-stimulation epochs are denoted as PRE-STIM, STIM and POST-STIM in the rest of this paper. Typically, 2 stimulation protocols selected randomly were tested in a rat per day. Stimulation experiments where performed over 2-4 consecutive days in each rat during the period in which the rats had the most seizures. The order of stimulation protocols tested on any day was chosen randomly. At least 4 and up to 6 rats were tested with each stimulation protocol. Manual monitoring and video recording of data was performed during all experimental sessions. When possible, (during all asynchronous stimulation trials and a few synchronous stimulation trials through microelectrodes) neural data was also recorded.

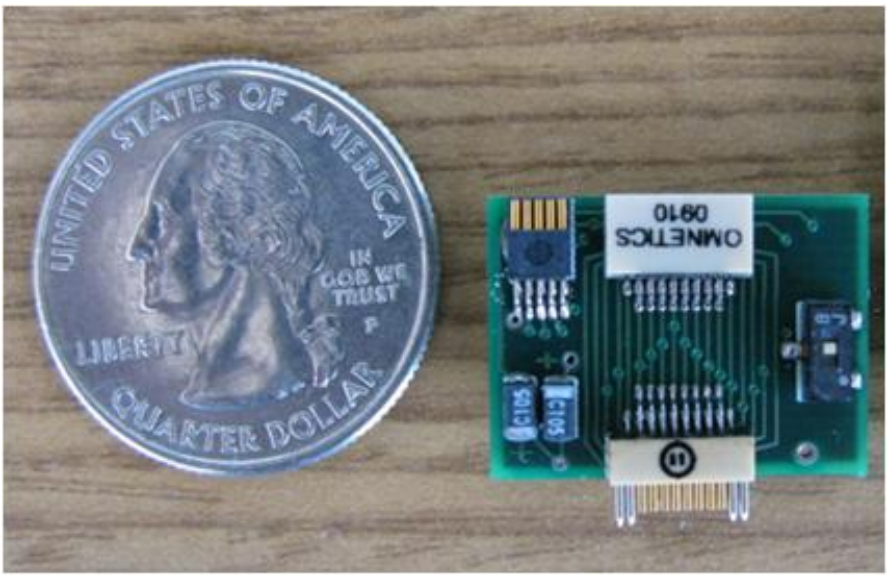

Figure 4.4 Stimulator headstage with multiplexer.
Picture of a headstage that was built to demultiplex the stimulation pulse over 16 microelectrodes in the microelectrode array. This headstage readily interfaces with the recording headstage from TBSI.

4.2.3 Seizure classification and counting

Only Racine scale 4 (rearing) and scale 5 (rearing and falling) seizures (Racine et al. 1972) are taken into account for this study. Seizure classification was performed by multiple blinded observers. Video recording was primarily used for classifying and counting seizures. Where neural data was available, 100% correlation was observed between classified seizures and neural ictal events. The total number of seizures during the stimulation and post-stimulation epochs were normalized with respect to the number of seizures in the pre-stimulation epoch.

4.2.4 Cognition test

Morris water maze training was performed to assess cognitive performance of epileptic rats when compared to controls. 8 epileptic and 8 control rats were tested.

Details of this procedure can be found in (Morris et al. 1982). Briefly, rats were trained to find an invisible escape platform located 1 cm below the water surface in a water-filled tub. Each rat was given 4 trials/day for 4 days with a 10-min intertrial interval. The maximum trial length was 60 seconds, and if rats did not reach the escape platform in the allotted time, they were manually guided to it. Upon reaching the invisible escape platform, rats were left on it for an additional 10 seconds to allow survey of spatial cues in the environment to guide future navigation to the platform. All trials were video-taped and performance was analyzed by means of MazeScan (Clever Sys Inc, VA).

4.2.5 Data analysis and test for significance

MATLAB was used for data analysis. Power spectral densities (PSDs; Figure 4.5) of 30-minute local field potential (LFP) recordings from 8 control and 8 epileptic rats during walking and exploratory activity were derived using inbuilt MATLAB functions. Any seizures (if present) were eliminated from the data that were used for analyzing the PSD. Wave_clus (Quiroga et al. 2004) was used for clustering spontaneous and evoked action potentials (Figure 4). All other data analysis and plots were done using inbuilt MATLAB functions.

The unpaired 2 sample t-test was used for testing statistical differences between derived PSDs from epileptic and control rats. The unpaired 2 sample t-test was also used for testing significance of memory deficit between control and epileptic rats in the Morris water maze task. For testing significance between number of seizures recorded during the PRE-STIM, STIM and POST-STIM epochs, a paired t-test was used.

4.2.6 Immunohistochemistry

After about a month of experimentation, rats were deeply anesthetized with a lethal dose of Euthasol (130 mg/kg) injected intraperitoneally, and then perfused intracardially with 0.9% NaCl, followed with 4% paraformaldehyde in 0.1 M phosphate buffered saline at pH 7.2 (PBS) for 15 min at a rate of 20 ml per min. Brains with electrodes were soaked in 4% paraformaldehyde overnight. The following day, electrodes were removed from the brain and the brains were cryoprotected in 30% sucrose at 4°C, and the region spanning the entire electrode sectioned in the horizontal plane at 50 μm thickness using a freezing microtome, collected in series of 4 in 4% paraformaldehyde PBS, and rinsed in PBS. All sections were counterstained by incubation with the nuclear dye DAPI that labels all cell nuclei. Sections were rinsed with PBS, and then mounted on glass slides with Fluoromont-G mounting medium (SouthernBiotech) for fluorescence microscopy. Sections were visualized using a Nikon eclipse E400 microscope and electrode locations were verified. Figure 4.1 shows example images of sections from microelectrode array and macroelectrode implanted rats.

4.3 Results

4.3.1 Theta oscillations are significantly reduced in tetanus toxin epilepsy.

Tetanus toxin injected epileptic rats showed significantly ($P< 10^{-4}$) reduced theta oscillations Figure 4.5 A, B) compared to saline injected control rats which have a distinct peak between 7-8 Hz. Increase in power at lower frequencies outside the generally accepted theta range for rats (4-12 Hz) with a peak at 2.5 Hz was however

observed in the epileptic rats. One possible explanation for the loss of theta is cell death, which could have resulted from the toxin injection. But single-unit recording and histology confirmed that this was not the case. Several previous studies have also concluded the same (Brace et al. 1985; Jefferys et al. 1992; Lee et al. 1995). To find the point in time when the reduction in theta occurs post tetanus toxin injection, and to study any possible correlations between theta reduction and seizure beginning/frequency, 1 hour LFP recording was performed in one epileptic rat every day over a period of one month (beginning 4 hours post tetanus toxin and microarray electrode implantation surgery to 30 days post-surgery). PSD analysis showed that theta is reduced as soon as 4 hours post-surgery (even before seizures began), and continues to remain reduced through the peak seizure days (days 7-11 post surgery) and up to one-month post injection when seizures have completely stopped (Figure 4.5 C). This observation falls in line with several previous studies, which have reported persistent pro-epileptic changes at the cellular level in the hippocampi of tetanus toxin-injected rats (Brace et al. 1985; Vreugdenhil et al. 2002). However, the long-term effects of tetanus toxin injections on hippocampal oscillations have not been studied before. To check if theta reduction is restricted to the hippocampus where tetanus toxin-injection is administered, one tetanus toxin injected rat was implanted with a sonicoplated MEA in the left dorsal hippocampus, contralateral to the injection site. Reduction in theta in the contralateral hippocampus matched the reduction observed on the ipsilateral side (Figure 4.5 D). Previous studies have shown that intracellular changes post tetanus toxin injection in the dorsal hippocampus happen at the site of injection of tetanus toxin, which develops into the primary seizure focus. But such changes also happen in the contralateral hippocampus,

which often develops into a secondary seizure focus with 27% seizure onset (Jiruska et al. 2010). Such bilateral theta reduction and seizure generation supports our hypothesis that theta is anti-epileptic.

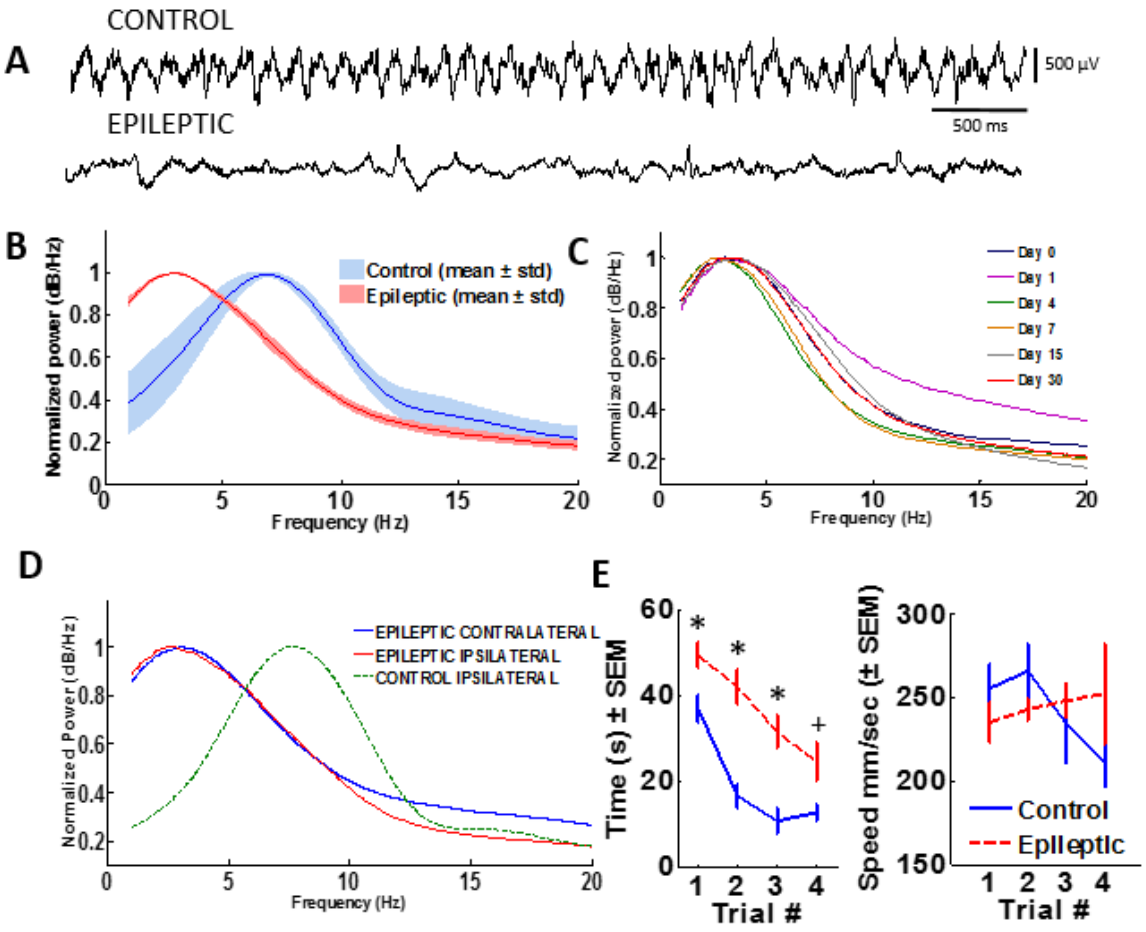

Figure 4.5 Abnormal theta oscillations in the tetanus toxin model of epilepsy.
(A) 5 second LFP traces from a control and epileptic rat during walking and exploring epochs. (B) Mean ± std. of normalized power spectral densities (nPSDs) from 8 control and epileptic rats. (C) nPSD from one epileptic rat recorded from 4 hours post surgery to 30 days post surgery. (D) nPSD from contralateral hippocampus (opposite to tetanus toxin injection site). (E) Morris water maze task plots (Left: Latency to mount platform, *P< 0.05, +P = 0.0537; Right: Swim speed).

In the pilocarpine model of temporal lobe epilepsy, theta was reduced in amplitude but was also shifted towards higher frequencies (controls had a theta peak at

3.8 Hz, while epileptic rats had theta peak at 4.25 Hz) (Colom et al. 2006). It should be noted that however that this observation was made when theta was evoked through tail pinch with rats under anesthesia, while in our study rats were awake and behaving when the hippocampal activity was recorded. Nevertheless, a more drastic theta reduction in the tetanus toxin rats along with the shift in peak toward 2.5 Hz (which is outside the theta range) may represent a more severe state of the same phenomenon.

With intrahippocampal tetanus toxin injections, persistent changes happen at the intracellular level having both pro-epileptic and anti-epileptic components, eventually reaching a balance leading to seizure remission (Jefferys and Williams 1987). Such persistent changes at the intracellular level have been thought to lead to the permanent cognitive impairments that are observed in tetanus toxin epileptic rats. Since theta is crucial for cognitive processing (Winson 1978), our observations on theta deficits outlasting seizures supports this theory and also explains the associated cognitive impairments. 8 epileptic rats were tested on the Morris water maze task 30 days post tetanus toxin injection (when seizures had completely stopped, but theta reduction was still persistent). The epileptic rats showed significant ($P<0.05$) memory deficits when compared to saline injected control rats (Figure 4.5 E). There was no significant difference in swim speed ($P> 0.2$).

This suggests that theta reduction not only represents a brain state that is pro-epileptic but also produces associated cognitive impairments.

4.3.2 Asynchronous theta microstimulation significantly reduces tetanus toxin epilepsy.

Previous studies looked at the effects of septal theta stimulation on epileptic spikes in anesthetized rats or its effects on seizure threshold (Miller et al. 1994; Colom et al. 2006). We tested for the anti-epileptic effects of theta stimulation at the epileptic focus on spontaneously occurring tonic-clonic seizures in awake and behaving rats. The distributed microstimulation approach that was shown to be effective in completely stopping seizure-like bursts *in vitro* (Wagenaar et al. 2005) was used for delivering stimulation. Supporting our observations of a theta peak between 7-8 Hz in saline injected controls (Figure 4.5), others have also reported 7.7 Hz to be the peak of theta in awake behaving rats (Shirvalkar et al. 2010). Square-wave pulses delivered at 7.7 Hz intended to enhance hippocampal theta power during medial septum inactivation, evoked stimulus-locked responses in the hippocampal pyramidal cells (Gray 1972; Scarlett et al. 2004).

Two different stimulation frequency range(s) were tested:

(1) Stimulation at theta peak: Biphasic 400 μs/phase pulses at 7.7 Hz/electrode delivered continuously or intermittently (2 minutes ON/OFF) on 15 microelectrodes for one hour.

(2) Stimulation within theta range: Biphasic 400 μs/phase pulses at a number of frequencies between 6-12 Hz/electrode delivered continuously or intermittently (2 minutes ON/OFF) on 15 microelectrodes for one hour.

In the first case, 7.7 Hz/electrode stimulation (or an aggregate frequency of 115.5 Hz over 15 microelectrodes) was delivered asynchronously as described in the methods

section (Figure 4.3 A) to 15 microelectrodes (8 in CA1 and 7 in CA3). Stimulation was either delivered continuously (denoted by the continuous blue line over STIM in figures 4.6 and 4.7) or intermittently with 2 minutes ON/OFF switching for 1-hour periods (denoted by the dotted blue line). One hour of spontaneous recording was performed before and after the one-hour STIM epochs (i.e., the PRE-STIM and POST-STIM epochs). In the second case, three different frequencies were used (6.28, 9.33, and 12 Hz/electrode) with aggregate frequencies of 94 Hz, 140 Hz or 180 Hz. Stimulation was delivered asynchronously (Figure 4.3 A) on 15 microelectrodes as in (1). A mean of 46% reduction in seizure frequency was observed across all situations ($P<0.05$) compared to baseline spontaneous seizures.

Similar to findings in the *in vitro* multielectrode stimulation study with stimulation delivered on 25 microelectrodes, multi-unit recording obtained on the 16 microelectrodes during theta asynchronous microstimulation showed increased neuronal firing during stimulation in some units. During seizures, the single-unit firing rate recorded on the microelectrodes was higher than the firing rate recorded during spontaneous no-seizure/interictal spike recording, or the firing rate recorded during theta stimulation. The difference between the firing rate during seizure and firing rate during theta stimulation varied on different units and electrodes, but the firing rate during seizures was always higher (Figure 4.6 shows an example). We hypothesize that the asynchronous multielectrode stimulation increases background firing analogous to what was observed in Wagenaar et al., (Wagenaar et al. 2005) maintaining the hippocampus in a state that is anti-epileptic. The mean frequency of evoked activity in single units varied over a wide range and did not seem to correspond with the stimulation frequency. It should however

be noted that the cellular properties of these neurons have changed following insult through tetanus toxin injection, which will affect their firing (Brace et al. 1985).

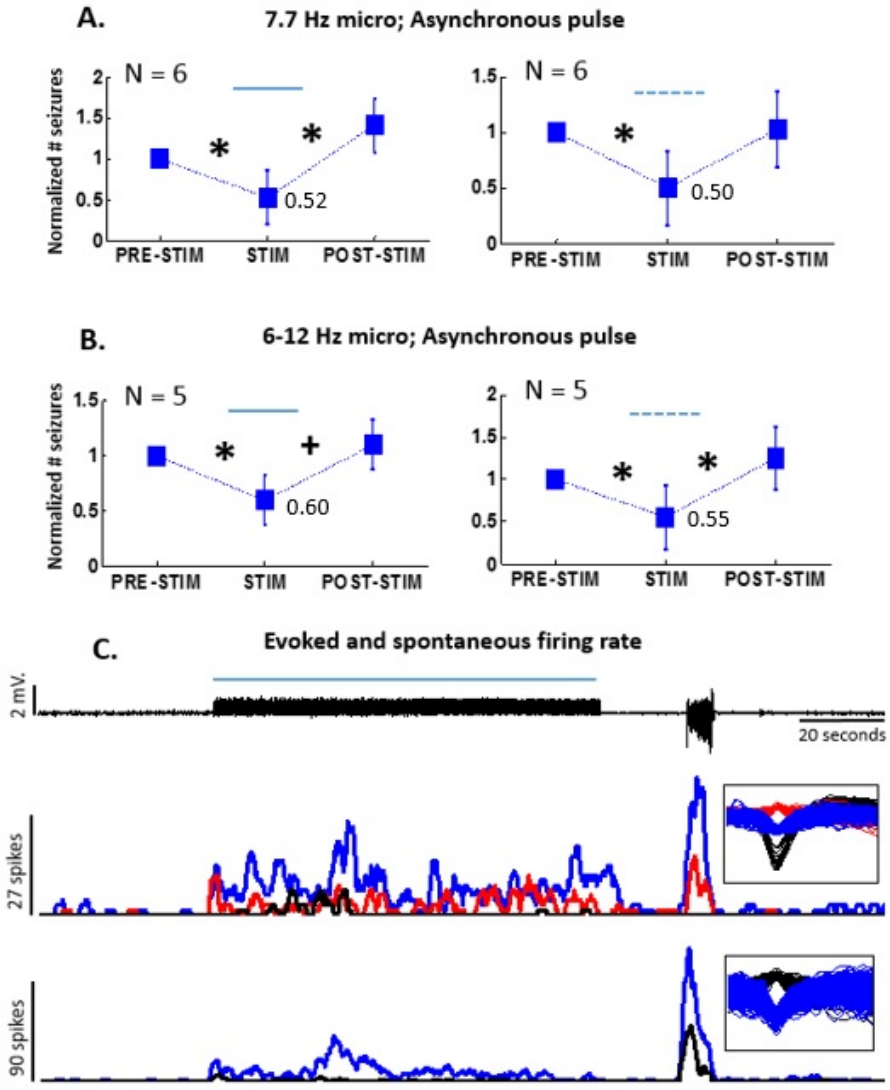

Figure 4.6 Seizure reduction is obtained with asynchronous distributed microstimulation in theta frequency range.

(A) (left) 7.7 Hz continuous stimulation, (right) 7.7 Hz intermittent stimulation. (B) (left) 6-12 Hz continuous stimulation, (right) 6-12 Hz intermittent stimulation are effective in significantly (* $p< 0.05$; + $p<0.1$; Student's t-test) reducing seizures compared to baseline spontaneous seizures. (C) Increased firing rate is observed with the asynchronous distributed 7.7 Hz stimulation during stimulation (indicated by the blue line). In comparison, the firing rate is higher during seizures (an example seizure follows the

stimulation epoch). Example firing rate on two different microelectrodes in the CA3 is shown below the LFP data. Spikes sorted with wave_clus are shown on the right.

We hypothesize that the asynchronous multielectrode stimulation increases background firing analogous to what was observed in Wagenaar et al., (Wagenaar et al. 2005) maintaining the hippocampus in a state that is anti-epileptic. The mean frequency of evoked activity in single units varied over a wide range and did not seem to correspond with the stimulation frequency. It should however be noted that the cellular properties of these neurons have changed following insult through tetanus toxin injection, which will affect their firing (Brace et al. 1985).

4.3.3 Neither theta synchronous stimulation nor asynchronous stimulation at higher frequencies reduced seizures

To test if the combination of pulse frequency (theta) and the distributed, asynchronous nature of the pulses in the dorsal hippocampus is necessary for seizure reduction, three sets of stimulation studies were performed. The motivation and results for each of these test cases is given below.

Is the asynchronous nature of stimulation necessary for seizure reduction?

To answer this question, 7.7 Hz pulses at 400 μs/phase or sinusoidal stimulation was delivered synchronously (in-phase) over 15 33-μm microelectrodes as explained in the methods section (Figure 4.3)

Biphasic 400 μs/phase pulses at 7.7 Hz delivered synchronously (Figure 4.3 B) and continuously or intermittently (2 minutes ON/OFF) on 15 microelectrodes did not reduce seizures. Similarly, sinusoidal 7.7 Hz (Figure 4.3 C) delivered continuously or

intermittently (2 minutes ON/OFF) on 15 microelectrodes resulted in no significant seizure reduction compared to baseline spontaneous recording (Figure 4.7 A)

Is the distributed nature of stimulation necessary for seizure reduction?

For testing this, we used a single macroelectrode for stimulation. Biphasic 400 μs/phase pulses at 7.7 Hz delivered continuously on a single macroelectrode resulted in no significant decrease in seizures compared to seizures during pre or post stim. Sinusoidal 7.7 Hz stimulation delivered continuously on a single macroelectrode also did not reduce seizures (Figure 4.7 B).

Is the theta frequency range crucial for seizure reduction?

For this, asynchronous 400 μs/phase at 16-22 Hz/electrode, 33-46 Hz/ electrode and 53.3 Hz/ electrode were delivered to each of the 15 33-μm microelectrodes. To reduce risk of capacitive charge build up leading to tissue damage, only intermittent stimulation (2 minutes ON/OFF) was performed at these high frequencies. Since stimulation at higher frequencies significantly ($P<0.05$ with data from all three high frequency range pulled together) increased seizures, only 4 rats were tested at these ranges. Data plotted in figure 4.7 C is from these 3 stimulation frequency range(s). 16-22 Hz/electrodes was tested in 2 60-minute sessions in 2 rats, 33-46 Hz/electrode and 53.3 Hz/electrode were each tested in one 60-minute session only. A second rat tested with 33-46 Hz/ electrodes developed too many seizures and had to be sacrificed.

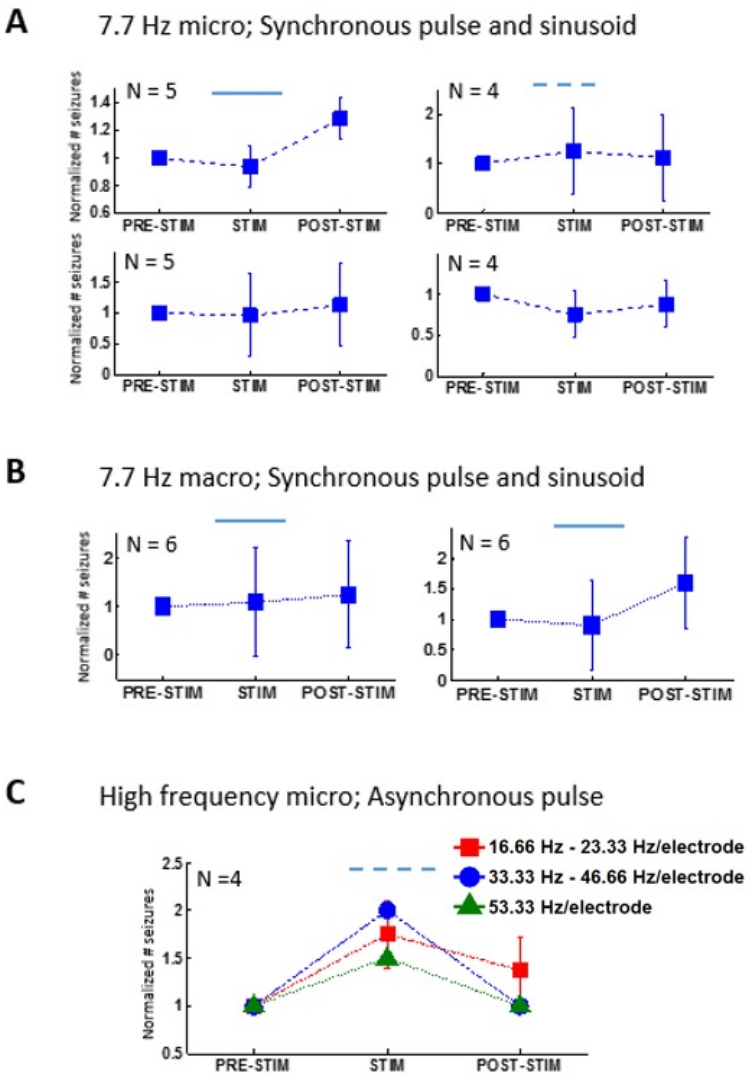

Figure 4.7 Some of the other stimulation protocols tested did not reduce seizures.
(A) Synchronous MEA stimulation: Top row (left) Synchronous 7.7 Hz pulses delivered continuously or (right) intermittently; bottom row (left) Synchronous 7.7 Hz sinusoidal stimulation delivered continuously or (right) intermittently did not reduce seizures significantly. (B) Macroelectrode stimulation. (Left) 7.7 Hz pulses or (right) sinusoidal stimulation did not significantly reduce seizures. (C) Asynchronous stimulation at higher frequencies tended to increase seizure frequency ($P<0.05$).

4.4 Discussion

Using the tetanus toxin model of temporal lobe epilepsy, we have shown that (A) theta oscillations are significantly reduced ($P<10^{-4}$) in the epileptic rats compared to saline injected controls. The reduction in theta is persistent even after seizures have stopped, with epileptic rats displaying associated memory deficits. (B) Theta asynchronous distributed microstimulation delivered unilaterally through a microelectrode array at the seizure focus was effective in significantly ($P<0.05$) reducing seizure by ~46% compared to baseline spontaneous epochs. Single unit recording performed during theta asynchronous stimulation revealed that the firing rate of the network increased during the stimulation epoch compared to baseline firing rate, but still remained lower than the network firing rate during seizures, similar to observations reported in the preceding *in vitro* study (Wagenaar et al. 2005).

Using our current electrophysiology recording setup, single units could not be reliably recorded during both the synchronous stimulation and high frequency asynchronous distributed microstimulation protocols. In future experiments, with changes to stimulation headstage design and with better stimulation artifact rejection, it should be possible to record single unit activity during these stimulation protocols as well. We hypothesize that the asynchronous distributed microstimulation at high frequencies may have increased the firing rate of the hippocampal network above an optimal level, which could have tipped the balance in favor of triggering seizures instead of suppressing them. The theta frequency stimulation range maintained the network firing at a level that resisted seizures similar to (Wagenaar et al. 2005).

The asynchronous and distributed nature of pulses was necessary to reduce seizure frequency in the tetanus toxin-injected epileptic rats. Synchronous theta pulse/sinusoidal stimulation delivered through microelectrodes and theta pulse/sinusoidal stimulation delivered through a single macroelectrode at the epileptic focus was ineffective in reducing seizures. In epilepsy, excessive network synchrony has often been blamed for triggering seizures (Wong et al. 1986). The asynchronous multisite stimulation approach we‘ve taken in this paper might serve to desynchronize local neuronal populations so that fewer seizures are triggered. In support of this hypothesis, it has been shown in a simulation study that a multi-site coordinated reset approach, where a sequence of high frequency stimuli was delivered via different sites, had powerful anti-kindling effects in epilepsy, while low frequency periodic pulse stimulation increased network synchrony and caused kindling (Tass and Majtanik 2006). In a more recent study, the co-ordinated reset approach was shown to be effective in reducing pathological synchronization and improving motor performance in the Parkinsonsian monkey (Tass et al. 2012).

By implanting microelectrode arrays with more than 16 microelectrodes in the dorsal hippocampus, sufficient single units may be recorded from the epileptic network to be used for tuning stimulation parameters in a closed-loop manner. Network firing rate may be continuously controlled to remain within pre-determined limits that are resistant to the evolution of seizures as was done in the *in vitro* study (Wagenaar et al. 2005). Our lab’s Application Programming Interface (API) for NeuroRighter will greatly simplify the process of implementing closed-loop algorithms for such experiments (Newman et al. 2012). Other ictal biomarkers such as evoked high frequency oscillations (Rolston et al. 2010) and microseizures (Stead et al. 2010) may also be used to trigger stimulation on

only a few microelectrodes local to where the biomarkers are recorded, controlling the spread of seizures and minimizing stimulation side effects. Stimulation through several microelectrodes will additionally cover larger volumes of the hippocampus, potentially producing better seizure-reduction outcomes (Chapter 3). Even with tetanus toxin injections administered only in one hippocampus, 27% seizures have been shown to begin on the contralateral hippocampus (Jiruska et al. 2010). An approach where stimulation is performed bilaterally with microelectrodes distributed in both hippocampi may produce better seizure control.

Finally, only a very small subset of all the possible spatio-temporal stimulation patterns through microelectrode arrays have been tested and reported in this chapter. We have highlighted the potential of multi-microelectrode stimulation for applications in epilepsy. Fine-tuning of the stimulation parameters described here, or closed-loop techniques may achieve more effective seizure control.

CHAPTER V

BEHAVIORAL DEFICITS ASSOCIATED WITH TETANUS TOXIN EPILEPSY

5.1 Introduction

In chapter 4, it was shown that tetanus toxin injected epileptic rats have significantly ($P<10^{-4}$) reduced theta oscillations even 30 days after the injection is administered, when spontaneous seizures have completely stopped. It is widely known that hippocampal theta oscillations are crucial for cognitive well being (Lega et al. 2012; Buzsaki and Moser 2013). There is also evidence for depression in patients with theta abnormality (Linkenkaer-Hansen et al. 2005). In this chapter, results of behavior studies where rats are tested in the Morris Water Maze task for assessing spatial memory (Vorhees and Williams 2006) and in the forced swim task or assessing depression are reported (Can et al. 2012). Additionally, preliminary results on theta electrical stimulation on behavior performance are also reported.

Most of the previous studies, which have tested for memory deficits in the tetanus toxin model, have used the radial arm maze task (Brace et al. 1985; Jefferys and Williams 1987). While this method has been used extensively for several years for spatial memory testing, the Morris water maze task has certain advantages including 1) the lack of local cues such as scent and 2) eliminating the need for depriving animals of food and water which is the main incentive in the radial arm maze task (Vorhees and Williams 2006). Rats make good progress in the water maze task, because they want to escape being in the water. Additionally, to the best of our knowledge, no studies have looked at the

effects of tetanus toxin injections in the ventral hippocampus, on memory. It would be very interesting to look at the effects the ventral hippocampal epileptic focus will have spatial memory task performance, since the ventral hippocampus in considered to have minimal contributions to spatial memory performance; hippocampal lesions have been shown to have no effects on memory, unlike lesions to the dorsal hippocampus (Moser et al. 1993; Hock and Bunsey 1998). In this chapter we have compared the effects of ventral and dorsal tetanus toxin injections in the spatial memory task performance.

5.2 Methods

All animal procedures were conducted in accordance with the National Institute of Health Guide for the Care and Use of Laboratory Animals and approved by the Emory University Institutional Animal Care and Use Committee. 26 male Sprage Dawley rats (~ 300 grams) were used in these studies. Six of these 26 rats were used from previous studies. 20 new rats underwent the surgery procedure described below.

5.2.1 Surgery

The surgery procedure for injecting tetanus toxin is similar to the procedure described in the previous chapters. Briefly, rats were anesthetized with isoflurane, the scalp was cut open and a craniectomy was made over the right dorsal hippocampus corresponding to the anterior-posterior and medial-lateral coordinates of the tetanus toxin injection. 8 rats were made epileptic with tetanus toxin injection into the right dorsal hippocampus as before. 4 rats were made epileptic with tetanus toxin injection into the right ventral hippocampus. The remaining 8 rats served as control and were injected with saline (4 received injections in the right dorsal hippocampus and 4 received injections in

the right ventral hippocampus). The scalp was stitched together with sterilized staples to close the craniectomy and rats were allowed to rest and recover for a month in their home cages.

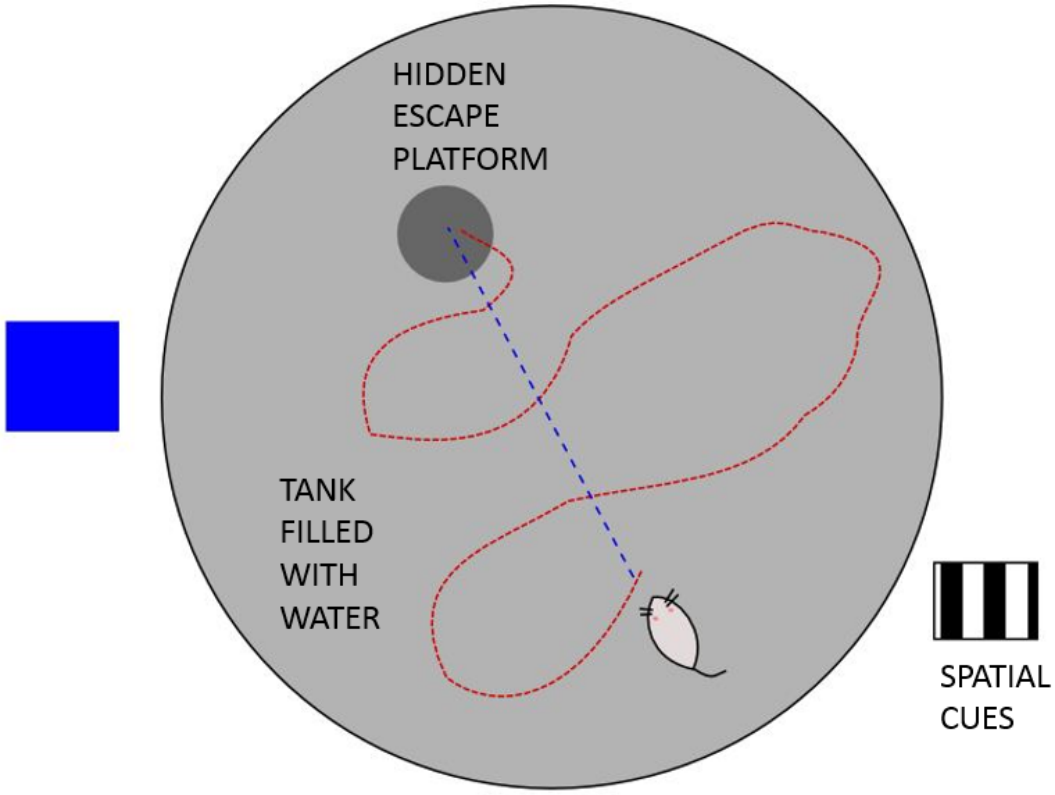

Figure 5.1 The Morris water maze setup.
A circular tank filled with black-paint mixed water is used to hide a black escape platform. The room is filled with spatial cues such as posters, a water sink, etc. Rats are trained to find the escape platform through several trials performed on consecutive days. In the first few attempts, rats usually swim around the tank to find the platform (an example swim path is shown in red), but in subsequent trials normal rats remember the location of the platform and swim directly towards it (swim path shown in blue).

5.2.2 Morris water maze task

The Morris water maze training was performed to assess cognitive performance of epileptic rats when compared to controls. 12 epileptic (8 with injections in dorsal

hippocampus and 4 with injections in ventral hippocampus) and 8 control rats were tested. Details of this procedure can be found in (Morris et al. 1982). Briefly, rats were trained to find an invisible escape platform located 1 cm below the water surface in a water-filled tub (Figure 5.1). Each rat was given 4 trials/day for 4 days with a 10-min inter-trial interval. The maximum trial length was 60 seconds and if rats did not reach the escape platform in the allotted time, they were manually guided to it. Upon reaching the invisible escape platform, rats were left on it for an additional 10 seconds to allow survey of spatial cues in the environment to guide future navigation to the platform. All trials were video-taped and performance was analyzed by means of MazeScan (Clever Sys, Inc).

5.2.3 Forced Swim test

The Forced Swim test was performed to assess depression in rats (Can et al. 2012). 8 epileptic (all with dorsal hippocampal tetanus toxin injection) and 8 control rats were tested. In two sessions separated by 24 hrs., rats were forced to swim in a narrow cylinder from which they cannot escape. The first session, lasting 15 min, was conducted without behavioral recording. This was done to habituate the rats to the test situation, thereby providing a stable, high level of immobile behavior during the 5-min test session. 24 hr. later, rats were forced to swim for 15 min in fresh 25° C water on the first day. On day 2, rats were forced to swim and videotaped for 5-min in 25° C fresh water. In this test, struggling, swimming, and immobile floating behavior was observed, with immobility considered a "depression-like" phenotype. A rat was considered immobile when it was only making movements necessary to remain floating. Subtle movements of feet, tail or head required to maintain the eyes, ears, and nose above the surface of the

water were considered as immobility. The videotapes were scored for latency to immobility and total time spent immobile. The rats were then removed from the water, dried, and returned to their home cage. The cage was placed half-on, half-off a heating pad until the rats dried completely.

5.2.4 Morris Water Maze test with electrical stimulation

6 rats (5 tetanus toxin injected and 1 saline injected control) implanted with a microelectrode array for stimulation and recording experiments in chapter 4 were used in this study too. A month after the tetanus toxin/saline injection and electrode implantation surgery, and experimentation using a few stimulation protocols as explained in Chapter 4, when seizures had completely abated in the epileptic rats, they were tested in the Morris water maze task with the implanted electrodes connected via long wires to the NeuroRighter electrophysiology platform. 2 out of the 5 tetanus toxin injected rats were implanted with a macroelectrode, while 3 had a microelectrode array implanted in the dorsal hippocampus. 3 of these rats (1 tetanus toxin microelectrode array, 1 tetanus toxin macroelectrode and 1 saline macroelectrode) did not receive any electrical stimulation, while the remaining three rats received ± 1 V, 400 μm/phase, biphasic pulses at 7.7 Hz (theta) pulse stimulation through the macroelectrode or synchronously on all electrodes on the microelectrode array. Asynchronous distributed microstimulation (which was effective in reducing seizures) was not performed.

For sealing the electrodes and avoiding any exposed metal contacts from coming in contact with the paint-mixed-water, which has substantial electrical conductivity, the

electrode-headstage junction was filled with water immiscible putty and the wires coming out of the headstage were coated with black insulating tape to provide an additional layer of insulation (Shirvalkar et al. 2010). Several rounds of testing were performed to make sure that the putty completely prevented water from coming in contact within enclosed electronics. To ensure that the headstage was completely covered in putty, rats were lightly anesthetized with isoflurane and were placed in the stereotaxic frame when the application of putty was performed. Once the application of putty was complete, rats were allowed to recover over a period of one hour before behavioral testing in the Morris water maze began.

With rats implanted with electrodes and connected to the NeuroRighter electrophysiology platform (Rolston et al. 2009), the Morris Water Maze protocol was altered to complete testing in one day. Instead of performing 4 test sessions on 4 consecutive days as before, 8 trials were performed on the same day. Each trial lasted a maximum of 60 seconds as before, but the trials were separated only by 2 minutes. The modification reduced stress/burden on rats.

5.3 Results

5.3.1 *Dorsal and ventral tetanus toxin injected rats showed significant memory impairments when compared to saline injected controls.*

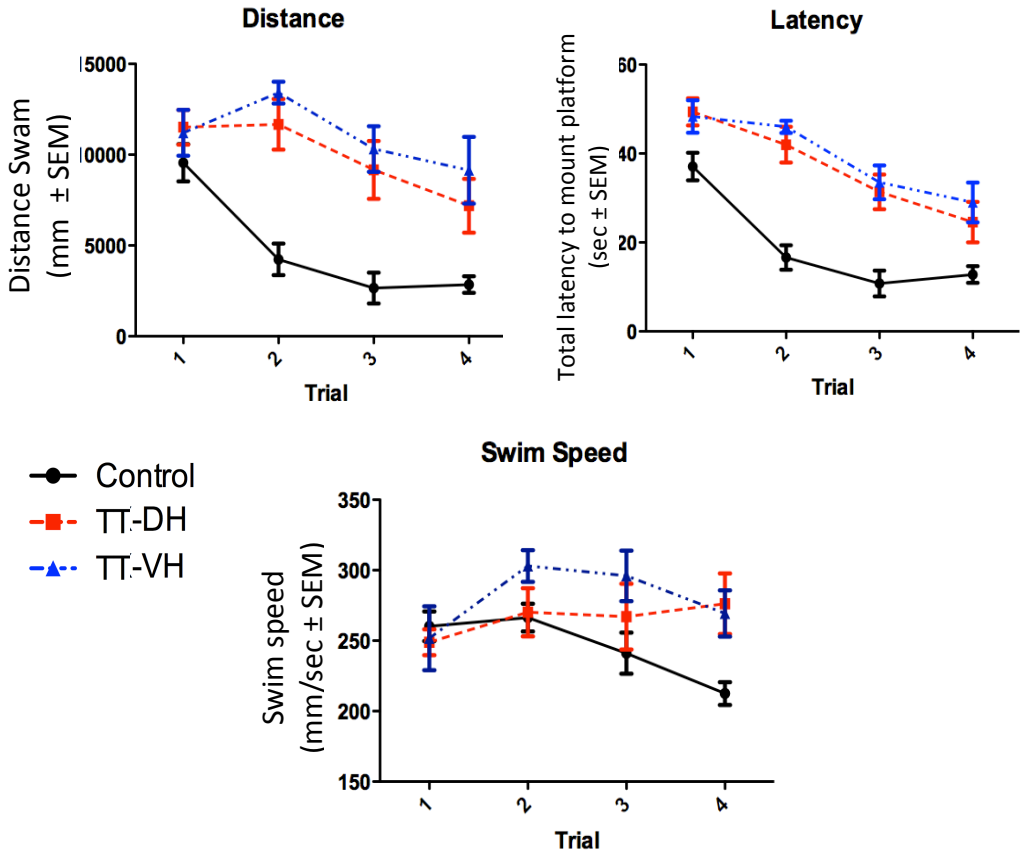

Figure 5.2 Morris water task performance by epileptic and control rats.
Epileptic rats showed significant memory impairment (P<0.05; t-test) compared to saline injected control rats. Top: (Left) Latency to mount escape platform; (Right) Distance swam before mounting escape platform. Bottom: Swim speed.

Both the dorsal and ventral hippocampus tetanus toxin injected epileptic rats groups took significantly (P< 0.05) longer to mount the escape platform compared to saline injected control rats (Figure 5.2). The distance these two tetanus toxin injected groups swam before mounting platform was also significantly longer. The swim speeds in the two epileptic groups was however significantly different from the control group on

the 4th day of testing. The swim speed of the control groups was specifically lower compared to the 1st three days of tests. This might be because of the reduced urgency to 'find' the escape platform since the control rats have already learnt its location. The swim speed in the epileptic rats however remained within comparable levels over all days of testing. No differences were seen between the dorsal-and ventral-injected tetanus toxin injected rats.

Previous studies have shown that the dorsal hippocampus is more involved in cognitive functions including memory compared to the ventral hippocampus, whereas the ventral hippocampus is more involved in functions related to emotions compared to the dorsal (Moser et al. 1993; Shirvalkar et al. 2010). Additionally, dorsal but not ventral hippocampal lesions produce memory deficits in rodents. Since we see similar effects on memory with both dorsal and ventral tetanus toxin injections, we hypothesize that one or both of the following may be true:

(1) The underlying epileptic conditions may have broader-effects (dorsal-ventral hippocampus, bilaterally) and not just at the injection site, impacting normal brain functioning including a loss of theta oscillations. Although we have not recorded theta activity in the dorsal hippocampus with tetanus toxin injected in the ventral, we expect dorsal hippocampal theta to be disrupted as well.

(2) A secondary seizure focus may have developed in the dorsal hippocampus with cell properties being altered (Brace et al. 1985), which may then produce similar effects as injecting the tetanus toxin directly into the dorsal hippocampus.

5.3.2 Epileptic rats did not display significant depression compared to controls

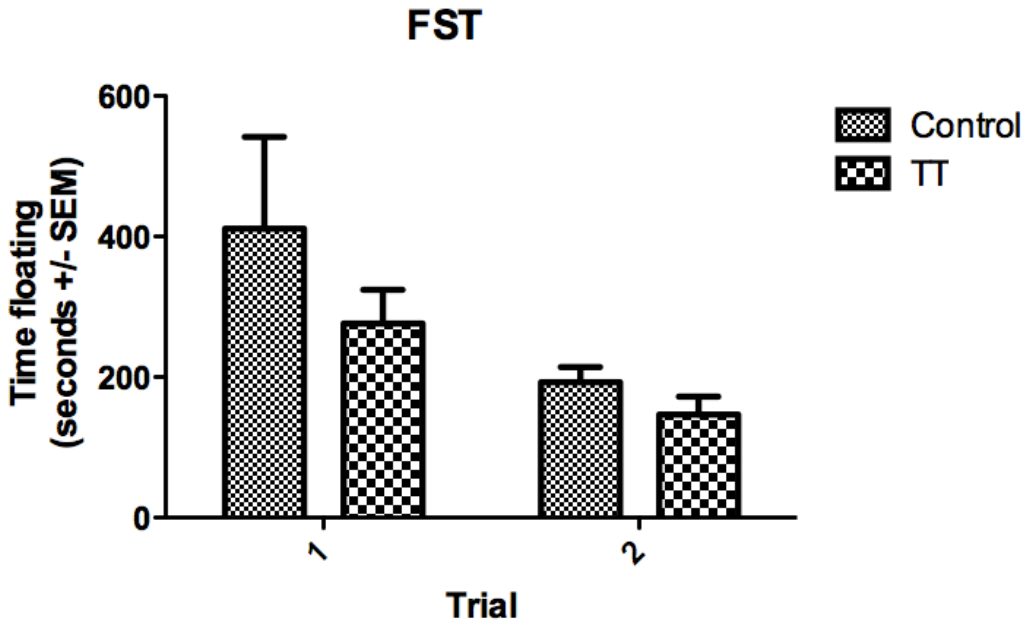

Figure 5.3 Forced swim task performance by epileptic and control rats.
Epileptic rats are not depressed when compared to saline injected controls. In the forced swim test task for depression, the epileptic and saline injected control rats did not show any significant differences.

Although studies have shown that integrity of hippocampal theta is important for preventing depression in human patients, we did not observe any significant differences in tetanus toxin and saline injected controls in the forced swim task. Although not significant, rats in the tetanus toxin injected group floated for less time compared to saline injected controls (Figure 5.3 time spent floating is comparable to depression in the forced swim task).

5.3.3 Theta synchronous microstimulation was ineffective in improving memory in preliminary studies.

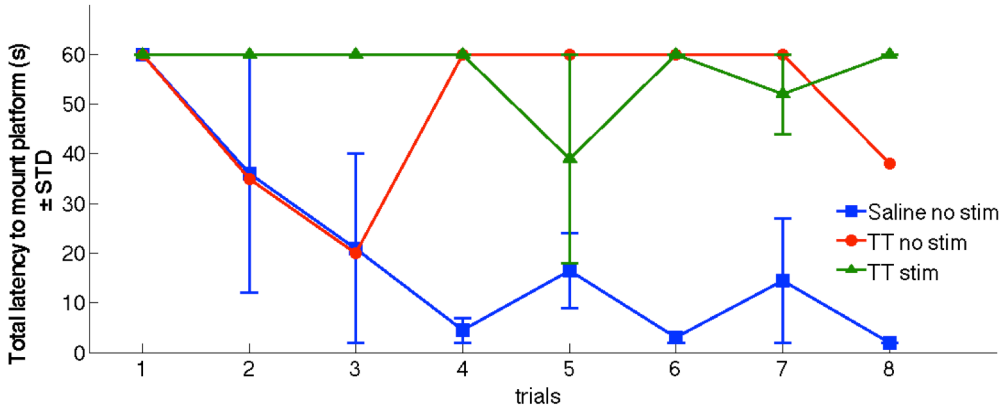

Figure 5.4 Morris water task with electrical stimulation in epileptic rat.
Preliminary studies show that theta synchronous stimulation through microelectrodes in the dorsal hippocampus (n = 2) did not improve memory in the tetanus toxin injected epileptic rats.

One of the 5 epileptic rats tested developed seizures when he was introduced into the water in the Morris water maze test for memory, hence, tests on him were aborted. Another rat lost his headcap during task performance due to strain on the wires connecting the headstage with the NeuroRighter hardware, hence further testing on him had to be aborted as well. In the remaining rats, we found that the new memory test protocol with 8 trials performed on the same day was effective in reproducing difference in memory performance observed between the control and tetanus toxin injected rats. It was also found that theta synchronous microstimulation was not effective in improving memory performance (Figure 5.4).

5.4 Discussion

While several previous studies have shown spatial memory deficits in the tetanus toxin injected rats, most of these studies have been performed on the radial arm maze task (Brace et al. 1985; Jefferys and Williams 1987). Through studies in the Morris water maze task, which has certain advantages over the radial arm maze task including lack of local scent cues and eliminating the need for food and water deprivation in rats, we have reproduced similar results. Additionally, we have shown that tetanus toxins injections in the dorsal and ventral hippocampus have the same effects on spatial memory performance. In the forced swim task for test for depression, the dorsal tetanus toxin rats did not show any significant differences compared to saline injected control rats.

In a modified version of the Morris water maze task where 8 trials were performed on the same day, we were able to reproduce the same results as before, where a saline-injected control rat with an implanted and unstimulated microelectrode array in the dorsal hippocampus successfully learnt the location of the platform, whereas a similarly implanted tetanus toxin injected epileptic rat, did not. Synchronous pulses at 7.7 Hz delivered on 15 microelectrodes in 2 epileptic rats implanted with microelectrode arrays, failed to improve the rats' memory performance in preliminary studies. Due to certain technical difficulties, the asynchronous distributed micro stimulation protocol, which was effective in reducing seizure frequency, (as shown in the previous chapter) could not be performed with the rats in the Morris water maze.

Acknowledgements

We wish to acknowledge help provided by Jason Schroeder of the Emory rodent behavioral core facility in designing and conducting the Morris water maze and Forced swim tasks. We would also like to acknowledge help from Dr.Joseph Manns, Department of Psychology at Emory University for helpful suggestions in setting up the Morris water maze task with electrical stimulation.

CHAPTER VI

CLOSED-LOOP STIMULATION FOR EPILEPSY

6.1 Introduction

Conventional electrical stimulation in DBS is through open-loop electrical stimulation where stimulation is performed continuously regardless of the underlying brain state (Ben-Menachem et al. 1994; Krause et al. 2001; Benabid et al. 2009). That is, whether the patient is asleep, postprandial or exercising, stimulation at the same stimulation parameters is performed. Given the dynamic nature of the brain, it is easy to envision that an adaptive electrical stimulation approach where stimulation is changed based on the brain state, could only be more effective. In addition, closed-loop electrical brain stimulation may have other advantages including: (1) Fewer side effects compared to open-loop stimulation, where the continuous stimulation may lead to habituation and subsequent functional impairment. (2) Extended battery life, since the stimulation engine will run for less time compared to continuous open-loop stimulation.

A primary problem in implementing closed-loop stimulation is the sheer number of combinations of stimulation parameters and control algorithms. There are theoretically an infinite number of stimulation parameters and an infinite number of control algorithms that transform recorded activity (or other biometrics) into changes in these stimulation parameters. Searching this space for the optimal parameters and algorithms is, therefore, incredibly difficult. One approach towards attempting to solve such a comprehensive

problem is breaking it into two sub problems (A) Finding electrical stimulation patterns that are effective in an open-loop approach, and (B) Identifying biomarkers that indicate the onset of the disease state. For example, in epilepsy, the biomarker could be the seizure itself (Sun et al. 2008). The closed-loop algorithm would then involve sending out electrical stimulation identified to be effective in (A) when a disease state biomarker (B) is identified. In a 2013 paper (Little et al. 2013), it was shown that a closed-loop technique based on this approach was more effective by 29% in controlling the symptoms of Parkinson's disease compared to open-loop stimulation, which by itself significantly suppressed symptoms. We took a similar approach for controlling seizures in the tetanus toxin model of temporal lobe epilepsy.

Through open-loop studies performed in the tetanus toxin epileptic rats, the asynchronous distributed microstimulation technique was identified to be effective in suppressing seizures (Chapter 4). The next problem was to identify biomarkers that indicated the disease state. One of the important constraints in biomarker identification is that the bio-signal used for biomarker extraction should be reliable over time. Local field potentials (LFP), which are the summed synaptic activity recorded extracellularly from a population of neurons, can reliably be extracted on both micro and macroelectrodes for several years post-electrode implantation. Unlike chronic single- and multi-unit recording where continued fine adjustments in electrode positioning are often required for reliably picking up good signals, LFP is less affected by exact positioning of electrodes and can be recorded on fixed electrode over several years (Rolston et al. 2011).

Interictal spikes, recorded in the local field potential activity from epileptic brains, have a strong correlation with the presence of seizures in that their presence is often used

to support the diagnosis of epilepsy and sometimes is even used for localizing the epileptogenic area (de Curtis and Avanzini 2001). While interictal spikes herald the onset of seizures, the ictal-interictal relationship remains largely elusive with some studies supporting their protective nature while others support their precipitating relationship to seizures (Avoli et al. 2006; Staley et al. 2011). If a correlation is found between frequency of interictal spiking and ictal events (seizures), interictal spike frequency may be used as a biomarker for turning on electrical stimulation in anticipation of seizures. In the tetanus toxin model of temporal lobe epilepsy, we show that interictal spike frequency reduces by 55% in 80% of the studied seizures in epileptic rats, indicating a protective nature these spikes.

6.2 Methods

For studying the relationship between interictal spikes and seizures, 10 seizures from 10 randomly selected rats were analyzed. The procedure for rendering rats epileptic, implanting microelectrode arrays and performing recording and stimulation is similar to the procedures described in the previous chapters. Briefly, rats were made epileptic with tetanus toxin injection in the right dorsal hippocampus and local field potential (LFP) was recorded using 16-wire microelectrode arrays implanted ipsilateral (same side) to injection site in 9 rats and contralateral (opposite side) to the injection site in one rat. Our lab's custom-built electrophysiology suite, NeuroRighter was used for recording and performing the closed-loop stimulation experiments (Rolston et al. 2010; Newman et al. 2012). Interictal spikes were identified as excursions in the signal >6 times the room mean square (RMS) of the recording.

Closed-loop electrical stimulation was performed on 4 rats made epileptic with tetanus toxin injection and implanted with microelectrode array as described above. In 2 rats, a responsive neurostimulation approach was employed where theta asynchronous distributed microstimulation was delivered on detection of seizures. Multi-electrode stimulation was triggered in response to detected seizures while the rat moved around its cage. To accomplish this, a "line length" measure on each LFP channel, which has been shown to be effective for threshold based seizure detection, was calculated online (Esteller et al. 2004). A line length increment for a single LFP channel is defined as absolute difference between successive samples of the LFP,

$$l_k[t] = |x_k[t] - x_k[t - T_s]|$$

where $x_k[t]$ is the LFP value on the kth channel at time t, and T_s is the LFP sampling period of 500 μs. $l_k[t]$ was passed through a first order averaging filter,

$$L_k^{\tau_{filt}}[t + T_s] = l_k[t] + \exp\left(\frac{-T_s}{\tau_{filt}}\right) \cdot \left(L_k^{\tau_{filt}}[t] - l_k[t]\right)$$

where τ_{filt} is the filter time constant was set to 60 seconds. The threshold for seizure detection was set such that stimulation would be turned on when 3 or more ictal/interictal spikes occurred consecutively (Newman et al. 2012). This did trigger a number of false detects (i.e., had low specificity), but stimulation was triggered 100% times when

seizures occurred (i.e., 100% sensitivity). Upon detection, 15 electrodes, 8 in the CA1 and 7 in CA3 were stimulated sequentially at 115.5 Hz (aggregate frequency) for 10 s using biphasic, ± 1 V, 400 μs per phase, square waves.

In 2 rats, closed-loop stimulation was triggered based on the frequency of the interictal spikes. A 300 seconds (60-360 seconds prior to seizures) moving average window was used for computing the baseline level of interictal spikes. If the number of interictal spikes in the immediate 30 second window fell below 30% of the baseline number of interictal spikes, 30 seconds of asynchronous electrical stimulation on 15 microelectrodes was performed as before.

6.3 Results

6.3.1 Biomarker identification

Interictal spike frequency reduces by > 55% in 80% of seizures.

Data analysis from 10 randomly chosen seizures from 10 rats showed that the number of interictal spikes in the 60-second window immediately preceding seizures was significantly reduced ($P<0.005$) when compared to the number of interictal spikes that happen in the 60-360 second window preceding seizures.

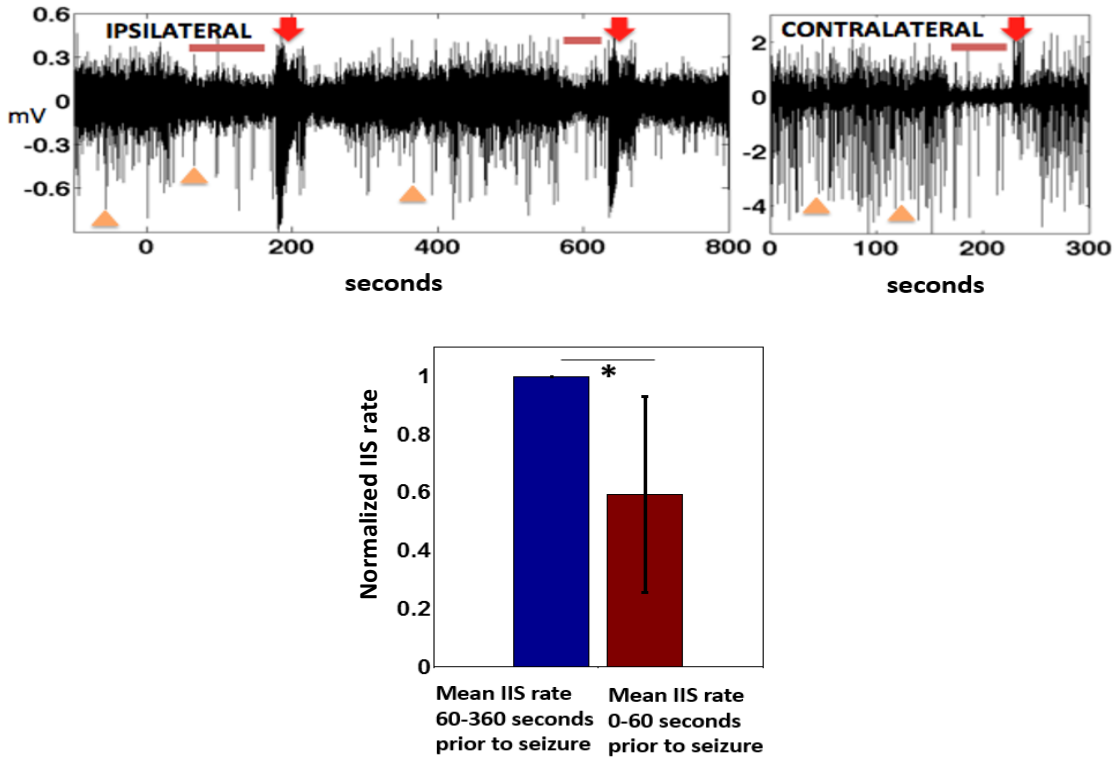

Figure 6.1 Temporal variation of interictal spikes with respect to seizures.

(Top) Ipsilateral and contralateral local field potential recordings from tetanus toxin injected epileptic rats' shows a marked decrease in interictal spiking activity prior to the onset of seizures. The red arrows indicate seizures, range arrow heads point to a few example interictal spikes. Notice a decrease in interictal spiking activity prior to onset of seizures (indicated by a red bar). (Bottom and Table 6.1). In 8 out of 10 randomly chosen seizures from 10 different rats, 8 rats showed reduced interictal spikes in the 60 seconds prior to seizure onset compared to the interictal spiking activity 60-360 (baseline) prior to seizure onset. Even with including data from the 2 rats that had increased interictal activity prior to seizures, on the whole there is a significant ($P<0.005$; Student's paired t-test) difference between numbers of interictal prior to seizures compared to baseline. Interictal spikes in the 0-60 seconds prior to seizures are normalized with respect to baseline in each case.

Table 6.1 Interictal spike rate in 60 seconds prior to seizures normalized with respect to baseline interictal spike rate.

Rat #	Normalized IIS rate in 60 seconds prior to seizure
1	0.31
2	0.41
3	0.46
4	0.29
5	0.60
6	0.53
7	0.41
8	0.51
9	1.26
10	1.15

In only 2 out of the 10 rats was a small increase in interictal spiking rate observed preceding seizures. Figure 6.1 (top) shows LFP recording from ipsilateral and contralateral sides' with respect to the tetanus toxin injection site in the dorsal hippocampus. Note the reduction in interictal spikes preceding seizures, which are indicated by red arrows. A few example interictal spikes are indicated with orange arrow heads. The number of interictal spikes were counted in 30 second windows preceding the 10 randomly chosen seizures. Mean number of interictal spikes in 2 30-second windows preceding seizures (times 0 to -60 seconds with respect to seizures) were normalized to the mean number of interictal spikes in 10 30-second windows preceding the 2-30 second windows discussed above. (i.e., -60 to -360 seconds with respect to seizures). Figure 6.1

(bottom) shows the mean ± standard deviation interictal spikes in the 60 seconds preceding seizures, normalized with respect to the interictal spikes in 360 to 60 seconds preceding seizures. A significant reduction ($P< 0.005$; paired t-test) was observed even when the two cases with a small increase in interictal spike rate was taken into account for calculations (Table 6.1).

One explanation for this observed relation between the interictal spike rate and seizures is that the increased network neuronal firing observed during interictal spikes (Rolston et al. 2010) may play a protective role similar to the open-loop stimulation showed in chapter 4 and (Wagenaar et al. 2005). In both these studies, the electrical stimulation pulses increased network firing which played a role in stopping/reducing seizure frequency. Since a similar correlation is observed between interictal spikes and seizures, we posit that the short bursts of multi-unit firing during interictal spikes (Rolston et al. 2010) may put the network in a refractory state (similar to electrical stimulation), thus preventing the onset of seizures. Similar relationship between interictal spikes and seizures has been shown to exist *in vitro (Avoli 2001)*.

Two types of closed-loop stimulation protocols were implemented.

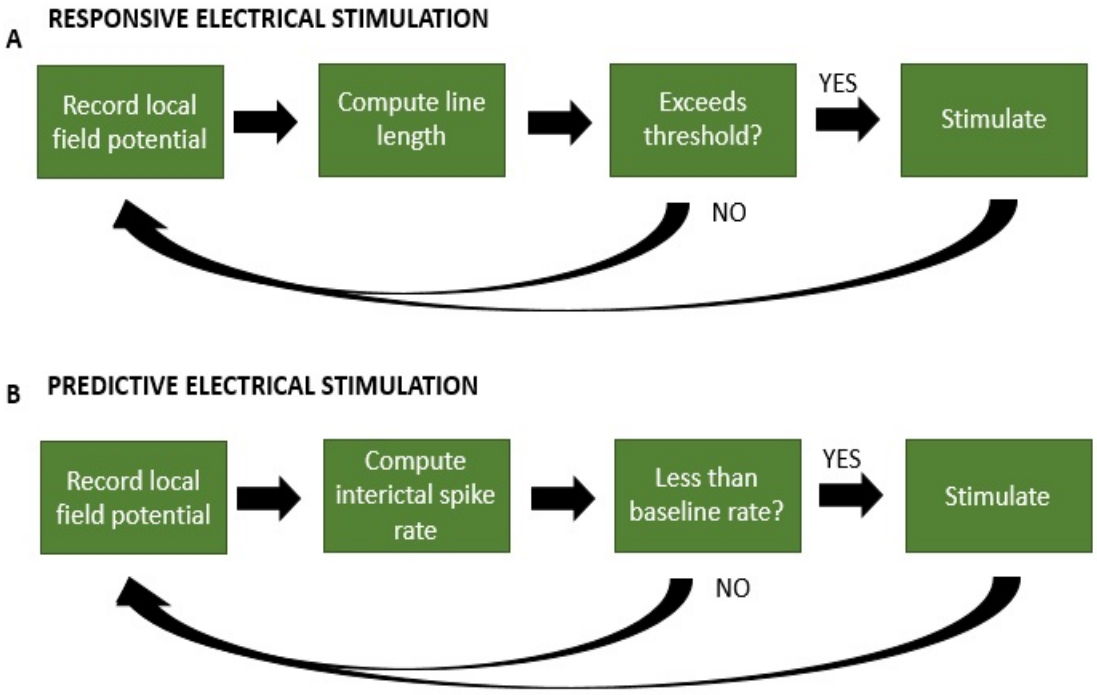

Figure 6.2 Two types of electrical closed-loop stimulation were performed in the tetanus toxin model of temporal lobe epilepsy.
(A) Responsive closed loop stimulation was performed to turn ON stimulation on detecting increase in line length pertaining to 3 interictal/ictal spikes. This method triggered a lot of false positives, but was also quick in responding to seizures. (B) Predictive closed-loop stimulation was performed when a 30% decrease in interictal spiking rate was detected in 30 seconds moving average windows compared to a baseline rate calculated in a 5 minutes moving average window (30 – 330 seconds preceding the current sample time).

6.3.2 Responsive closed-loop stimulation

Closed-loop responsive stimulation stimulation was turned on when 3 or more consecutive spikes were detected.

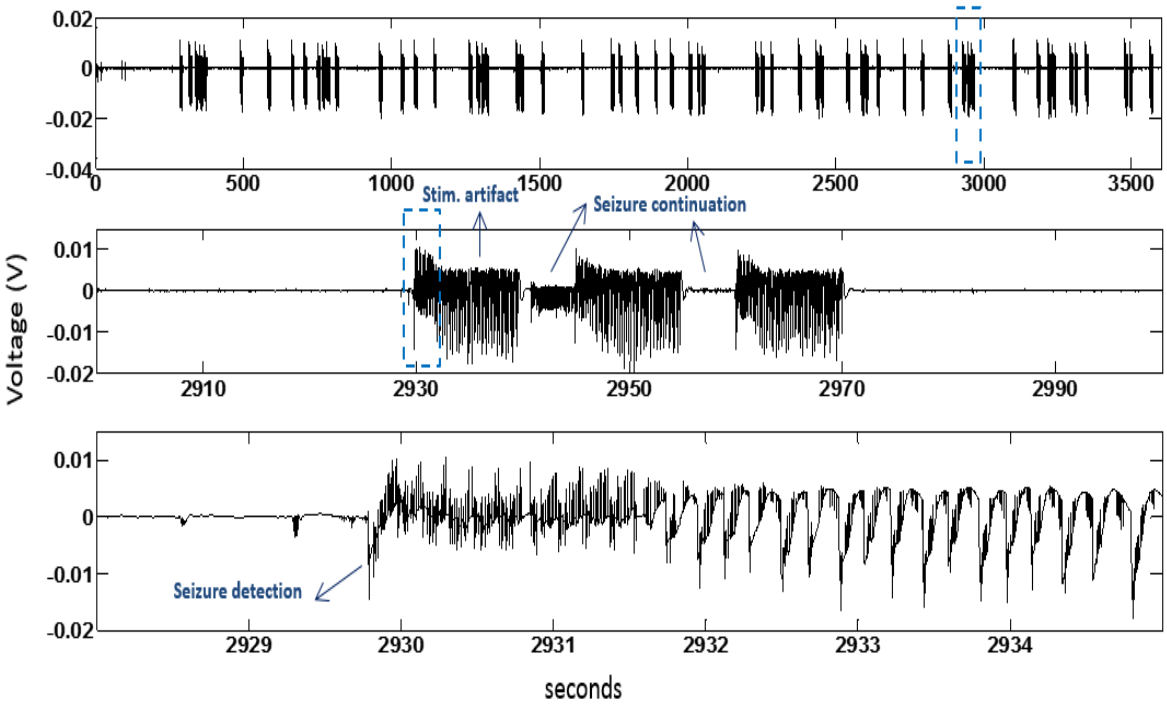

Figure 6.3 Responsive closed-loop stimulation for epilepsy.
Stimulation that was turned on when 3 or more interictal/ictal spikes were detected failed to stop seizures. In the figure above, the top row shows a 1-hour recording with several 10 second long stimulation epochs. This approach had a very high false positive rate, but the line length threshold was kept intentionally low to have a fast reaction time to seizures. The center plot shows one example where stimulation was performed on correct detection of seizure. The data within the boxed region is zoomed in, in the bottom plot. Notice that the stimulation did not stop the seizure. In the bottom plot it can be seen that stimulation comes on less than a second after the seizure began.

In 2 rats, asynchronous distributed microstimulation at theta frequency, which was effective in reducing seizure frequency by ~50% (Chapter 4), failed to stop seizures when the stimulation was turned On, in a responsive manner when 3 or more spikes (ictal/interictal) were detected. Figure 6.3 shows a closed-loop example where stimulation was performed on detection of 3 intericatl/ictal spikes. Notice the large number of false positives. The line length threshold was intentionally kept small to reduce detection to stimulation latencies. The portion within the blue dotted boxes is

zoomed in in the respective bottom plots. Notice that the stimulation comes on less than a second after the seizure starts. The stimulation was however ineffective in stopping the seizure. Bottom-most plot shows seizure continuation even after stimulation was delivered.

6.3.3 Predictive closed-loop stimulation

Closed-loop anticipative stimulation was turned on when a decrease in interictal spiking was detected.

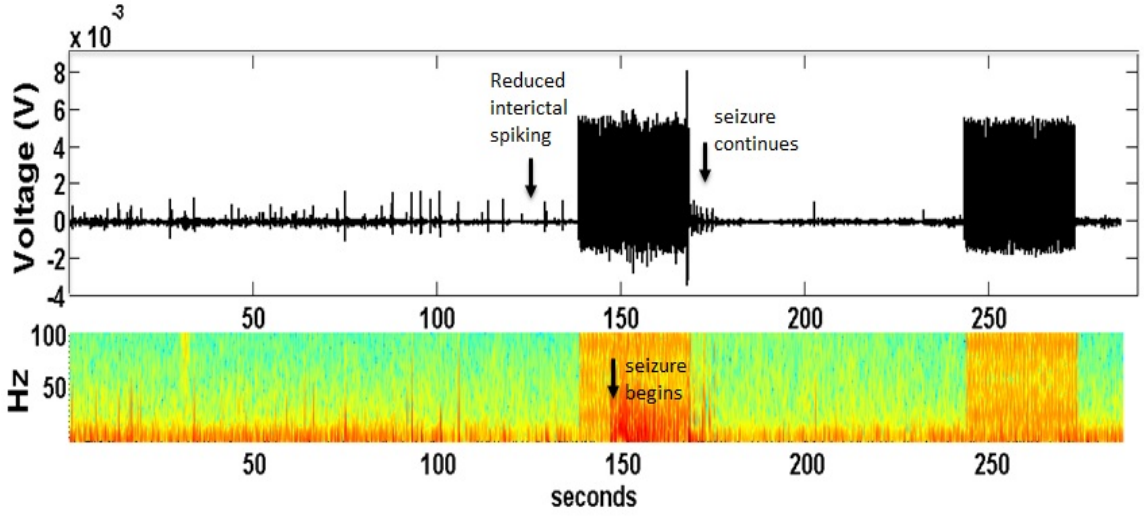

Figure 6.4 Predictive closed-loop stimulation for epilepsy.

Stimulation that was delivered on 15 microelectrodes in anticipation of oncoming seizures, when a decrease in interictal spiking rate was detected, was not effective in stopping seizures. The figure above shows an example raw LFP recording and corresponding spectrogram where 30 second 7.7 Hz/electrode pulses were delivered asynchronously on 15 microelectrodes when a 30% reduction in interictal spiking rate with respect to baseline spiking was detected. Although the stimulation pulses were delivered even before the seizure began, it was ineffective in stopping it, as can be seen by the seizure continuing even after the pulses stopped.

In 2 rats, asynchronous distributed theta stimulation was performed when a 30% decrease in interictal spiking rate was detected in a 30-second moving average window, compared to a baseline level calculated in a 300-second moving average window, preceding the 30 second window. As can be seen from the above figure (Figure 6.4), this stimulation protocol caused stimulation to come on before the seizure started, but this did not prevent the seizure from occurring.

6.4 Discussion

Through spontaneous hippocampal recording in the tetanus toxin model of temporal lobe epilepsy, we show that interictal spike rate reduces significantly ($P<0.005$) preceding seizures supporting the notion that interictal spikes may have anti-seizure roles. We hypothesize that the short bursts of multi-unit activity recorded during interictal spikes (Rolston et al. 2010) may play a protective role in epilepsy by sending neurons into a refractory state where they are unable to give rise to seizures, similar to open-loop electrical stimulation in chapter 4 and (Wagenaar et al. 2005). Indeed, a similar relation between interictal spikes and seizures was reported *in vitro* (Avoli 2001).

Theta electrical distributed microstimulation delivered in response to seizure detection (Esteller et al. 2004), and in a predictive approach in response to reduction in interictal spike rate, failed to stop seizures in preliminary experiments. Even though the closed-loop experiments were performed in a total of only 4 rats, these initial results seem to suggest that with the theta asynchronous multisite pulses, continuous neuromodulation where these pulses are delivered continuously and in response to biomarkers may be necessary to maintain the brain in an anti-epileptic state. Sending

these pulses after, or a few seconds before seizures begin may not be sufficient to induce the anti-epileptic state to stop oncoming seizures. Perhaps, the hippocampal network enters an epileptic state prior to the actual start of seizures and hence even the predictive closed-loop stimulation approach was ineffective in stopping seizures. Since we did not perform sufficient number of trials, we are unable to compare the effectiveness of the closed and open-loop (Chapter 4) approaches in seizure reduction. There may be other stimulation frequencies/parameters that will be more effective in closed-loop stimulation

CHAPTER VII

DEVELOPMENT OF A RAPID ALGORITHM PROTOTYPING TOOL FOR CLOSED-LOOP DEEP BRAIN STIMULATION SYSTEMS[4]

7.1 Introduction

There are several potential areas where closed-loop brain stimulation may have advantages over open-loop stimulation in human deep brain stimulation applications. Some of these include epilepsy, Parkinson's disease and essential tremor. In addition to being possibly more effective than open-loop stimulation, closed-loop systems may have other advantages including reduced side effects and extended battery life. Extending battery life of the implanted neurostimulator (INS), which would imply patients having to undergo fewer battery replacements surgeries, is in itself a significant need driving research and product development involving closed-loop systems for human applications (Sun et al. 2008).

Closed-loop system design involves the following components: (A) Biomarker: Biosignal indicative of the disease state (E.g. LFP broad-band energy in epilepsy (Sun et al. 2008); LFP beta energy in Parkinson's disease (Little et al. 2013), (B) Control policy: the closed-loop algorithm that determines stimulation output for the detected biomarker,

[4] Isaacson, B.P., Dani, S.P., Desai, S.A., Denison, T., Afshar, P., (2013) A rapid algorithm prototyping algorithm tool for bi-directional neural interfaces. Conf Proc IEEE Neural Engineering, 2013.

and (C) Effector: Stimulator engine that sends out electrical stimulation based on the control policy. One of the main requirements in designing effective closed-loop systems is determining the control policy, i.e., the closed-loop algorithm. The optimal algorithm may have any level of complexity ranging from applying a simple threshold to the biomarker to more complicated forms such as computing cross-frequency coherences, phase-amplitude coupling, and weighted averaging or Kalman filtering of two or more biomarkers (e.g. combination of LFP and EMG). Determining the optimal algorithm will undoubtedly require systematically trying out several. Additionally, these algorithms may depend on persistent data storage. For example, some machine learning algorithms may depend on stored data for updating its linear discriminant parameters. While embedded systems may be capable of storing the required amount of data, they lack the flexibility required for rapidly testing several algorithms due to firmware limitations. One method of enabling such rapid algorithm prototyping is to transmit the data out of the implanted device onto a computer where algorithms can be rapidly prototyped and transmit stimulation requests back to the INS. Such a platform would allow researchers to rapidly test a number of algorithms of any level of complexity and will certainly open up several new avenues of understanding the underlying disease condition and deriving algorithms that are more effective than the currently used ones. Once knowledge about effective algorithms is obtained, future generation closed-loop systems that are intended for chronic implants may be built with the new improved algorithms contained entirely within firmware, thus avoiding the need of having an external component for closing the loop.

In order for such an effort to be truly successful, researchers in many different research sites around the globe should be able to independently test closed-loop algorithms in patients. Efforts focused on collaboratively analyzing data gathered by the different sites will then prove effective in deciding on the most promising algorithms quickly. Given that researchers at the various research sites may have different preferences in the types of algorithms tested and the algorithm prototyping tools used to build them, to enable such large-scale data collection, the closed-loop platform should have two main features: (1) Researchers should have the flexibility of testing any algorithm. (2) Researchers should have the flexibility of using any algorithm prototyping tool that they are familiar with.

Medtronic Neuromodulation, located in Minneapolis is developing such a system that would allow researchers to rapidly prototype different closed-loop algorithms for application in various brain disorders. As part of an internship with the Neuromodulation team at Medtronic, I worked in team to develop and test an application programming interface (API) that will readily interface with the bi-directional neural implant through a streaming telemetry system on one end and can be easily plugged into any signal processing tool on a host computer on the other end. Some examples of the signal processing tools include MATLAB, Simulink and LabVIEW.

7.2 System overview

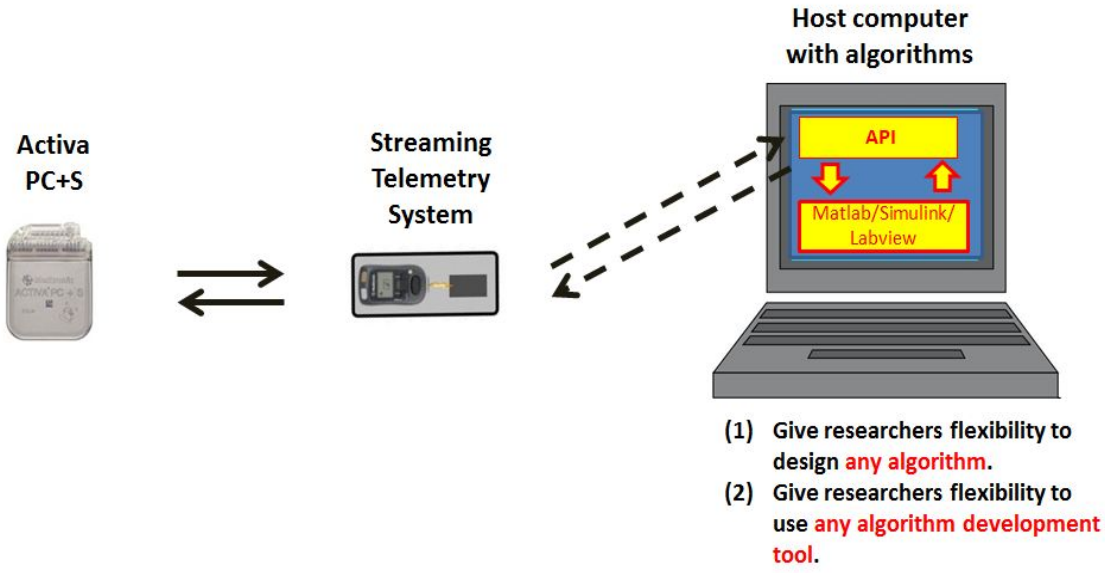

Figure 7.1 The Medtronic closed-loop research tool.
(Previous page) Left – Medtronic's implantable neurostimulator also capable of sensing neural signals. Center – A streaming telemetry system that communicates bidirectionally with the neurostimulator on one side and a host computer on the other side. Right – host laptop containing the API which communicates bidirectionally with the streaming telemetry system and readily plugs into algorithms written in Matlab/Simulink/LabVIEW.

The closed-loop system with the rapid algorithm prototyping tool consists of the following components:

(A) Activa PC+S: Bi-directional Neural Interface (BNI) that can both sense/record neural data and perform stimulation.

(B) STS (Streaming Telemetry System): The STS has an antenna which when placed over the BNI can communicate with it bi-directionally, receiving data and sending stimulation command updates to it.

(C) Host computer with algorithms: An example for this would be a laptop PC with closed-loop algorithms developed using the MATLAB signal processing software. The API (built in Java) resides on the host processor and serves as the communication layer between the host processor and the STS. Its function is to translate commands from the host-processor into low-level commands interpreted by the host processor, while hiding low-level hardware communication complexities from algorithm developers. One of the key requirements in developing the API was that the API should not add any significant latency to the closed-loop system. Additionally, the API was built keeping data security and integrity in mind. Any data missed or corrupted can be identified by the host processor, which can then restore stimulation settings to the default values.

7.3 Characterizing system latencies

There are several sources of latencies for a closed-loop system of the kind described above, including but not restricted to, the telemetry communication latency, latency introduced by the signal processing algorithm and API latency. Since the signal processing latency will depend extensively on the nature of the algorithm used, (For example, a 400 ms. moving average filter has an inherent latency of 200 ms.), for the purpose of characterizing the closed-loop system latency, a simple threshold detector algorithm was implemented.

Test Setup

The closed-loop system was validated using a test bed as illustrated in Figure. 7.2 Signals from a signal generator were input to the bi-directional neural interface (BNI) and

telemetry was used to stream data from the BNI to the host computer running the API and Matlab/Simulink. Data from the BNI were sent in packets of 400 ms to the host processor; hence, 2.5 packets would contain 1 second worth of sensed data.

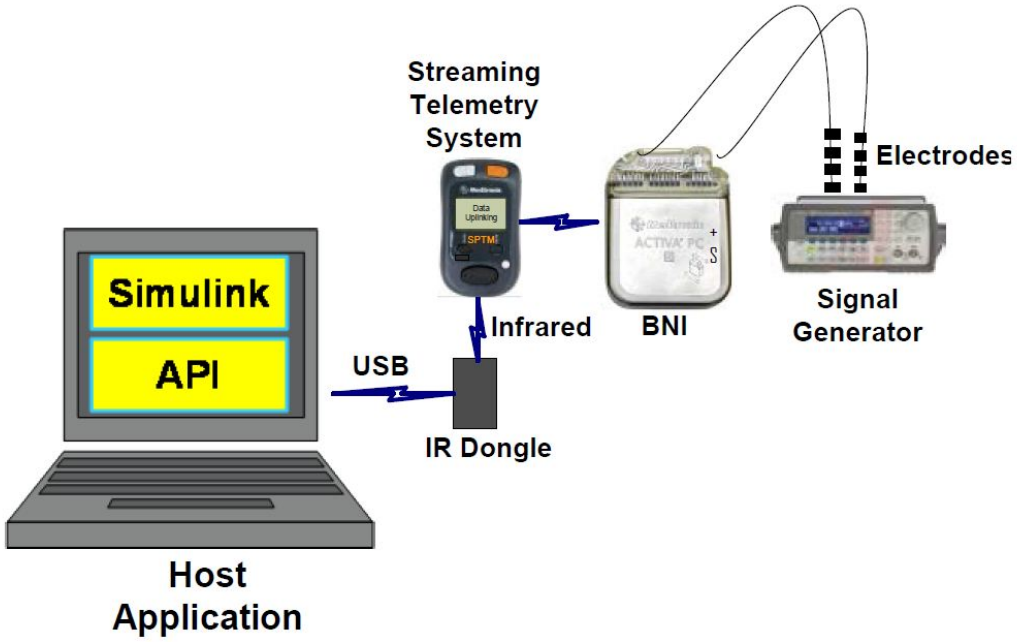

Figure 7.2 Test setup for characterizing latencies of the closed-loop research too.
A signal generator provided a single pulse to the bidirectional neural interface, signals from BNI were then sent through telemetry to the streaming telemetry system. The API residing on a host computer made periodic requests for signals to the streaming telemetry system

Signal Input/Biomarker

Sixty-six square pulses from a signal generator, each 20 Hz at 50% duty cycle and 300 mV peak-to-peak, attenuated by a factor of 2000, were input to the BNI and retrieved by the host processor through the API. The pulses were distributed over 10 minutes and the spacing between them was chosen to randomly position them in the 400 ms. data

packets sent from the BNI to the host processor through telemetry (Oscilloscope screenshot in Figure. 7.3 shows the distribution of the pulse positions within the 400 ms. data packets).

Bi-Directional Neural Interface

The bi-directional neural interface (BNI) used in this setup has the capability of streaming data at 200 or 422 Hz in time domain, and 5Hz when transmitting power in a pre-defined frequency band. For the results in this chapter, 422 Hz sampling was used. Details of the bi-directional neural interface may be found in (Stanslaski et al. 2012).

Telemetry device

Data packets from the BNI were transmitted through a low-frequency proximal (~4 cm) inductive telemetry device to the host processor. The stimulation programs on the BNI were setup by the standard clinician programmer (Medtronic, Inc. model 8840). The closed-loop system could only vary stimulation parameters within the bounds set by the clinician programmer.

Application Programming Interface

The API, written in Java, utilized a multithreaded telemetry execution engine to process the transfer and receipt of commands over a generic connection interface which was implemented using various physical layers (e.g., USB, Bluetooth, etc.). The host processor instantiated an instrument instance, requested data from and sent stimulation updates to the BNI.

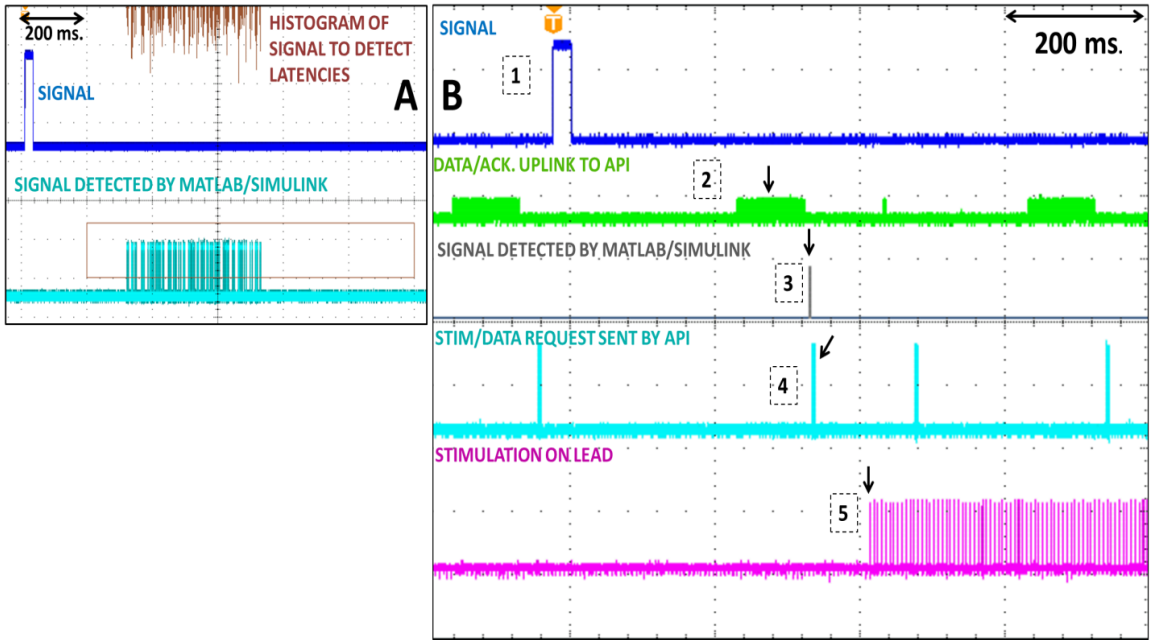

Figure 7.3 Oscilloscope screenshots showing signal and stimulation command transmission between the implanted pulse generator and algorithm on host computer. (A) Cyan traces (detection of pulses by Simulink) and histogram show that the signal occurrence to detect latency depends on position of pulse (blue trace) within the 400 ms. data packet. (B) A random trial of full closed-loop system latency computation with the Inc. command (Increment amplitude command). (1) A single square pulse is input to the BNI; (2) the pulse is sent within a 400 ms packet to the API; (3) the pulse is detected by Simulink; (4) Stim (Inc) command is sent by API when pulse is detected; (5) Stimulation appears on lead.

Host Processor and Algorithm

For this work, a PC-based host processor running MATLAB and Simulink (Mathworks) for algorithm development was selected. The algorithm consisted of a classifier to identify states of interest from the input signal and a control policy to modify stimulation based on identified state. The classifier was an empirically derived linear threshold on the amplitude of the raw signal. The corresponding control policy toggled stimulation OFF (0V) and ON (6V) based on the classifier output.

7.4 RESULTS

7.4.1 Latency characterization

Table 7.1 Signal to detection latency with Medtronic's closed-loop research tool.

Sensing Latency					
Command	Description	Mean (ms)	Min (ms)	Max (ms)	Std (ms)
Get Data	Get data packets from the INS	508.6	311.2	716.9	116.2

Table 7.2 Stimulation command to actuation latency with Medtronic's closed-loop research tool.

Stimulation Latency					
Command	Description	Mean (ms)	Min (ms)	Max (ms)	Std (ms)
Therapy On	Switch ON stim engine	354.6	343.9	372.4	7.1
Therapy Off	Switch OFF stim engine	52.4	45.1	61.1	4.3
Group Switch	Change multiple parameters	495.9	490.5	505.1	3.7
Inc/Dec (Amp,PW,Freq.)	Increase/decrease stimulation amplitude, pulse width or frequency	80.9	76.0	84.6	2.6

For the system described in this chapter, latencies were introduced by numerous individual system elements in addition to the API latency, such as telemetry, detection,

etc. Latency was calculated separately for sensing commands and stimulation control. Sensing latency was computed by measuring the time elapsed between the occurrence of the signal on the leads and its detection by the host processor (time between 1 and 3 in Figure 7.3). Stimulation latency was computed by measuring the time between detection/issuing a command to change stimulation and the stimulation change at the electrode (time between 3 and 5 in Figure 7.3). All latency measurements and statistics computations were automated using a Tektronix MSO 4034 Mixed Signal Oscilloscope.

Tables 7.1 and 7.2 show the latencies for the system from signal input to stimulation on the lead. Table 7.1 contains Sensing latency statistics and Table 7.2 contains Stimulation latency statistics. To get the entire closed-loop system latency, numbers in table 7.1 should be added to the appropriate latency numbers in table 7.2. For example, when the Inc/Dec (increment/decrement) command is used, the mean closed loop system latency from Signal to Stimulation would be 508.6 ms + 80.86 ms ~ 590 ms. Figure 7.3 is an oscilloscope screenshot illustrating the different latency steps from signal to stimulation in a randomly selected trial.

The main contributor to the total latency comes from packaging of data samples in 400 ms packets and transmission of these packets via telemetry (sensing latency). The large variance in this sensing latency (~ 400 ms; table 7.1) is due to the variance in positioning of the signal of interest (pulse signal in this study) within the 400 ms data packets (Figure 7.3 A). Pulse signals occurring at the very end of the data packet produce total closed-loop system latency with Inc/Dec of ~ 390 ms. On the other hand pulse

signals occurring at the very beginning of the data packet produce total latency of ~ 790 ms.

Complex algorithms or signal processing chains with inherent delays may cause additional sense to stimulation latencies. For example, a 400 ms boxcar moving average filter would introduce an average 200 ms. delay regardless of host processor speed. By processing data outside the implantable device one can leverage greater computational power as compared to running algorithms in embedded firmware and thus gain processing advantage. Design of closed-loop systems should balance latency, computational complexity, and memory requirements. The API described in this work provides simplicity, flexibility, low-latency, and security for researchers interested in prototyping algorithms. This approach allows for rapid and broad algorithm development. Algorithms that meet performance needs for closed loop systems may then be implemented in device firmware optimizing for computation and power consumption. The proximal telemetry, the host application modifying stimulation parameters only within boundaries set by clinical programmers, the ability of the API to detect data loss or corruption provide a robust setting for developing closed-loop neurostimulation algorithms. Biomarkers extracted from multiple signal sources representative of a disease state or through other processing methods are convenient to explore with the flexibility on the host processor that the API enables. Examples of these could be activity or position sensors. The Java implementation of the API also opens the possibility for mobile applications to interact with devices so long as data security and privacy are maintained, which in the future, could allow for greater collaboration between researchers and reduce the learning time for understanding neural mechanisms.

7.4.2 Example applications of the rapid algorithm prototyping closed-loop research tool.

Example 1: Closed-loop algorithm for Parkinson's Disease.

Increasing evidence suggests that beta frequency band (13–30Hz) oscillations in the LFP can be consistently picked up in the subthalamic nucleus (STN) of patients with Parkinson's Disease and that their level correlates with motor impairment, with and without treatment (Moran et al. 2011; Little et al. 2013). The symptoms along with the amplitude of beta oscillations fluctuate on a moment by moment basis depending on factors such as cognitive and motor load and concurrent drug therapy. A very convincing study also shows that electrical deep brain stimulation at 130 Hz is effective in both suppressing beta oscillations and improving symptoms associated with Parkinson's Disease (Little et al. 2013). Closed-loop stimulation with 130 Hz stimulation delivered only when beta exceeds a pre-set threshold was 29% more effective in controlling the symptoms in advanced Parkinson's patients (Little et al. 2013).

Using the rapid algorithm prototyping tool with the implanted bi-directional neurostimulator described in the previous section, a straightforward closed-loop algorithm is to stream in the local field potential data from the DBS leads implanted in the subthalamic nucleus, into an external unit as such a host laptop, classify the signal (based on power in the beta band compared with a pre-set threshold) and send stimulation commands to the INS via telemetry (Figure 7.4).

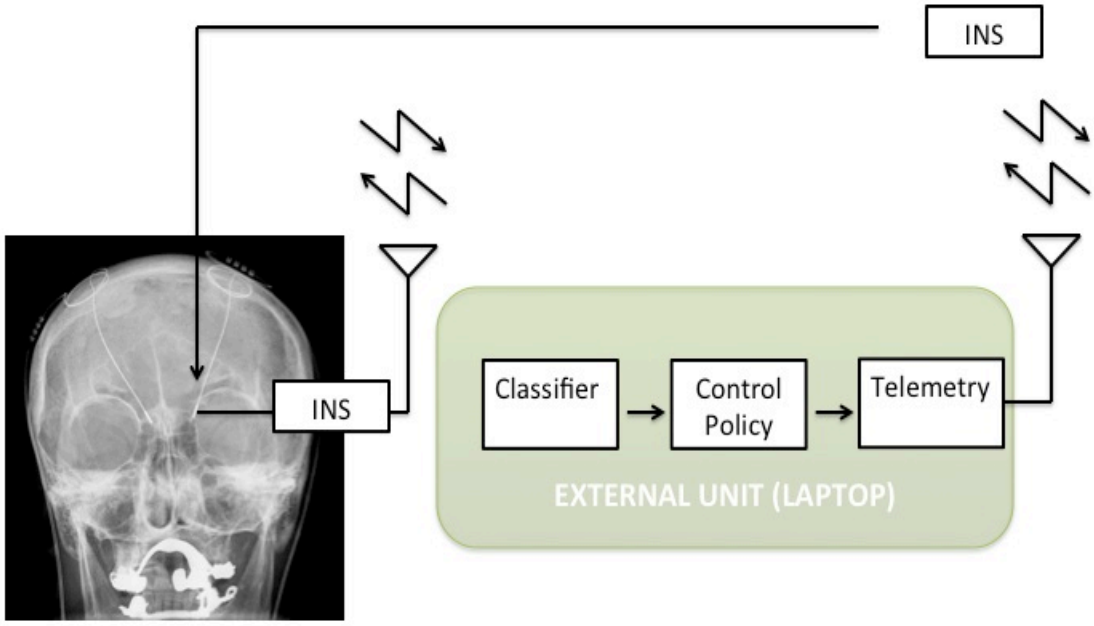

Figure 7.4 Application of the closed-loop research tool for Parkinson's disease.
Local field potential signals from the DBS leads is sent vis telemetry to an external unit (laptop computer) that contains the classifier, control policy and stimulation control blocks. The stimulation command is sent to the implanted neurostimulator through telemetry, closing the loop.

We implemented the closed-loop algorithm for this example in Simulink. In the Simulink model shown in figure 7.5, the first block in the extreme left is setup to stream in data in real time from the implanted neurostimulator through the application programming interface (API) described in the previous section. Once the data is received by the host laptop, the beta energy is extracted by passing the signal through a signal processing chain described below and stimulation command is sent to the implanted neurostimulator if the beta power exceeded a pre-set threshold.

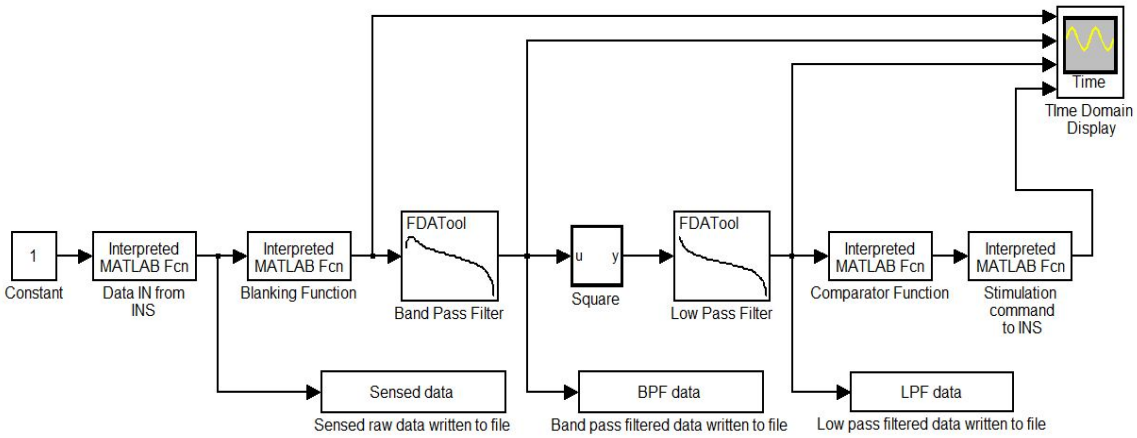

Figure 7.5 Simulink model example for Parkinson's disease.
Simulink model that was designed for extracting beta energy from local field potential data that is input from the BNI to the MATLAB environment though the API, comparing extracted beta energy with a pre-set threshold and sending out stimulation through the API to the BNI if beta energy above the threshold is detected.

The top-level signal processing flow for this algorithm is as follows:

(A) Data is streamed into Simulink through the JAVA API which communicates with the BNI through the STS.

(B) The data streamed in is passed through a 4 pole IIR Butterworth band pass filter with center frequency at 22 Hz and cut-off frequencies at 13 and 30 Hz.

(C) The band pass filtered data is then passed through a stage of rectification and low pass filtering (3 pole IIE Butterwork filter with cut-off frequency at 2.5 Hz), which performs smoothing.

(D) Data output from the smoothing filter is compared with a pre-set threshold.

(E) If a value above threshold is detected, a stimulation command is sent to the BNI through the Java API.

Example 2: Sensor fusion closed-loop algorithm based on inputs from two independent recording techniques for movement disorders (e.g. essential tremor).

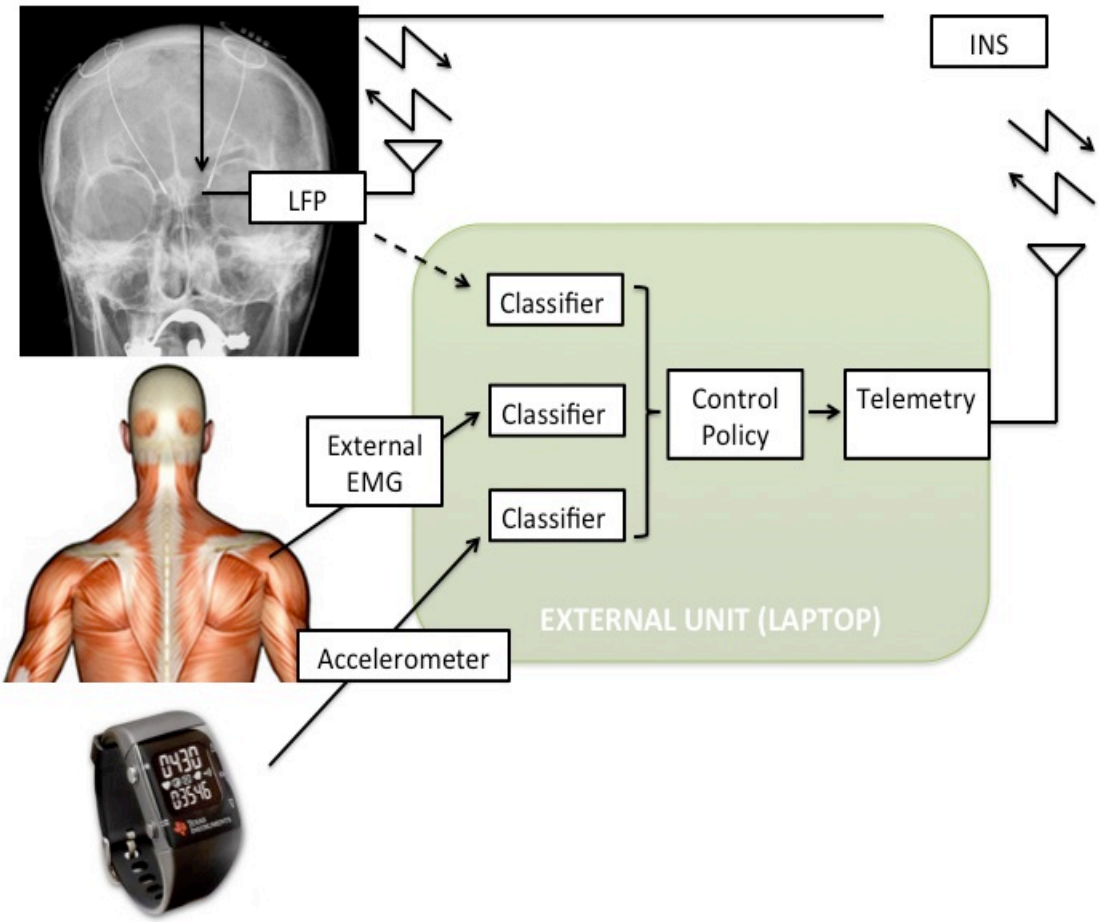

Figure 7.6 Application of the closed-loop research tool for essential tremor.
Sensor-fusion based closed-loop algorithm for essential tremor. Bio-signals from three different sources 1) local field potential from DBS electrodes, 2) external EMG from surface electrodes and 3) 3-axis accelerometer data from a Texas Instrument Chronos watch are sent to an external unit (laptop) where the three signals are processed separately and a control policy combines processed data from the three different sources to make a decision on when to send out a stimulation command to the INS through telemetry.

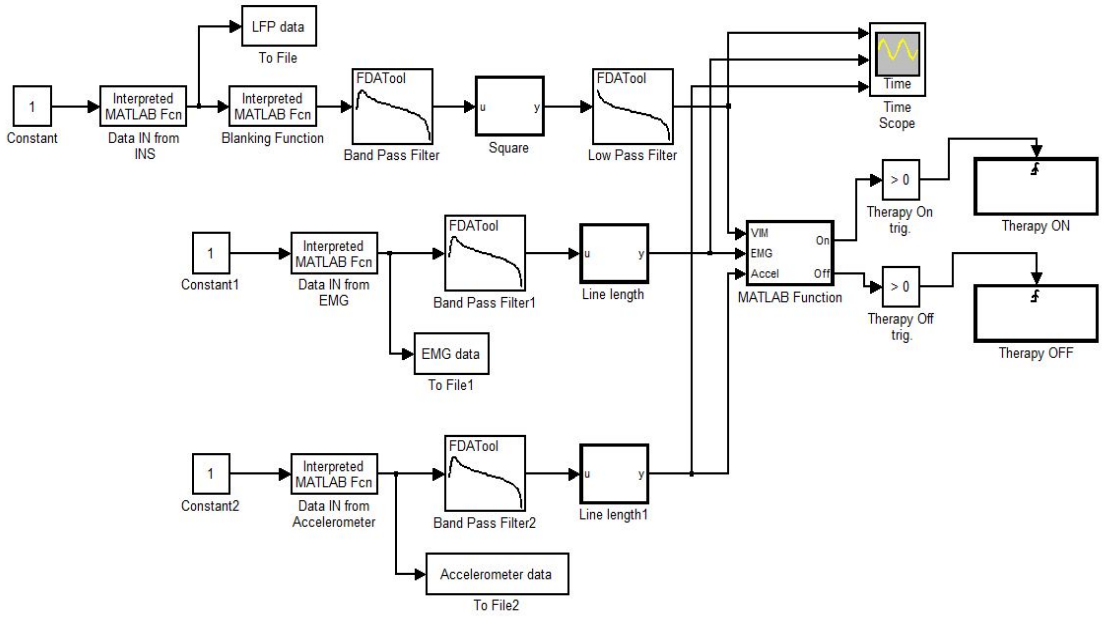

Figure 7.7 Simulink model example with sensor fusion for essential tremor.
This Simulink model is an example of an algorithm based on senor fusion data input. Data from 2 different sources (E.g. Neural data from deep brain stimulation electrodes sensed by the BNI and EMG/accelerometer data from the BNI or any other sensing device) can be streamed into the Simulink model on a computer. The two data streams can then be individually processed and a weighted average function can be used to Turn On/Off stimulation based on the two inputs.

The second example shows a closed-loop algorithm in Simulink where three types of data are received by the host processor. The 1st data stream is a thalamic LFP signal and the second is a EMG signal and the third is an accelerometer signal (Figure 7.7). These three data streams are processed separately where band pass filtering, rectification and smoothing is performed on the LFP signal while band pass filtering and line length computation is performed on the EMG and accelerometer signals. These signals are then passed to a Simulink block, which performs a weighted average on the three signals streams. The weights of this weighted average function can be moved to favor one signal

over the others in during different states. The resulting value from this block is compared to a pre-set threshold to Turn On or Off stimulation. A sensor-fusion based closed-loop signal processing algorithm of the type described here will have applications in cases where EMG/accelerometer data can be used to derive information about the disease state in addition to LFP signals from the brain. One example for this is essential tremor, where tremors surface only when the patient intends to make a physical movement and is tremor free when no volitional movement is made.

Using a wired signal processing tool like Simulink for building closed-loop algorithms allows researchers to easily visualize the signal processing flow while also allowing them to quickly select any particular block to change parameters. Also, Simulink contains an extensive library with several pre-built signal processing blocks that the research can drag, drop and wire together to create/modify algorithms quickly.

7.5 CONCLUSION

The API described in this chapter easily plugs into commonly used signal processing platforms such as MATLAB providing simplicity and flexibility for prototyping closed-loop algorithms. Once optimal algorithms are found, those that meet performance needs for closed-loop systems may then be implemented in device firmware optimizing for computation and power consumption. Biomarkers extracted from multiple signal sources representative of disease state or through other processing methods can be easily imported into the host computer and algorithms can be designed that take a sensor fusion approach for turning On and Off stimulation, thus providing added reliability and flexibility in closed-loop DBS applications.

Acknowledgements

I wish to thank Dr. Timothy Denison, Director of Core Technology at Medtronic Neuromodulation for giving me the opportunity to work on this project. I would like to acknowledge Ben Isaacson, Siddharth Dani, Dr. Pedram Afshar and Scott Stanslaski of Medtronic Neuromodulation for collaborating with me on this project. Additionally, I wish to thank Eric Panken, David Carlson, David Linde, Randy Jensen and Terry Ahrens of Medtronic Neuromodulation for their valuable inputs.

CHAPTER VIII

CONCLUSION AND FUTURE DIRECTION

8.1 CONCLUSION

In this dissertation I have described a novel method of electrical brain stimulation for seizure control in temporal lobe epilepsy. While multi-electrode arrays have been used extensively for stimulation studies in brain-machine interfaces (Nicolelis et al. 1997; Pais-Vieira et al. 2013), they have not been explored for treating brain disorders such as epilepsy, Parkinson's disease or essential tremor. A previous study from the Potter group has shown that a multielectrode microstimulation technique can completely stop seizure-like spontaneous bursting events in cultures of cortical neurons grown on glass dishes (Wagenaar et al. 2005). In this dissertation, I have worked on translating this finding to a rodent model of temporal lobe epilepsy.

It was first necessary to improve impedance properties of *in vivo* multielectrodes to allow better recording during stimulation (an important feature for closed-loop stimulation). Impedance of microelectrode arrays additionally plays an important role in determining the signal to noise ratio (SNR) of the neural data recorded. Reducing impedance of microelectrode arrays will theoretically increase the SNR, reduce stimulation artifact pickup and reduce stimulation voltage requirements for injecting a given amount of current, compared to unplated high-impedance microelectrodes. One method of reducing impedance is through electroplating the base metal with a non-toxic material such as platinum black. But the traditional DC electroplating method has not

been popular with this material in chronic brain implants because of low durability of the electroplated material. In Chapter 2 of this dissertation, I have described a novel technique called sonicoplating, which solved this issue by significantly ($P<0.05$) increasing the adherence of platinum black on the base metal. In sonicoplating, ultra high frequency vibrations are applied to the electroplating setup. While improvement in signal to noise ratio could not be demonstrated, significant reduction in stimulation artifact ($P<0.01$) and voltage requirements ($P<0.005$) were achieved, compared to unplated controls.

There are no studies that have directly compared the spatial extent of activation with micro (<30 μm) and macro (>100 μm) electrode stimulation in deep brain structures. Further, with voltage-controlled stimulation, sonicoplated microelectrodes may have higher neuronal activation compared to unplated microelectrodes of the same diameter. In chapter 3 of this dissertation, I have compared spatial activation in the dorsal hippocampus with macroelectrodes, microelectrodes and sonicoplated microelectrodes. A macroelectrode has an activation radius of 200 μm, a microelectrode has an activation radius of 100 μm and an electroplated microelectrode has an activation radius of 150 μm. With 20 unplated or sonicoplated microelectrodes (which would occupy less volume compared to a single macroelectrode), 3.5 or 7.5 times more neurons would be activated when compared to single macroelectrode. Hence, microelectrode arrays may not only cause less tissue damage due to implantation compared to a single macroelectrode, but would also cause more neuronal activation.

Microelectrodes arrays allow several different spatio-temporal patterns of stimulation, which are not possible through macroelectrodes. In the tetanus toxin model

of temporal lobe epilepsy, spontaneous local field potential recordings from the epileptic focus showed reduced theta oscillations ($P<10^{-4}$) compared to theta oscillations recorded from saline-injected control rats. Asynchronous multi-microelectrode stimulation in the theta frequency range significantly reduced seizures by ~50% ($P<0.05$) when compared to baseline spontaneous recording. Synchronous theta stimulation through microelectrode arrays or theta stimulation through a single macroelectrode was ineffective in reducing seizures significantly, while high frequency stimulation increased seizures. Epileptic rats tested in the Morris water maze task showed significant ($P<0.05$) memory deficits when compared to saline injected controls. Chapters 4 and 5 of this dissertation describe these results in detail.

I found that interictal spikes significantly ($P<0.005$) reduced in the 60 seconds prior to the onset of seizures. For closed-loop stimulation, two approaches were taken. A. Responsive neurostimulation – stimulation was turned on when seizures were detected and B. Predictive neurostimulation – stimulation was turned on when a decrease in interictal spike rate was detected. Both these approaches failed to stop seizures. From these preliminary results, I hypothesize that once the hippocampal network enters a pro-epileptic state, it is too late to stop the seizures with the theta multielectrodes microstimulation approach. Continuous open-loop or closed-loop neuromodulation may be necessary to prevent the network from entering the pro-epileptic state to begin with. Perhaps, increasing the number of microelectrodes implanted at the epileptic focus or with movable microelectrodes (Jackson and Fetz 2007), sufficient single unit activity may be recorded to implement closed-loop algorithms similar to (Wagenaar et al. 2005). Such an approach might help control the epileptic network better (i.e., changes in single

unit firing may be more sensitive to temporal network properties, thus closed-loop stimulation based on single-unit firing may interfere with the epileptic network even before it enters the pro-epileptic state described above) than the approach described in chapter 6 which used LFP biomarkers.

Through an internship at Medtronic Neuromodulation in Minneapolis, I implemented an application programming interface based rapid prototyping research tool which can be easily used by researched and clinicians to quickly test any desired algorithm on a wide range of signal processing tools including MATLAB/Simulink and Labview. I characterized the latencies of the closed-loop system in detail and have provided example Simulink models for two different neurological disorders.

8.2 FUTURE DIRECTIONS

A number of future steps may be taken to improve the work presented in this dissertation. In this section, I list a few points that may help direct future research based on this dissertation.

1) Building and improving technology that will allow superior research in closed-loop deep brain stimulation.

By DC electroplating microwire arrays under sonication (sonicoplating), impedance of the microelectrodes was durably reduced ($P<0.05$). However, only one electroplating material, platinum black, was used in this work. Other materials like the conductive polymer PEDOT (Xiao et al. 2004), which has recently gained popularity in the field of Neuroscience, may also potentially be electroplated through this technique. Further, this technique may also be tested on DBS macroelectrodes used in stimulation

studies for reducing voltage requirements and consequently improving battery life (Gross et al. 2004). Through my internship at Medtronic Neuromodulation, I have contributed to building technology that will allow rapid-prototyping of algorithms to find optimal stimulation patterns for closed-loop DBS in human patients. However, the technology has significant closed-loop latencies (390 ms. to 790 ms.), which may not be within acceptable limits in certain applications. Methods to improve the telemetry latency, or designing tools that will allow rapid and flexible algorithm prototyping within the implanted neurostimulator (i.e., without the need for streaming data out of the implanted device through telemetry) will definitely broaden the scope of the closed-loop algorithms tested.

2) Understanding spatial activation profiles with microelectrode and macroelectrodes used in DBS.

The results through my work described in chapter 3, will help in designing and spacing microelectrodes for achieving desired activation patterns/levels for different anatomical structures. However, in this dissertation, only one stimulation parameter was tested (25 Hz, ± 1 V, 400 μs/phase biphasic square pulses). Creating an extensive database with several different clinically relevant stimulation parameters will prove very useful in informing the selection of optimal stimulation parameters for disease control. Further, a collaborative approach with data from immunohistochemistry (such as used in my work), simulation studies (E.g. finite element analysis) (Chaturvedi et al. 2010) and real-time brain activity visualization techniques such calcium imaging (Histed et al.

2009) and MRI (Jech et al. 2001) in the presence of macro and microelectrode deep brain stimulation will prove very useful in understanding how exactly DBS works.

3) Understanding epilepsy and introducing a new approach for DBS.

The tetanus toxin model used in this dissertation is a non-lesional model of human temporal lobe epilepsy (Brace et al. 1985). Through extensive local field potential recordings in this model, I have shown that theta oscillations (~7.5 Hz center frequency) are reduced ($P<10^{-4}$) compared to controls and asynchronous theta stimulation performed through microelectrode arrays reduced seizures by ~50% ($P<0.05$). A number of alterations to experimental design may lead to better seizure control including a) Increasing the number of microelectrodes implanted in the dorsal hippocampus for influencing more hippocampal tissue. In the current study 16 electrode microwire arrays were used for stimulating the epileptic focus. 32-or 64-electrode mirowires can be used to affect more neuronal tissue. Our lab's electrophysiology suite, NeuroRighter (Rolston et al. 2010; Newman et al. 2012) already has the capability for supporting such high electrode numbers. Since 27% of seizures begin from the hippocampus contralateral to the injection site (Jiruska et al. 2010), microelectrodes arrays implanted bilaterally may be more effective than unilateral stimulation. Additionally, increasing the number of implanted microelectrodes will also increase the recorded single/multi-unit activity, which may be used for designing closed-loop control algorithms (Wagenaar et al. 2005), instead of the LFP biomarkers described in chapter 6 of this dissertation. b) Achieving better targeting with movable microelectrode arrays. The positioning of microelectrode arrays we used in this dissertation could not be adjusted once implanted. Brain micromotion (Gilletti and Muthuswamy 2006), gliosis (Polikov et al. 2005) and other

factors often lead to tiny changes in the electrode positions with time, moving the microelectrodes away from the targets they were originally implanted at. To achieve optimal electrical stimulation throughout the course of study, it may be better to use movable microelectrodes where fine adjustments to electrode positions can be made when desired (Jackson and Fetz 2007). Single, multi-unit and local filed potential recording can be used to continuously guide the microelectrodes towards the right targets. c) Stimulation of other targets in the brain such as the fimbria/fornix (major hippocampal input/output pathway) and/or the theta pacemaker, medial septum (both part of the septohippocampal system) that have wide projections to the hippocampus (Colom et al. 2006; Garcia-Hernandez et al. 2010), might be more effective in influencing larger hippocampal volumes compared to the approach taken in this dissertation, having better control on the bilateral seizure foci. Stimulating these alternative targets may additionally play a role in improving memory deficits associated with temporal lobe epilepsy (Helmstaedter 2002). Stimulation of the fimbria/fornix has been shown to improve memory in Alzheimer's disease (Hamani et al. 2008). d) Optogenetics is a new and exciting field where a subpopulation of neurons made to express light sensitive ion channels may be selectively activated or depressed by shining light of different wavelengths (Deisseroth 2011). Depressing overly synchronized neurons at the epileptic focus or activating neurons to maintain a tonic background-firing rate (Wagenaar et al. 2005), are potential stimulation techniques that may be effective in controlling seizures. A few studies have indeed already shown successful closed-loop seizure control with optogenetic light stimulation in awake behaving rodents (Krook-Magnuson et al. 2013; Paz et al. 2013).

APPENDIX

C-fos immunohistochemistry to study spatial neuronal activation with optogenetic light stimulation in the hippocampus of rodents

Introduction

Optogenetics is a technology that allows targeted and fast control of precisely defined events in biological systems as complex as freely moving mammals (Deisseroth 2011). By delivering optical control at the speed (millisecond-scale) and with the precision (cell type–specific) required for biological processing, optogenetic approaches have opened new landscapes for the study of biology, both in health and disease (Deisseroth 2011).

A number of studies have already shown that this technology can be successfully used for controlling seizures in *in vivo* models of epilepsy (Krook-Magnuson et al. 2013; Paz et al. 2013). However, this technology is still in its infancy and there remains a lot of work that needs to be done before it can have any human translation. In comparison, even though the mechanisms of action of electrical deep brain stimulation remain elusive, electrical DBS is FDA approved and has been successful in treating several disorders. e.g., Parkinson's disease (Little et al. 2013). One of the several studies that would perhaps ease any translational efforts with optogenetics is comparing its spatial activation with electrical DBS. In chapter 3 of this dissertation, we described a method involving c-fos immunohistochemistry to study the spatial extent of activation in the dorsal hippocampus using macroelectrode, microelectrode and sonicoplated microelectrode stimulation. Using the same technique for analyzing neuronal excitation (i.e., c-fos immunohistochemistry), and similar stimulation experimental conditions (i.e., with rats

under anesthesia), we performed some preliminary experiments to try to compare spatial excitation using electrical and optogenetic stimulation in the dorsal hippocampus.

Although the results obtained through these preliminary studies are somewhat inconclusive because of the large variability in both the positioning of the fiber optic and the light-gated cation channel expression (ChR2) in the dorsal hippocampus, widespread c-fos expression was seen in the pyramidal cell bodies in the hippocampus of rats with ChR2 expression and 2.5 hours of light stimulation. The c-fos expression in most cases, however, did not overlap with the ChR2 expressing cell bodies, suggesting that mechanisms such as summation of post-synaptic potentials might be the responsible for the neuronal activation observed. Studies with better viral injections and fiber optic placements in the dorsal hippocampus are necessary to arrive at any conclusions. The results presented in this appendix are very preliminary and should be treated as a guiding point for any future studies conducted along these lines.

Methods

All animal procedures were conducted in accordance with the National Institutes of Health Guide for the Care and Use of Laboratory Animals and approved by the Emory University Institutional Animal Care and Use Committee. Ten adult male Sprague Dawley rats were used for this study. Rats were anesthetized with 1.5-3% inhaled isoflurane. A craniotomy was made over the right hippocampus in all rats. In half the rats selected at random, 1.8 µl of 10^12 virions/mL AAV5-hsyn-ChR2-EYFP was injected into the dorsal hippocampus at 3.3 mm posterior and 3.2 mm lateral to bregma, and 3.1 mm ventral to pia. In the other half 1.8 µl of 10^12 virions/mL AAV5-hsyn-EYFP (no

channel; control) was injected instead. The periosteum was replaced and the scalp was stapled closed and rats were allowed to rest and recover in BSL2 quarantine housing for 3 days after which they are moved to the normal rat monitoring rooms. Two week later, all rats underwent a second surgery where a fiber optic/ferrule was implanted. While anesthetized, 10 ms long pulses were delivered at 25Hz with 18 mW/mm^2 intensity for 2.5 hours. Following stimulation, the fiber optic was removed and each rat was deeply anesthetized with a lethal dose of Euthasol (130 mg/kg) injected intraperitoneally and then perfused intracardially with 0.9% NaCl, followed by 4% paraformaldehyde in 0.1 M phosphate buffered saline at pH 7.2 (PBS) for 15 min at a rate of 20 ml per min. Brains were removed and cryoprotected in 30% sucrose at 4°C, and the region spanning the entire fiber optic track sectioned in the horizontal plane at 50 μm thickness using a freezing microtome, collected in series of 4 in 4% paraformaldehyde PBS, and rinsed in PBS. To identify the number and identity of the cells activated by the optogenetic stimulation, we performed double immunofluorescence labeling for the immediate early gene, c-Fos, and the neuronal marker, NeuN. Free-floating sections were rinsed in PBS, blocked in 5% normal donkey serum (NDS) and 0.1% Triton-X for 30 min and rinsed in PBS. After rinses in PBS, sections were incubated overnight at 4°C in rabbit anti-cfos (1:5000; Calbiochem) and mouse anti NeuN (1:1000; Millipore) in PBS containing 1% NDS. Sections were rinsed in PBS and incubated in Alexa 594-conjugated donkey anti-rabbit (1:1000; Jackson Immunoresearch) and Alexa 488-conjugated donkey antimouse (1:1000; Jackson Immunoresearch) in 1% NDS for 1 hr. Sections were rinsed with PBS, then mounted on glass slides with Fluoromont-G mounting medium (SouthernBiotech) for fluorescence microscopy. For each double-label experiment, controls included

omission of one or both primary antibodies. Sections were visualized using a Nikon eclipse E400 microscope equipped with 4 fluorescent cubes, a monochrome and color digital camera and Nikon BR software (Nikon Instruments Inc, Melville, NY). For each brain at least 2 series were stained and images corresponding to the tip of the fiber optic are used for making figures A-1 and A-2 below.

Results

(A) Blue light stimulation in the dorsal hippocampus of rats with AAV5-hSYn-ChR2-EYPF showed widespread c-fos expression

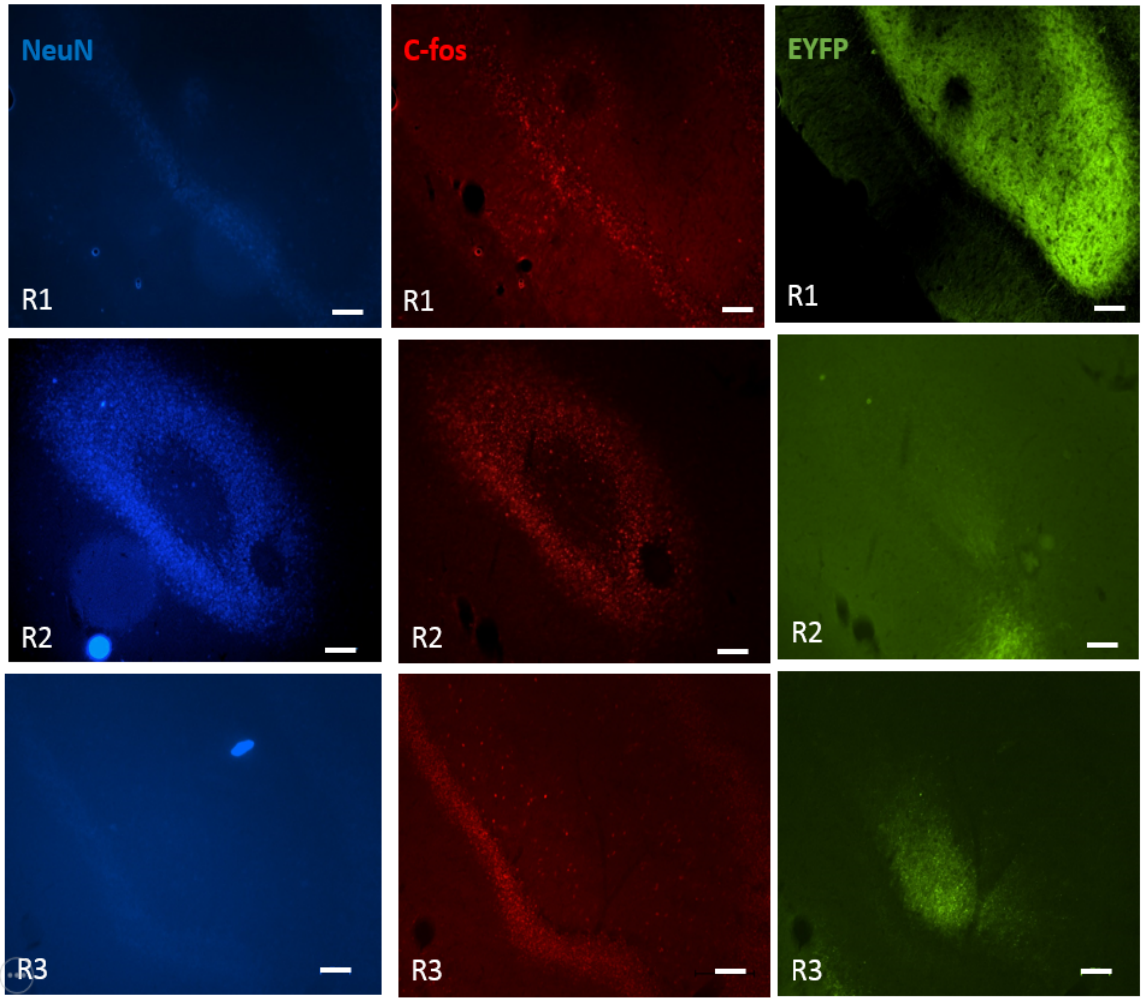

Figure A.1 Optogenetic light stimulation in dorsal hippocampus with ChR2 expression. (Previous page) Blue light stimulation in the dorsal hippocampus of rats with ChR2-EYPF showed widespread c-fos expression. Example images with NeuN, c-fos stained and ChR2-EYFP expressing horizontal sections from 3 rats (R1, R2, and R3) are shown in this figure. All three rats were injected with AAV5-hsyn-ChR2-EYFP in the right dorsal hippocampus, two weeks prior to receiving 2.5 hours of blue light stimulation under isoflurane anesthesia. Histology revealed that the ChR2 expression was not uniform in these rats, with some rats having drastically more (E.g. Rat1) ChR2 expression in the dorsal hippocampus when compared to others (E.g. Rat 2 and 3). Even so, widespread c-fos expression was found in the dorsal hippocampal pyramidal cell layers near the tip of the fiber optic. Scale bar: 100 µm.

(A) Blue light stimulation in the dorsal hippocampus of rats with AAV5-hSyn-EYFP expression showed widespread c-fos expression

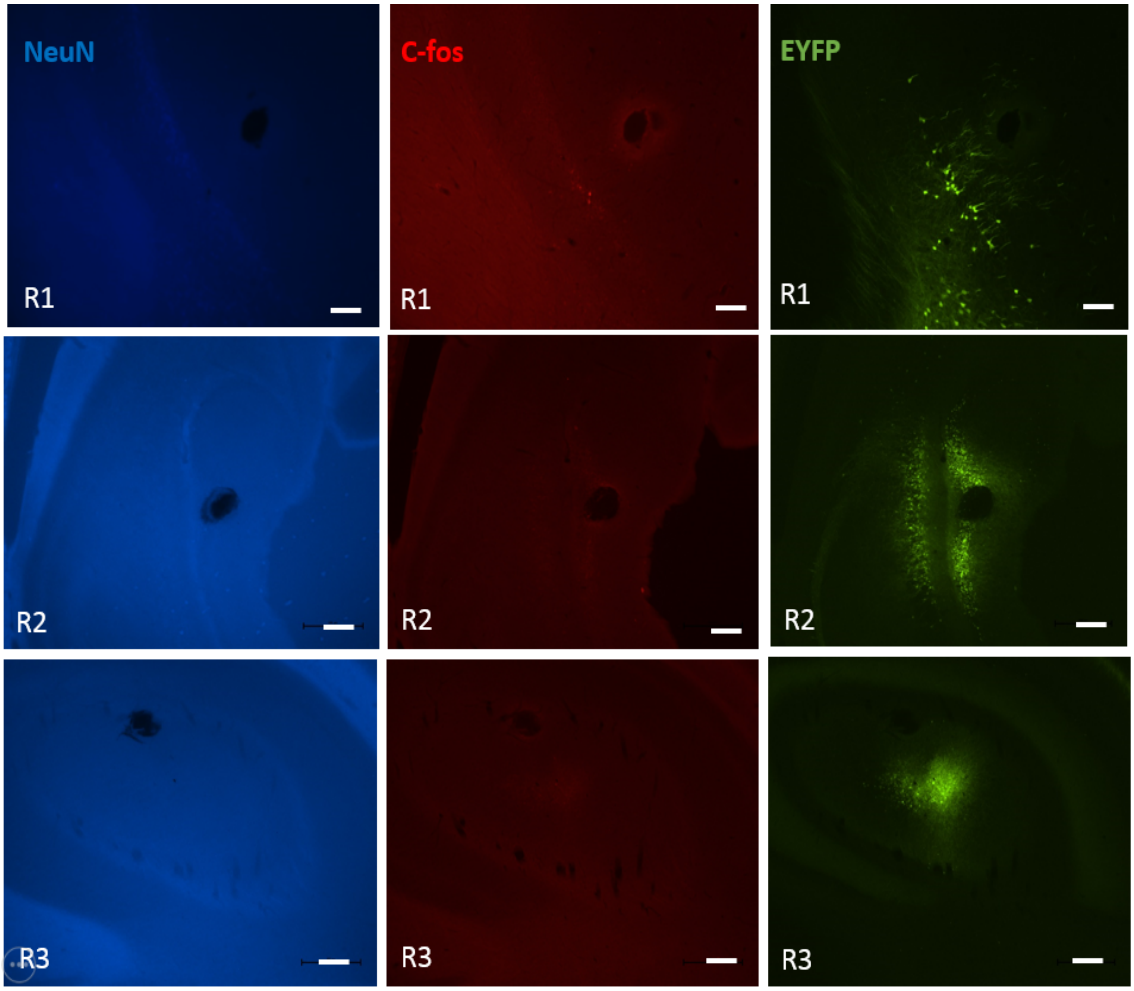

Figure A.2 Optogenetic light stimulation in dorsal hippocampus with ChR2 expression.
(Previous page) Blue light stimulation in the dorsal hippocampus of control rats with EYPF expression showed negligible c-fos expression. Example images with NeuN, c-fos stained and ChR2-EYFP expressing horizontal sections from 3 rats (R1, R2 andR3) are shown in this figure. All three rats were injected with AAV5-hsyn-EYFP in the right dorsal hippocampus, two weeks prior to receiving 2.5 hours of blue light stimulation under isoflurane anesthesia. Histology revealed negligible c-fos expression in the pyramidal cell layers of the dorsal hippocampus. Scale bar: 100 μm.

Discussion

Preliminary experiments performed to study spatial activation in the dorsal hippocampus of ChR2 expressing rats with 2.5 hours of light stimulation, showed widespread c-fos expression. Results obtained with c-fos immunohistochemistry following electrical stimulation (Chapter 3) showed c-fos expression concentrated to a tissue volume surrounding the tip of the electrode tracks. With optogenetic excitatory blue light stimulation in ChR2 expressing rats, this did not seem to be the case. Very few cell bodies expressing ChR2-EYFP or EYFP (controls) were seen in the dorsal hippocampus corresponding to the sections that contained the tip of the fiber track. Most of the ChR2-EYFP/EYFP expression was seen in the neuropil. Widespread c-fos expression in the light stimulated dorsal hippocampal pyramidal cell bodies with no ChR2 expression in non-control rats, suggests mechanisms such as algebraic summation of several post-synaptic potentials behind neuronal activation. Electrical stimulation and optogenetic stimulation may hence have completely different mechanisms of action and a direct and fair comparison of spatial activation with these two neuronal stimulation methods may not be possible.

In the experiments described above, even though the c-fos expression was seen only in the ChR2 expressing dorsal hippocampus with light stimulation, the variability in

both the positioning of the fiber optic and ChR2 expression within the hippocampus made it difficult to arrive at any major conclusions. Further, poor histology resulted in bad sections from 2 animals in each group (ChR2 expressing and control) that did not stain well for c-fos and NeuN and hence were not included in the results. Further experiments with better targeting of the viral injections and fiber optic for light stimulation will be necessary to confirm the results described in this appendix. Future c-fos immunohistochemistry experiments with different promoters that will selectively express the ChR2 light-sensitive channels in particular neuronal subpopulations will be helpful in understanding some of the mechanisms of neuronal activation with optogenetic light stimulation.

Acknowledgements

I thank Claire-Anne Gutekunst and Neal Laxpati for collaborating with me in designing, conducting experiments and producing results presented in this Appendix.

REFERENCES

Anderson, R. J., M. A. Frye, O. A. Abulseoud, K. H. Lee, J. A. McGillivray, M. Berk and S. J. Tye (2012). "Deep brain stimulation for treatment-resistant depression: efficacy, safety and mechanisms of action." Neurosci Biobehav Rev **36**(8): 1920-1933.

Arsiero, M., H. R. Luscher and M. Giugliano (2007). "Real-time closed-loop electrophysiology: towards new frontiers in in vitro investigations in the neurosciences." Arch Ital Biol **145**(3-4): 193-209.

Avoli, M. (2001). "Do interictal discharges promote or control seizures? Experimental evidence from an in vitro model of epileptiform discharge." Epilepsia **42 Suppl 3**: 2-4.

Avoli, M., G. Biagini and M. de Curtis (2006). "Do interictal spikes sustain seizures and epileptogenesis?" Epilepsy Curr **6**(6): 203-207.

Ben-Menachem, E., R. Manon-Espaillat, R. Ristanovic, B. J. Wilder, H. Stefan, W. Mirza, W. B. Tarver and J. F. Wernicke (1994). "Vagus nerve stimulation for treatment of partial seizures: 1. A controlled study of effect on seizures. First International Vagus Nerve Stimulation Study Group." Epilepsia **35**(3): 616-626.

Benabid, A. L., S. Chabardes, J. Mitrofanis and P. Pollak (2009). "Deep brain stimulation of the subthalamic nucleus for the treatment of Parkinson's disease." Lancet Neurology **8**(1): 67-81.

Bewernick, B. H., R. Hurlemann, A. Matusch, S. Kayser, C. Grubert, B. Hadrysiewicz, N. Axmacher, M. Lemke, D. Cooper-Mahkorn, M. X. Cohen, H. Brockmann, D. Lenartz, V. Sturm and T. E. Schlaepfer (2010). "Nucleus accumbens deep brain stimulation decreases ratings of depression and anxiety in treatment-resistant depression." Biol Psychiatry **67**(2): 110-116.

Bland, B. H. and L. V. Colom (1993). "Extrinsic and intrinsic properties underlying oscillation and synchrony in limbic cortex." Prog Neurobiol **41**(2): 157-208.

Brace, H. M., J. G. Jefferys and J. Mellanby (1985). "Long-term changes in hippocampal physiology and learning ability of rats after intrahippocampal tetanus toxin." J Physiol **368**: 343-357.

Bragin, A., J. Engel, Jr., C. L. Wilson, I. Fried and G. Buzsaki (1999). "High-frequency oscillations in human brain." Hippocampus **9**(2): 137-142.

Branner, A., R. B. Stein and R. A. Normann (2001). "Selective stimulation of cat sciatic nerve using an array of varying-length microelectrodes." J Neurophysiol **85**(4): 1585-1594.

Butson, C. R., S. E. Cooper, J. M. Henderson, B. Wolgamuth and C. C. McIntyre (2011). "Probabilistic analysis of activation volumes generated during deep brain stimulation." Neuroimage **54**(3): 2096-2104.

Butson, C. R., C. B. Maks and C. C. McIntyre (2006). "Sources and effects of electrode impedance during deep brain stimulation." Clinical Neurophysiology **117**(2): 447-454.

Butson, C. R. and C. C. McIntyre (2006). "Role of electrode design on the volume of tissue activated during deep brain stimulation." J Neural Eng **3**(1): 1-8.

Buzsaki, G. (2002). "Theta oscillations in the hippocampus." Neuron **33**(3): 325-340.

Buzsaki, G. (2004). "Large-scale recording of neuronal ensembles." Nat Neurosci **7**(5): 446-451.

Buzsaki, G. and E. I. Moser (2013). "Memory, navigation and theta rhythm in the hippocampal-entorhinal system." Nat Neurosci **16**(2): 130-138.

Can, A., D. T. Dao, M. Arad, C. E. Terrillion, S. C. Piantadosi and T. D. Gould (2012). "The mouse forced swim test." J Vis Exp(59): e3638.

Chaturvedi, A., C. R. Butson, S. F. Lempka, S. E. Cooper and C. C. McIntyre (2010). "Patient-specific models of deep brain stimulation: influence of field model complexity on neural activation predictions." Brain Stimul **3**(2): 65-67.

Cogan, S. F. (2008). "Neural stimulation and recording electrodes." Annual Review of Biomedical Engineering **10**: 275-309.

Colom, L. V., A. Garcia-Hernandez, M. T. Castaneda, M. G. Perez-Cordova and E. R. Garrido-Sanabria (2006). "Septo-hippocampal networks in chronically epileptic rats: potential antiepileptic effects of theta rhythm generation." J Neurophysiol **95**(6): 3645-3653.

Cusin, C., K. C. Evans, L. L. Carpenter, B. D. Greenberg, D. A. Malone, E. Eskandar and D. D. Dougherty (2010). "Deep Brain Stimulation for Treatment Resistant Depression: The Role of the Ventral Capsule/Ventral Striatum." Psychiatric Annals **40**(10): 477-484.

de Curtis, M. and G. Avanzini (2001). "Interictal spikes in focal epileptogenesis." Prog Neurobiol **63**(5): 541-567.

Deadwyler, S. A. and R. E. Hampson (2004). "Differential but complementary mnemonic functions of the hippocampus and subiculum." Neuron **42**(3): 465-476.

Deisseroth, K. (2011). "Optogenetics." Nat Methods **8**(1): 26-29.

Desai, S. A., J. D. Rolston, L. Guo and S. M. Potter (2010). "Improving impedance of implantable microwire multi-electrode arrays by ultrasonic electroplating of durable platinum black." Front Neuroengineering **3**: 5.

Donoghue, J. P. (2002). "Connecting cortex to machines: recent advances in brain interfaces." Nat Neurosci **5 Suppl**: 1085-1088.

Dragunow, M. and R. Faull (1989). "The use of c-fos as a metabolic marker in neuronal pathway tracing." J Neurosci Methods **29**(3): 261-265.

Engel, J., Jr. (1996). "Introduction to temporal lobe epilepsy." Epilepsy Res **26**(1): 141-150.

Esteller, R., J. Echauz and T. Tcheng (2004). "Comparison of line length feature before and after brain electrical stimulation in epileptic patients." Conf Proc IEEE Eng Med Biol Soc **7**: 4710-4713.

Ferguson, J. E., C. Boldt and A. D. Redish (2009). "Creating low-impedance tetrodes by electroplating with additives." Sensors and Actuators a-Physical **156**(2): 388-393.

Fisher, R., V. Salanova, T. Witt, R. Worth, T. Henry, R. Gross, K. Oommen, I. Osorio, J. Nazzaro, D. Labar, M. Kaplitt, M. Sperling, E. Sandok, J. Neal, A. Handforth, J. Stern, A. DeSalles, S. Chung, A. Shetter, D. Bergen, R. Bakay, J. Henderson, J. French, G. Baltuch, W. Rosenfeld, A. Youkilis, W. Marks, P. Garcia, N. Barbaro, N. Fountain, C. Bazil, R. Goodman, G. McKhann, K. Babu Krishnamurthy, S. Papavassiliou, C. Epstein, J. Pollard, L. Tonder, J. Grebin, R. Coffey and N. Graves (2010). "Electrical stimulation of the anterior nucleus of thalamus for treatment of refractory epilepsy." Epilepsia **51**(5): 899-908.

Ganguly, K., L. Secundo, G. Ranade, A. Orsborn, E. F. Chang, D. F. Dimitrov, J. D. Wallis, N. M. Barbaro, R. T. Knight and J. M. Carmena (2009). "Cortical representation of ipsilateral arm movements in monkey and man." J Neurosci **29**(41): 12948-12956.

Garcia-Hernandez, A., B. H. Bland, J. C. Facelli and L. V. Colom (2010). "Septo-hippocampal networks in chronic epilepsy." Exp Neurol **222**(1): 86-92.

Gilletti, A. and J. Muthuswamy (2006). "Brain micromotion around implants in the rodent somatosensory cortex." J Neural Eng **3**(3): 189-195.

Gimsa, J., B. Habel, U. Schreiber, U. van Rienen, U. Strauss and U. Gimsa (2005). "Choosing electrodes for deep brain stimulation experiments--electrochemical considerations." J Neurosci Methods **142**(2): 251-265.

Gray, J. A. (1972). "Effects of septal driving of the hippocampal theta rhythm on resistance to extinction." Physiol Behav **8**(3): 481-490.

Greenberg, B. D., D. A. Malone, G. M. Friehs, A. R. Rezai, C. S. Kubu, P. F. Malloy, S. P. Salloway, M. S. Okun, W. K. Goodman and S. A. Rasmussen (2006). "Three-year outcomes in deep brain stimulation for highly resistant obsessive-compulsive disorder (vol 31, pg 2384, 2006)." Neuropsychopharmacology **31**(11): 2394-2394.

Griffith, R. W. and D. R. Humphrey (2006). "Long-term gliosis around chronically implanted platinum electrodes in the Rhesus macaque motor cortex." Neuroscience Letters **406**(1-2): 81-86.

Grill, W. M. (1999). "Modeling the effects of electric fields on nerve fibers: Influence of tissue electrical properties." Ieee Transactions on Biomedical Engineering **46**(8): 918-928.

Gross, R. E., E. G. Jones, J. O. Dostrovsky, C. Bergeron, A. E. Lang and A. M. Lozano (2004). "Histological analysis of the location of effective thalamic stimulation for tremor - Case report." Journal of Neurosurgery **100**(3): 547-552.

Guehl, D., E. Cuny, A. Benazzouz, A. Rougier, F. Tison, S. Machado, D. Grabot, C. Gross, B. Bioulac and P. Burbaud (2006). "Side-effects of subthalamic stimulation in Parkinson's disease: clinical evolution and predictive factors." Eur J Neurol **13**(9): 963-971.

Hamani, C., M. P. McAndrews, M. Cohn, M. Oh, D. Zumsteg, C. M. Shapiro, R. A. Wennberg and A. M. Lozano (2008). "Memory enhancement induced by hypothalamic/fornix deep brain stimulation." Ann Neurol **63**(1): 119-123.

Hariz, M. I. (2002). "Complications of deep brain stimulation surgery." Movement Disorders **17**: S162-S166.

Helmchen, F. and W. Denk (2005). "Deep tissue two-photon microscopy." Nat Methods **2**(12): 932-940.

Helmstaedter, C. (2002). "Effects of chronic epilepsy on declarative memory systems." Prog Brain Res **135**: 439-453.

Heuschkel, M. O., M. Fejtl, M. Raggenbass, D. Bertrand and P. Renaud (2002). "A three-dimensional multi-electrode array for multi-site stimulation and recording in acute brain slices." J Neurosci Methods **114**(2): 135-148.

Histed, M. H., V. Bonin and R. C. Reid (2009). "Direct activation of sparse, distributed populations of cortical neurons by electrical microstimulation." Neuron **63**(4): 508-522.

Hock, B. J., Jr. and M. D. Bunsey (1998). "Differential effects of dorsal and ventral hippocampal lesions." J Neurosci **18**(17): 7027-7032.

Jackson, A. and E. E. Fetz (2007). "Compact movable microwire array for long-term chronic unit recording in cerebral cortex of primates." Journal of Neurophysiology **98**(5): 3109-3118.

Jech, R., D. Urgosik, J. Tintera, A. Nebuzelsky, J. Krasensky, R. Liscak, J. Roth and E. Ruzicka (2001). "Functional magnetic resonance imaging during deep brain stimulation: a pilot study in four patients with Parkinson's disease." Mov Disord **16**(6): 1126-1132.

Jefferys, J. G., B. J. Evans, S. A. Hughes and S. F. Williams (1992). "Neuropathology of the chronic epileptic syndrome induced by intrahippocampal tetanus toxin in rat: preservation of pyramidal cells and incidence of dark cells." Neuropathol Appl Neurobiol **18**(1): 53-70.

Jefferys, J. G. and S. F. Williams (1987). "Physiological and behavioural consequences of seizures induced in the rat by intrahippocampal tetanus toxin." Brain **110 (Pt 2)**: 517-532.

Jiruska, P., G. T. Finnerty, A. D. Powell, N. Lofti, R. Cmejla and J. G. Jefferys (2010). "Epileptic high-frequency network activity in a model of non-lesional temporal lobe epilepsy." Brain **133**(Pt 5): 1380-1390.

Jobst, B. C. (2010). "Electrical stimulation in epilepsy: vagus nerve and brain stimulation." Curr Treat Options Neurol **12**(5): 443-453.

Keating, J. G. and G. L. Gerstein (2002). "A chronic multi-electrode microdrive for small animals." Journal of Neuroscience Methods **117**(2): 201-206.

Kerr, L. D., J. T. Holt and L. M. Matrisian (1988). "Growth factors regulate transin gene expression by c-fos-dependent and c-fos-independent pathways." Science **242**(4884): 1424-1427.

Krause, M., W. Fogel, A. Heck, W. Hacke, M. Bonsanto, C. Trenkwalder and V. Tronnier (2001). "Deep brain stimulation for the treatment of Parkinson's disease: subthalamic nucleus versus globus pallidus internus." J Neurol Neurosurg Psychiatry **70**(4): 464-470.

Krook-Magnuson, E., C. Armstrong, M. Oijala and I. Soltesz (2013). "On-demand optogenetic control of spontaneous seizures in temporal lobe epilepsy." Nat Commun **4**: 1376.

Kumar, R., A. M. Lozano, Y. J. Kim, W. D. Hutchison, E. Sime, E. Halket and A. E. Lang (1998). "Double-blind evaluation of subthalamic nucleus deep brain stimulation in advanced Parkinson's disease." Neurology **51**(3): 850-855.

Lebedev, M. A. and M. A. Nicolelis (2006). "Brain-machine interfaces: past, present and future." Trends Neurosci **29**(9): 536-546.

Lee, C. L., R. A. Hrachovy, K. L. Smith, J. D. Frost, Jr. and J. W. Swann (1995). "Tetanus toxin-induced seizures in infant rats and their effects on hippocampal excitability in adulthood." Brain Res **677**(1): 97-109.

Lega, B. C., J. Jacobs and M. Kahana (2012). "Human hippocampal theta oscillations and the formation of episodic memories." Hippocampus **22**(4): 748-761.

Linkenkaer-Hansen, K., S. Monto, H. Rytsala, K. Suominen, E. Isometsa and S. Kahkonen (2005). "Breakdown of long-range temporal correlations in theta oscillations in patients with major depressive disorder." J Neurosci **25**(44): 10131-10137.

Little, S., A. Pogosyan, S. Neal, B. Zavala, L. Zrinzo, M. Hariz, T. Foltynie, P. Limousin, K. Ashkan, J. Fitzgerald, A. L. Green, T. Z. Aziz and P. Brown (2013). "Adaptive deep brain stimulation in advanced Parkinson disease." Ann Neurol **74**(3): 449-457.

Maher, M. P., J. Pine, J. Wright and Y. C. Tai (1999). "The neurochip: a new multielectrode device for stimulating and recording from cultured neurons." J Neurosci Methods **87**(1): 45-56.

Mayberg, H. S., A. M. Lozano, V. Voon, H. E. McNeely, D. Seminowicz, C. Hamani, J. M. Schwalb and S. H. Kennedy (2005). "Deep brain stimulation for treatment-resistant depression." Neuron **45**(5): 651-660.

McCreery, D., A. Lossinsky, V. Pikov and X. Liu (2006). "Microelectrode array for chronic deep-brain microstimulation and recording." IEEE Trans Biomed Eng **53**(4): 726-737.

Mccreery, D. B., W. F. Agnew, T. G. H. Yuen and L. Bullara (1990). "Charge-Density and Charge Per Phase as Cofactors in Neural Injury Induced by Electrical-Stimulation." Ieee Transactions on Biomedical Engineering **37**(10): 996-1001.

McIntyre, C. C., S. Mori, D. L. Sherman, N. V. Thakor and J. L. Vitek (2004). "Electric field and stimulating influence generated by deep brain stimulation of the subthalamic nucleus." Clinical Neurophysiology **115**(3): 589-595.

McIntyre, C. C., M. Savasta, L. Kerkerian-Le Goff and J. L. Vitek (2004). "Uncovering the mechanism(s) of action of deep brain stimulation: activation, inhibition, or both." Clin Neurophysiol **115**(6): 1239-1248.

Merrill, D. R., M. Bikson and J. G. Jefferys (2005). "Electrical stimulation of excitable tissue: design of efficacious and safe protocols." J Neurosci Methods **141**(2): 171-198.

Miller, J. W., G. M. Turner and B. C. Gray (1994). "Anticonvulsant effects of the experimental induction of hippocampal theta activity." Epilepsy Res **18**(3): 195-204.

Montgomery, E. B., Jr. and J. T. Gale (2008). "Mechanisms of action of deep brain stimulation(DBS)." Neurosci Biobehav Rev **32**(3): 388-407.

Montplaisir, J., M. Laverdiere, J. M. Saint-Hilaire and I. Rouleau (1987). "Nocturnal sleep recording in partial epilepsy: a study with depth electrodes." J Clin Neurophysiol **4**(4): 383-388.

Moran, R. J., N. Mallet, V. Litvak, R. J. Dolan, P. J. Magill, K. J. Friston and P. Brown (2011). "Alterations in brain connectivity underlying beta oscillations in Parkinsonism." PLoS Comput Biol **7**(8): e1002124.

Morgan, J. I. and T. Curran (1991). "Stimulus-transcription coupling in the nervous system: involvement of the inducible proto-oncogenes fos and jun." Annu Rev Neurosci **14**: 421-451.

Mormann, F., T. Kreuz, R. G. Andrzejak, P. David, K. Lehnertz and C. E. Elger (2003). "Epileptic seizures are preceded by a decrease in synchronization." Epilepsy Res **53**(3): 173-185.

Moro, E., R. J. Esselink, J. Xie, M. Hommel, A. L. Benabid and P. Pollak (2002). "The impact on Parkinson's disease of electrical parameter settings in STN stimulation." Neurology **59**(5): 706-713.

Morris, R. G., P. Garrud, J. N. Rawlins and J. O'Keefe (1982). "Place navigation impaired in rats with hippocampal lesions." Nature **297**(5868): 681-683.

Moser, E., M. B. Moser and P. Andersen (1993). "Spatial learning impairment parallels the magnitude of dorsal hippocampal lesions, but is hardly present following ventral lesions." J Neurosci **13**(9): 3916-3925.

Mullen, R. J., C. R. Buck and A. M. Smith (1992). "Neun, a Neuronal Specific Nuclear-Protein in Vertebrates." Development **116**(1): 201-211.

Muller, R., R. Bravo, J. Burckhardt and T. Curran (1984). "Induction of C-Fos Gene and Protein by Growth-Factors Precedes Activation of C-Myc." Nature **312**(5996): 716-720.

Newman, J. P., R. Zeller-Townson, M. F. Fong, S. Arcot Desai, R. E. Gross and S. M. Potter (2012). "Closed-Loop, Multichannel Experimentation Using the Open-Source NeuroRighter Electrophysiology Platform." Front Neural Circuits **6**: 98.

Nicolelis, M. A., A. A. Ghazanfar, B. M. Faggin, S. Votaw and L. M. Oliveira (1997). "Reconstructing the engram: simultaneous, multisite, many single neuron recordings." Neuron **18**(4): 529-537.

O'Doherty, J. E., M. A. Lebedev, T. L. Hanson, N. A. Fitzsimmons and M. A. Nicolelis (2009). "A brain-machine interface instructed by direct intracortical microstimulation." Front Integr Neurosci **3**: 20.

Pais-Vieira, M., M. Lebedev, C. Kunicki, J. Wang and M. A. Nicolelis (2013). "A brain-to-brain interface for real-time sharing of sensorimotor information." Sci Rep **3**: 1319.

Pancrazio, J. J., P. P. Bey, Jr., A. Loloee, S. Manne, H. C. Chao, L. L. Howard, W. M. Gosney, D. A. Borkholder, G. T. Kovacs, P. Manos, D. S. Cuttino and D. A. Stenger (1998). "Description and demonstration of a CMOS amplifier-based-system with measurement and stimulation capability for bioelectrical signal transduction." Biosens Bioelectron **13**(9): 971-979.

Paz, J. T., T. J. Davidson, E. S. Frechette, B. Delord, I. Parada, K. Peng, K. Deisseroth and J. R. Huguenard (2013). "Closed-loop optogenetic control of thalamus as a tool for interrupting seizures after cortical injury." Nat Neurosci **16**(1): 64-70.

Percha, B., R. Dzakpasu, M. Zochowski and J. Parent (2005). "Transition from local to global phase synchrony in small world neural network and its possible implications for epilepsy." Phys Rev E Stat Nonlin Soft Matter Phys **72**(3 Pt 1): 031909.

Perez Velazquez, J. L. and P. L. Carlen (2000). "Gap junctions, synchrony and seizures." Trends Neurosci **23**(2): 68-74.

Perlmutter, J. S. and J. W. Mink (2006). "Deep brain stimulation." Annu Rev Neurosci **29**: 229-257.

Pike, F. G., R. S. Goddard, J. M. Suckling, P. Ganter, N. Kasthuri and O. Paulsen (2000). "Distinct frequency preferences of different types of rat hippocampal neurones in

response to oscillatory input currents." Journal of Physiology-London **529**(1): 205-213.

Polikov, V. S., P. A. Tresco and W. M. Reichert (2005). "Response of brain tissue to chronically implanted neural electrodes." J Neurosci Methods **148**(1): 1-18.

Potter, S. M. and T. B. DeMarse (2001). "A new approach to neural cell culture for long-term studies." J Neurosci Methods **110**(1-2): 17-24.

Quiroga, R. Q., Z. Nadasdy and Y. Ben-Shaul (2004). "Unsupervised spike detection and sorting with wavelets and superparamagnetic clustering." Neural Comput **16**(8): 1661-1687.

Racine, R., V. Okujava and S. Chipashvili (1972). "Modification of seizure activity by electrical stimulation. 3. Mechanisms." Electroencephalogr Clin Neurophysiol **32**(3): 295-299.

Ramachandran, A., M. Schuettler, N. Lago, T. Doerge, K. P. Koch, X. Navarro, K. P. Hoffmann and T. Stieglitz (2006). "Design, in vitro and in vivo assessment of a multi-channel sieve electrode with integrated multiplexer." J Neural Eng **3**(2): 114-124.

Rolston, J. D., S. A. Desai, N. G. Laxpati and R. E. Gross (2011). "Electrical stimulation for epilepsy: experimental approaches." Neurosurg Clin N Am **22**(4): 425-442, v.

Rolston, J. D., D. J. Englot, D. D. Wang, T. Shih and E. F. Chang (2012). "Comparison of seizure control outcomes and the safety of vagus nerve, thalamic deep brain, and responsive neurostimulation: evidence from randomized controlled trials." Neurosurg Focus **32**(3): E14.

Rolston, J. D., R. E. Gross and S. M. Potter (2009). "A low-cost multielectrode system for data acquisition enabling real-time closed-loop processing with rapid recovery from stimulation artifacts." Front Neuroeng **2**: 12.

Rolston, J. D., R. E. Gross and S. M. Potter (2009). "NeuroRighter: closed-loop multielectrode stimulation and recording for freely moving animals and cell cultures." Conf Proc IEEE Eng Med Biol Soc **2009**: 6489-6492.

Rolston, J. D., R. E. Gross and S. M. Potter (2010). "Closed-loop, open-source electrophysiology." Front Neurosci **4**.

Rolston, J. D., N. G. Laxpati, C. A. Gutekunst, S. M. Potter and R. E. Gross (2010). "Spontaneous and evoked high-frequency oscillations in the tetanus toxin model of epilepsy." Epilepsia **51**(11): 2289-2296.

Rose, T. L. and L. S. Robblee (1990). "Electrical stimulation with Pt electrodes. VIII. Electrochemically safe charge injection limits with 0.2 ms pulses." IEEE Trans Biomed Eng **37**(11): 1118-1120.

Rosin, B., M. Slovik, R. Mitelman, M. Rivlin-Etzion, S. N. Haber, Z. Israel, E. Vaadia and H. Bergman (2011). "Closed-loop deep brain stimulation is superior in ameliorating parkinsonism." Neuron **72**(2): 370-384.

Ross, J. D., S. M. O'Connor, R. A. Blum, E. A. Brown and S. P. DeWeerth (2004). "Multielectrode impedance tuning: reducing noise and improving stimulation efficacy." Conf Proc IEEE Eng Med Biol Soc **6**: 4115-4117.

Rozman, J., I. Milosev and M. Jenko (2000). "Platinum stimulating electrodes in physiological media." J Med Eng Technol **24**(3): 123-128.

Rudge, J. S., G. M. Smith and J. Silver (1989). "An in vitro model of wound healing in the CNS: analysis of cell reaction and interaction at different ages." Exp Neurol **103**(1): 1-16.

Saryyeva, A., M. Nakamura, J. K. Krauss and K. Schwabe (2011). "c-Fos expression after deep brain stimulation of the pedunculopontine tegmental nucleus in the rat 6-hydroxydopamine Parkinson model." J Chem Neuroanat **42**(3): 210-217.

Scarlett, D., A. T. Dypvik and B. H. Bland (2004). "Comparison of spontaneous and septally driven hippocampal theta field and theta-related cellular activity." Hippocampus **14**(1): 99-106.

Schachter, S. C. and C. B. Saper (1998). "Vagus nerve stimulation." Epilepsia **39**(7): 677-686.

Shi, L. H., F. Luo, D. J. Woodward, D. C. McIntyre and J. Y. Chang (2007). "Temporal sequence of ictal discharges propagation in the corticolimbic basal ganglia system during amygdala kindled seizures in freely moving rats." Epilepsy Res **73**(1): 85-97.

Shirvalkar, P. R., P. R. Rapp and M. L. Shapiro (2010). "Bidirectional changes to hippocampal theta-gamma comodulation predict memory for recent spatial episodes." Proc Natl Acad Sci U S A **107**(15): 7054-7059.

Staley, K. J., A. White and F. E. Dudek (2011). "Interictal spikes: harbingers or causes of epilepsy?" Neuroscience Letters **497**(3): 247-250.

Stanslaski, S., P. Afshar, P. Cong, J. Giftakis, P. Stypulkowski, D. Carlson, D. Linde, D. Ullestad, A. T. Avestruz and T. Denison (2012). "Design and validation of a fully implantable, chronic, closed-loop neuromodulation device with concurrent sensing and stimulation." IEEE Trans Neural Syst Rehabil Eng **20**(4): 410-421.

Stead, M., M. Bower, B. H. Brinkmann, K. Lee, W. R. Marsh, F. B. Meyer, B. Litt, J. Van Gompel and G. A. Worrell (2010). "Microseizures and the spatiotemporal scales of human partial epilepsy." Brain **133**(9): 2789-2797.

Stoney, S. D., W. D. Thompson and H. Asanuma (1968). "Excitation of Pyramidal Tract Cells by Intracortical Microstimulation - Effective Extent of Stimulating Current." Journal of Neurophysiology **31**(5): 659-&.

Sun, F. T., M. J. Morrell and R. E. Wharen, Jr. (2008). "Responsive cortical stimulation for the treatment of epilepsy." Neurotherapeutics **5**(1): 68-74.

Tass, P. A. and M. Majtanik (2006). "Long-term anti-kindling effects of desynchronizing brain stimulation: a theoretical study." Biol Cybern **94**(1): 58-66.

Tass, P. A., L. Qin, C. Hauptmann, S. Dovero, E. Bezard, T. Boraud and W. G. Meissner (2012). "Coordinated reset has sustained aftereffects in Parkinsonian monkeys." Ann Neurol **72**(5): 816-820.

Velasco, A. L., F. Velasco, M. Velasco, F. Jimenez, J. D. Carrillo-Ruiz and G. Castro (2007). "The role of neuromodulation of the hippocampus in the treatment of intractable complex partial seizures of the temporal lobe." Acta Neurochir Suppl **97**(Pt 2): 329-332.

Velasco, F., M. Velasco, A. L. Velasco, D. Menez and L. Rocha (2001). "Electrical stimulation for epilepsy: Stimulation of hippocampal foci." Stereotactic and Functional Neurosurgery **77**(1-4): 223-227.

Venkatraman, S., K. Elkabany, J. D. Long, Y. Yao and J. M. Carmena (2009). "A System for Neural Recording and Closed-Loop Intracortical Microstimulation in Awake Rodents." Biomedical Engineering, IEEE Transactions on **56**(1): 15-22.

Vetter, R. J., J. C. Williams, J. F. Hetke, E. A. Nunamaker and D. R. Kipke (2004). "Chronic neural recording using silicon-substrate microelectrode arrays implanted in cerebral cortex." IEEE Trans Biomed Eng **51**(6): 896-904.

Volkmann, J., E. Moro and R. Pahwa (2006). "Basic algorithms for the programming of deep brain stimulation in Parkinson's disease." Movement Disorders **21**: S284-S289.

Vorhees, C. V. and M. T. Williams (2006). "Morris water maze: procedures for assessing spatial and related forms of learning and memory." Nat Protoc **1**(2): 848-858.

Vreugdenhil, M., S. P. Hack, A. Draguhn and J. G. Jefferys (2002). "Tetanus toxin induces long-term changes in excitation and inhibition in the rat hippocampal CA1 area." Neuroscience **114**(4): 983-994.

Wagenaar, D. A., R. Madhavan, J. Pine and S. M. Potter (2005). "Controlling bursting in cortical cultures with closed-loop multi-electrode stimulation." J Neurosci **25**(3): 680-688.

Wagenaar, D. A., J. Pine and S. M. Potter (2004). "Effective parameters for stimulation of dissociated cultures using multi-electrode arrays." Journal of Neuroscience Methods **138**(1-2): 27-37.

Wagenaar, D. A. and S. M. Potter (2002). "Real-time multi-channel stimulus artifact suppression by local curve fitting." J Neurosci Methods **120**(2): 113-120.

Warren, C. P., S. Hu, M. Stead, B. H. Brinkmann, M. R. Bower and G. A. Worrell (2010). "Synchrony in normal and focal epileptic brain: the seizure onset zone is functionally disconnected." J Neurophysiol **104**(6): 3530-3539.

Wei, X. F. and W. M. Grill (2009). "Analysis of high-perimeter planar electrodes for efficient neural stimulation." Front Neuroeng **2**: 15.

Winson, J. (1978). "Loss of hippocampal theta rhythm results in spatial memory deficit in the rat." Science **201**(4351): 160-163.

Wong, R. K., R. D. Traub and R. Miles (1986). "Cellular basis of neuronal synchrony in epilepsy." Adv Neurol **44**: 583-592.

Xiao, Y. H., X. Y. Cui and D. C. Martin (2004). "Electrochemical polymerization and properties of PEDOT/S-EDOT on neural microelectrode arrays." Journal of Electroanalytical Chemistry **573**(1): 43-48.